Forschungsbericht 2025-34

Buckling prediction of cylindrical shells by vibration considering stochastic modelling, combined loading and industrial-scale validation

Theodor Dan Baciu

Deutsches Zentrum für Luft- und Raumfahrt
Institut für Systemleichtbau
Braunschweig

Deutsches Zentrum
DLR für Luft- und Raumfahrt

Forschungsbericht 2025-34

Buckling prediction of cylindrical shells by vibration considering stochastic modelling, combined loading and industrial-scale validation

Theodor Dan Baciu

Deutsches Zentrum für Luft- und Raumfahrt
Institut für Systemleichtbau
Braunschweig

185 Seiten
68 Bilder
14 Tabellen
104 Literaturstellen

Deutsches Zentrum
DLR für Luft- und Raumfahrt

Herausgeber:

Deutsches Zentrum
für Luft- und Raumfahrt e. V.
Wissenschaftliche Information
Linder Höhe
D-51147 Köln

ISSN 1434-8454
ISRN DLR-FB-2025-34
Erscheinungsjahr 2025
DOI:10.57676/2wtf-wb30

Vibration-Correlation Technique, Beulen, Zylinderschalen, Schwingung, zerstörungsfreie Prüfung

Theodor Dan BACIU
DLR, Institut für Systemleichtbaus, DLR, Braunschweig

Beulvorhersage von Zylinderschalen durch Vibration unter Berücksichtigung stochastischer Modellierung, kombinierter Belastung und Validierung im industriellen Maßstab

Universität Bremen

Die Vibrationskorrelationsmethode (VCT) hat sich als ein verlässliches Verfahren zur Bestimmung der Beullasten zylindrischer Schalen unter Druckbeanspruchung etabliert. Dennoch wurde die Methode bislang nicht als hinreichend ausgereift angesehen, um in industriellen Versuchsprogrammen Anwendung zu finden, da verschiedene Aspekte einer vertieften Untersuchung bedurften. Im Rahmen dieser Dissertation werden mehrere dieser Aspekte eingehend analysiert. Zunächst wird die Empfindlichkeit der Methode gegenüber wesentlichen Messparametern untersucht. Anschließend erfolgt eine Bewertung des Einflusses unterschiedlicher Amplituden von Form- und Belastungsimperfektionen auf die Robustheit der Methode. Daraufhin wird der Einfluss zusätzlicher Biege-, Schub- und/oder Torsionsbelastungen auf die VCT-basierte Abschätzung der axialen Beullast analysiert. Abschließend werden die experimentellen Ergebnisse einer zylindrischen Schale vorgestellt, die eine realmaßstäbliche Trägerstruktur eines Raumfahrzeugs repräsentiert und unter zwei kombinierten Biege-Druck-Lastfällen geprüft wurde.

Vibration-Correlation Technique, buckling, cylindrical shells, vibration, non-destructive testing
(Published in English)

Theodor Dan BACIU
German Aerospace Center (DLR), Institute of Lightweight Systems, DLR, Braunschweig

Buckling Prediction of Cylindrical Shells by Vibration Considering Stochastic Modelling, Combined Loading and Industrial-Scale Validation

Bremen University (Doctoral thesis)

The Vibration-Correlation Technique (VCT) has established itself as a reliable method to predict the buckling loads of cylindrical shells under compression. However, the method was not considered mature enough to deploy in industrial experimental campaigns, owing to several aspects that needed further investigation. In this dissertation, some of these aspects are investigated, starting with the method's sensitivity to key measurement parameters. Then, the influence of various amplitudes of shape and loading imperfections on the robustness of the method is assessed. Afterwards, the influence of applying additional bending, shear, and/or torsion loads on the VCT estimation of the axial buckling load was investigated. Lastly, the experimental results of a cylindrical shell representative of a real-scale launcher structure, tested under two bending-compression load cases, are presented.

BUCKLING PREDICTION OF CYLINDRICAL SHELLS BY VIBRATION CONSIDERING STOCHASTIC MODELLING, COMBINED LOADING AND INDUSTRIAL-SCALE VALIDATION

Vom Fachbereich Produktionstechnik
der
UNIVERSITÄT BREMEN

zur Erlangung des Würde
eines Doktor-Ingenieur (Dr.-Ing.)
genehmigte

Dissertation
von
M.Sc. Theodor Dan Baciu

Gutachter:

Prof. Dr.-Ing. Richard Degenhardt, Universität Bremen
Prof. Dr.-Ing. habil. Christian Mittelstedt, Technische Universität Darmstadt

Tag der mündlichen Prüfung: 20 Juni 2025

Abstract

The research summarised in this thesis focuses on advancing the state of the art regarding a non-destructive method to predict the buckling load of various structures, based on the change in their frequency response as a function of the load level applied, commonly known as the Vibration-Correlation Technique (VCT). The structures of choice for this research were cylindrical shells, for which VCT is particularly appealing, given their high sensitivity to imperfections, which often leads to large discrepancies between their theoretical and experimental buckling loads, as well as due to their unstable buckling response. Owing to the recent developments regarding this technique and its low adoption outside the academic environment, the research was focused on key areas that are equally relevant to both academic and industrial environments.

Firstly, the significance of the maximum load level measured and the number of measurements over the buckling load estimation provided by VCT was studied for multiple cylindrical shells, given the existing lack of agreement over these aspects of the experimental test setup. In an initial step, numerical data from the finite element models of 10 nominally identical cylindrical shells was used to investigate the influence of the aforementioned parameters over the VCT predictions. Then, in a second step, a similar study was performed using experimental data gathered from the existing literature, which confirmed the trends observed in the study based on numerical data. The main conclusions of this investigation were that the most important test parameter is the load level at which the vibration measurement is taken and that the number of measurements is mostly relevant in decreasing the possible errors given by unexpected frequency deviations among the multiple measurements. The VCT buckling load predictions of the structures studied had an insignificant variation with respect to the baseline predictions, for which all available measurements were used, regardless of the number of measurements taken into account, as long as the ratio between the highest load level considered and the buckling load was at least 70%. Conversely, having at least 9 measurements proved enough in ensuring a negligible variation of the predictions with respect to the baseline ones in the presence of frequency measurement deviations within ± 0.5Hz. Furthermore, it was also noticed that there are cases in which the VCT predictions decrease, rather than increase, with

increasing the load level taken into account. Although this behaviour is relatively easy to identify when performing VCT predictions while gradually increasing the maximum load level considered, the general conservative nature of the method in these cases may no longer be ensured.

Secondly, the sensitivity of VCT under various magnitudes of shape and loading imperfections was assessed. For this study, the FE model of a cylindrical shell with a large knock-down factor, related to its shape imperfection and for which VCT gave robust experimental buckling load predictions, was chosen as the baseline structure. Then, multiple magnitudes of its measured out-of-plane and of a realistic in-plane imperfection pattern were applied to the cylinder, such that the reliability of VCT to provide robust buckling load predictions in the presence of such imperfections could be investigated. It was found that the VCT predictions were generally insensitive to the aforementioned imperfections, provided that the maximum load ratio accounted for was in line with the one found to be sufficient in the first study. However, it was also found that there might be several shape imperfections for which VCT may be unreliable, primarily due to the VCT predictions decreasing when increasing the load ratio taken into account, aspect also highlighted in the first study. Furthermore, in the event of local buckling occurring, VCT proved unreliable in estimating the load level at which these events occur. Similarly, the VCT estimations of the global buckling load using the measurements before local buckling occurred were also relatively poor. Nevertheless, predicting the global buckling using VCT for these cases may be possible when taking into account exclusively the measurements beyond the point at which local buckling occurred. In these scenarios, the established VCT procedure often provided unconservative predictions, reason why using an empirical VCT procedure and taking shape imperfections into account in the buckling analysis is recommended, as the estimations provided in this case are generally more conservative.

Thirdly, the robustness of VCT for cylindrical shells subjected to combined loading was assessed. This numerical study used the finite element models of 6 cylindrical shells, in which additional bending, shear or torsion loads were applied, either individually or all together, alongside the main compressive load. The study revealed that VCT could provide reliable estimations of the axial loads at which cylinders buckle under the aforementioned combined loading scenarios, provided that the amounts of bending, shear, and/or torsion were relatively low. Moreover, whether the compression load was applied sequentially, or simultaneously with the additional ones was only relevant regarding the amount of the latter beyond which VCT failed to provide robust predictions. In this context, VCT provided better estimations when compression was applied after the aforementioned additional loads (sequential load introduction), so that the change in the frequency response reflected a change in the compression

load alone. In addition to that, it was also shown that VCT could provide good estimations on the compression load level at which cylinders buckle when bending, shear and torsion were applied together along with compression, also provided that the magnitudes of the former were small.

Lastly, the results of an experimental campaign covering aspects from all previous investigations conducted were shown to validate the results found. In this experimental campaign VCT was applied to a real-scale launcher structure, tested under two load cases in which uneven compression was applied. These load cases had significant bending components, given that they were defined so that buckling was precisely initiated in two key areas of the structure. During both of these tests, the vibration modes considered to provide reliable predictions were identified in situ. Taking into account the maximum load ratio of a valid vibration measurement during the first load case of 86%, the relative error of the VCT buckling load prediction was -5%. Conversely, the relative error of the VCT buckling load prediction for the second load case was -15%, as the load ratio of the last valid vibration measurement was lower than for the first load case, at 77%. Nevertheless, given the approximately linear relation between the VCT predictions and the maximum load level taken into account, an extrapolation of the VCT buckling load prediction corresponding to an 86% load ratio was made for the second load case, which yielded a relative error comparable to the one achieved for the first load case, namely -6%. Another positive outcome was that the preliminary numerical investigation performed in preparing the test provided valuable insights, confirmed later by experiment. Some of the key aspects accurately identified through numerical analyses were the frequency window in which the first vibration modes would occur, the span of the circumferential waves of the vibration modes, and the expected VCT prediction error as a function of the maximum load level used. In addition to this, a fair estimation of the frequency drop as the load applied increased was also provided by the preliminary numerical analysis.

Given the reliable in-situ VCT buckling load predictions and that in the post-test investigations a single vibration mode providing a better prediction than the in-situ ones was found, and only for the second load case, VCT can be considered a robust non-destructive method to determine the axial load level at which cylinders buckle. Furthermore, this was shown to hold true for a real-scale structure subjected to load cases with significant bending components, displaying thus the versatility of the method and its retained robustness when applied to structure sizes relevant to industrial environments. This feat is even more impressive when considering the test's important time restrictions and the occurrence of unexpected events, which for the first load case led to losing the track of the majority of vibration modes monitored beyond the 6^{th} vibration measurement, out of the 9 initially defined, while for the

second load case, it caused the loss of track of all previously tracked vibration modes beyond the 7^{th} vibration measurement, out of the 8 initially defined.

Zusammenfassung

Die in dieser Arbeit zusammengefasste Forschung konzentriert sich auf die Weiterentwicklung des Stands der Technik im Hinblick auf ein zerstörungsfreies Verfahren zur Vorhersage der Beullast verschiedener Strukturen. Grundlage ist dabei die Veränderung ihrer Frequenzantwort in Abhängigkeit von der aufgebrachten Last, die allgemein als Vibration-Correlation Technique (VCT) bekannt ist. Die für diese Untersuchung gewählten Strukturen waren Zylinderschalen, für die VCT besonders interessant ist, da ihre hohe Empfindlichkeit gegenüber Imperfektionen häufig zu großen Diskrepanzen zwischen theoretisch und experimentell ermittelten Beullasten führt und zudem ihr Beulverhalten instabil ist. Angesichts der jüngsten Entwicklungen dieser Methode und ihrer bislang geringen Anwendung außerhalb des akademischen Umfelds konzentrierte sich die Arbeit auf Schlüsselaspekte, die sowohl für die Wissenschaft als auch für die Industrie von gleicher Relevanz sind.

Zunächst wurde die Bedeutung des maximal gemessenen Lastniveaus und der Anzahl der Messungen für die Beullastabschätzung durch VCT untersucht, da über diese Aspekte im experimentellen Versuchsaufbau bislang Uneinigkeit herrscht. In einem ersten Schritt wurden numerische Daten aus Finite-Elemente-Modellen von zehn nominell identischen Zylinderschalen verwendet, um den Einfluss der genannten Parameter auf die VCT-Vorhersagen zu analysieren. In einem zweiten Schritt wurde eine ähnliche Untersuchung mit experimentellen Daten aus der Literatur durchgeführt, die in der numerischen Studie beobachteten Trends bestätigte. Die Hauptschlussfolgerung war, dass der wichtigste Testparameter das Lastniveau ist, bei dem die Schwing-ungsmessung erfolgt, während die Anzahl der Messungen vor allem dazu beiträgt, mögliche Fehler durch unerwartete Frequenzabweichungen zwischen den Messungen zu verringern. Die VCT-Beullastvorhersagen zeigten nur geringe Abweichungen von den Referenzwerten, für die alle verfügbaren Messungen berücksichtigt wurden – unabhängig von der Anzahl der Messungen, solange das Verhältnis zwischen der höchsten betrachteten Last und der tatsächlichen Beullast mindestens 70% betrug. Umgekehrt erwiesen sich mindestens neun Messungen als ausreichend, um Abwei-chungen der Vorhersagen bei Frequenzmessfehlern innerhalb von ±0,5Hz vernachlässigbar zu machen. Zudem wurde festgestellt, dass es Fälle gibt, in denen die VCT-Vorhersagen mit zunehmender Last nicht steigen, sondern sinken. Obwohl dieses

Verhalten bei schrittweiser Erhöhung des maximal berücksichtigten Lastniveaus relativ leicht zu erkennen ist, könnte die üblicherweise konservative Natur der Methode in solchen Fällen nicht mehr gewährleistet sein.

Im zweiten Schritt wurde die Sensitivität der VCT gegenüber Imperfektionen in Form und Belastung untersucht. Dazu diente das FE-Modell einer Zylinderschale mit einem großen Knock-down factor, der auf ihre Formimperfektion zurückzuführen ist und für die VCT robuste experimentelle Beullastvorhersagen lieferte. Anschließend wurden verschiedene Ausprägungen der gemessenen außeraxialen und einer realistischen in-plane-Imperfektion auf den Zylinder angewandt, um die Zuverlässigkeit von VCT unter solchen Bedingungen zu bewerten. Es zeigte sich, dass die VCT-Vorhersagen gegenüber diesen Imperfektionen im Allgemeinen unempfindlich waren, sofern das maximale berücksichtigte Lastverhältnis mit dem im ersten Schritt ermittelten Wert übereinstimmte. Es wurde jedoch auch festgestellt, dass es bestimmte Formimperfektionen geben könnte, bei denen VCT unzuverlässig ist, vor allem, wenn die Vorhersagen mit zunehmender Last sinken – ein Aspekt, der bereits in der ers-ten Untersuchung auffiel. Darüber hinaus erwies sich VCT als unzuverlässig bei der Abschätzung der Last, bei der lokales Beulen auftritt. Ebenso waren die globalen Beullastabschätzungen anhand der Messungen vor dem lokalen Beulen relativ ungenau. Dennoch könnte die globale Beullast mithilfe von VCT abgeschätzt werden, wenn ausschließlich Messungen nach Eintritt des lokalen Beulens berücksichtigt werden. In diesen Szenarien lieferte das etablierte VCT-Verfahren jedoch häufig nicht-konservative Ergebnisse. Daher wird empfohlen, ein empirisches VCT-Verfahren zu verwenden und Formimperfektionen explizit in die Beulanalyse ein zubeziehen, da die Schätzungen in diesem Fall im Allgemeinen konservativer ausfallen.

Im dritten Schritt wurde die Robustheit von VCT für Zylinderschalen unter kombinierter Belastung untersucht. In dieser numerischen Studie wurden FE-Modelle von sechs Zylinderschalen verwendet, bei denen zusätzlich Biegung, Schub oder Torsion – einzeln oder kombiniert – neben der axialen Drucklast aufgebracht wurden. Die Untersuchung zeigte, dass VCT zuverlässige Vorhersagen der axialen Beullast unter diesen kombinierten Belastungen liefern kann, solange die zusätzlichen Belastungen relativ gering waren. Ob die Drucklast nacheinander oder gleichzeitig mit den Zusatzlasten eingebracht wurde, war nur insofern relevant, als es den Schwellenwert der Zusatzlast bestimmte, oberhalb dessen VCT keine robusten Vorhersagen mehr liefern konnte. In diesem Zusammenhang erwies sich VCT als genauer, wenn die Drucklast nach den Zusatzlasten aufgebracht wurde (sequentielle Lastaufbringung), sodass die Änderung der Frequenzantwort nur die Drucklast widerspiegelte. Darüber hinaus konnte VCT auch gute Vorhersagen liefern, wenn Biegung, Schub und Torsion zusammen mit Druck aufgebracht wurden – vorausgesetzt, deren Intensität war gering.

Abschließend wurden die Ergebnisse einer experimentellen Kampagne vorgestellt, die Aspekte aller vorangegangenen Untersuchungen abdeckte und die gewonnenen Erkenntnisse validierte. In dieser Kampagne wurde VCT an einer realmaßstäblichen Trägerstruktur angewandt, die unter zwei Lastfällen getestet wurde, in denen ungleichmäßige Druckbelastungen aufgebracht wurden. Diese Lastfälle enthielten erhebliche Biegungsanteile, da sie so definiert waren, dass das Beulen gezielt in zwei Schlüsselbereichen der Struktur eingeleitet wurde. Während beider Tests wurden die Schwingungsmoden, die zuverlässige Vorhersagen ermöglichten, vor Ort identifiziert. Unter Berücksichtigung eines maximalen Lastverhältnisses von 86% bei einem gültigen Schwingungsmesspunkt im ersten Lastfall betrug der relative Fehler der VCT-Beullastvorhersage -5%. Im zweiten Lastfall lag der relative Fehler bei -15%, da das Lastverhältnis der letzten gültigen Messung geringer war (77%). Aufgrund der annähernd linearen Beziehung zwischen den VCT-Vorhersagen und dem maximal berücksichtigten Lastniveau konnte jedoch für den zweiten Lastfall eine Extrapolation auf ein Lastverhältnis von 86% durchgeführt werden, die einen vergleichbaren relativen Fehler von -6% ergab. Ein weiterer positiver Aspekt war, dass die vorberei-tenden numerischen Untersuchungen wertvolle Erkenntnisse lieferten, die im Experiment bestätigt wurden. Zu den Aspekten, die numerisch korrekt vorhergesagt wurden, gehörten u. a. das Frequenzfenster der ersten Schwingungsmoden, die Ausbrei-tung der Umfangswellen der Moden sowie der erwartete VCT-Vorhersagefehler in Abhängigkeit vom maximal berücksichtigten Lastniveau. Zudem lieferte die Voruntersuchung eine brauchbare Schätzung des Frequenzabfalls bei zunehmender Last.

Angesichts der zuverlässigen VCT-Beullastvorhersagen in situ und der Tatsache, dass nachträglich nur in einem einzigen Fall (im zweiten Lastfall) ein Schwingungs-Mode identifiziert wurde, die eine bessere Vorhersage als die in situ identifizierten ermöglichte, kann VCT als robustes zerstörungsfreies Verfahren zur Bestimmung der axialen Beullast von Zylinderschalen betrachtet werden. Dies gilt selbst für realmaßstäbliche Strukturen unter Lastfällen mit signifikanten Biegungsanteilen. Damit zeigt sich die Vielseitigkeit und Robustheit der Methode auch bei Strukturen von für die Industrie relevanter Größe. Besonders bemerkenswert ist dies angesichts der strengen Zeitvorgaben der Tests und des Auftretens unerwarteter Ereignisse, die im ersten Lastfall dazu führten, dass die Mehrheit der Schwingungsmoden ab der 6. von insgesamt 9 geplanten Messungen nicht mehr verfolgt werden konnte. Im zweiten Lastfall gingen alle zuvor verfolgten Moden ab der 7. von 8 geplanten Messungen verloren.

Acknowledgements

The research presented in this thesis was conducted within the two years of the ESIRA, and 1 year of the SIWIRA, research projects founded by ERDF (the former also being in collaboration with Faserinstitut Bremen e.V.), and within the two-year in-between scholarship at DLR through the DLR-DAAD PhD scholarship programme.

While the research work was performed by me, I could have not succeeded on my own, this accomplishment being impossible without the support of many people and organizations alike. Therefore, I feel compelled to express my gratitude to all, my acknowledgments being shown in a chronological order.

Firstly, I could have never dared to hope I'd be able to reach such an accomplishment without the emotional and financial support of my family. Supporting my studies abroad was anything but easy, yet they were always positive, supportive and believed in me. I was, am, and will forever be grateful to them, for this, as well as for all other things they did, are doing, or will do in the future.

Besides my family, I'm also thankful to my friends, who were next to me for better or worse. Be it during casual meetings inside or outside, at the sea or in the mountains, they listened to my troubles and made me either to temporarily forget them or to overcome them easier than on my own.

An important role throughout my career also had Professor Chiara Bisagni, my MSc supervisor at TU Delft. Besides offering valuable feedback on the published papers, she also reached out to me in the difficult times during Covid and put me in contact with Professor Richard Degenhardt, who would later become my work colleague and PhD supervisor. Needless to say, I'm ever grateful for her support throughout the past years, and I look forward to possible collaborations in the future.

Professor Richard Degenhardt, my PhD supervisor and colleague for the past 5 years, deserves many SPECIAL thanks. The option of doing a PhD was definitely not on my mind, not until he encouraged and supported me to apply for a PhD scholarship within the DLR-DAAD framework. From the onset of my PhD pursuit, as well as within the two years we worked together prior to that, he was always positive, supportive, optimistic and provided valuable feedback, while giving me the freedom I desired within my research as well. As if this was not enough, he also helped me a great

deal in establishing myself both within Germany, as well as within the department of Structural Mechanics at the DLR institute of Lightweight Systems. As my writing skills fail to match my gratitude to you Richard, I'll simply resort to a simple and sincere thank you, it has been a pleasure.

My gratitude also goes to Dr. Felipe Franzoni and to Dr. Adrian Gliszczyński, my colleagues within the ESIRA and SIWIRA projects. Working with them has been a pleasure, as they were always easy to reach, willing to hear my thoughts, and help me with the issues I was struggling with. From feedback on my research, support with Abaqus and Python scripts, and ideas on how I might tackle the challenges throughout my research, their contribution was highly valuable in improving the quality of my research and publications.

During my research I had the absolute privilege, possibly once in a lifetime, to be present at two experimental tests of a liquid hydrogen tank section of the liquid lower propulsion module of the Ariane 6 rocket. This embodied every researcher's dream, namely, to see their theoretical work validated by experiment and to publish the results of the first known application of the vibration-correlation technique to a real-scale launcher structure. Needless to say, such an effort could only be achieved with the involvement of a large number of people, all of whom have my deepest gratitude. I'm thankful to Dr. Jochen Albus from ArianeGroup, Mr. Klaus Stromer from MT Aerospace, and Dipl. Ing. (FH) IWE Jens Hornschuch from IMA Dresden, who allowed me and my colleagues to attend the test, provided the prerequisites needed to perform the theoretical studies prior to the test, and allowed publishing the results. In addition, their feedback on my research was also highly valued, as was their willingness to implement the changes suggested for enhancing the likelihood of a positive outcome of my research. My gratitude also goes to Dr. Kaspars Kalnins and Dr. Eduards Skukis, who performed the vibration measurements during those tests, shared their knowledge with me, and provided feedback on my research.

My second PhD supervisor, Professor Christian Mittelstedt, from TU Darmstadt, has my sincere appreciation as well. Easy to reach, quick in providing insightful comments and recommendations, positive and motivating, in short, everything you'd want from a PhD supervisor.

Further, I would also like to thank Ms. Katrin Bußmeier, from the DAAD's Information and Advisory Centre, for her continuous support during my scholarship. She was there every single time I needed information and guidance, providing me with clear answers, and in a short time.

I'm also thankful to my DLR colleagues, especially to Dr. Raffael Bogenfeld, Marc Garbade, and Dr. Martin Liebisch, who were always willing to help when I was struggling with my tasks, or when I had technical or software issues, and who made me feel included. I'm also thankful to the head of the department, Dr. Tobias Wille, who accepted and extended my PhD scholarship, while providing valuable feedback on the research performed within the department.

Many thanks also go to Professor Saullo Castro and Professor Mariano Arbelo for their willingness to share with me their incomparably vaster experience in the buckling and vibration-correlation technique fields, as well as their meaningful critique of the manuscripts published together.

Last, but not least, I would like to offer my gratitude to the members of the doctoral committee that were not mentioned earlier, namely to Dipl.-Ing.Christoph Hoffmeister, PhD candidate Gökdeniz Havuc, Professor David May, and Dr. Dirk Wilckens. Besides taking their time to attend my PhD defense, their positive and calm attitude during the defense, in contrast with my high running emotions and stress, was deeply appreciated.

Contents

List of Figures

List of Tables

Nomenclature

List of Symbols

AC	Actuator
Al	Aluminium
$C(n, r)$	Combinations of n taken k
D	Diameter [mm]
E	Elastic modulus [GPa]
E_1	Elastic modulus in the longitudinal direction [GPa]
E_{1C}	Elastic modulus in the longitudinal direction, under compression [GPa]
E_{1T}	Elastic modulus in the longitudinal direction, under tension [GPa]
E_2	Elastic modulus in the transversal direction [GPa]
E_{2C}	Elastic modulus in the transversal direction, under compression [GPa]
E_{2T}	Elastic modulus in the transversal direction, under tension [GPa]
ϵ_{nl-exp}	Relative error of P_{nl} with respect to P_{exp}
$\epsilon_{VCT-exp}$	Relative error of numerical P_{VCT} with respect to P_{exp}
ϵ_{VCT-nl}	Relative error of experimental P_{VCT} with respect to P_{nl}
f	Frequency ratio
f_k	Frequency ratio for vibration mode k
F	Frequency [Hz]
F_k	Frequency of vibration mode k [Hz]
G_{12}	Shear modulus in the 1-2 plane [GPa]
G_{13}	Shear modulus in the 1-3 plane [GPa]
G_{23}	Shear modulus in the 2-3 plane [GPa]
k	Vibration mode occurrence number
L	Axial length of the cylindrical shell [mm]
L_{free}	Free (unsupported) axial length of the cylindrical shell [mm]
L_{tot}	Total axial length of the cylindrical shell [mm]
ν	Poisson's ratio

ν_{12}	Poisson's ratio in the 1-2 plane
p	Axial load ratio
P	Axial load [kN]
P_{cr}	Theoretical axial buckling load [kN]
P_{cr_ci}	Theoretical axial buckling load of the imperfect structure under combined loading [kN]
P_{cr_cp}	Theoretical axial buckling load of the perfect structure under combined loading [kN]
P_{cr_i}	Theoretical axial buckling load of the imperfect structure [kN]
P_{cr_p}	Theoretical axial buckling load of the perfect structure [kN]
P_{exp}	Experimental buckling load [kN]
P_{VCT}	VCT buckling load prediction [kN]
$P_{VCT,k}$	VCT buckling load prediction for the kth vibration mode [kN]
P_{nl}	Non-linear axial buckling load [kN]
r	Pearson correlation coefficient
r_s	Spearman correlation coefficient
r_x	Rotation around the X axis [rad]
r_y	Rotation around the Y axis [rad]
r_z	Rotation around the Z axis [rad]
R	Radius [mm]
ρ	Density [g/cm^3]
σ	Variance
t	Thickness of the cylindrical shell [mm]
τ	Kendall correlation coefficient
u	Axial displacement [mm]
u_x	Displacement along the X axis [mm]
u_y	Displacement along the Y axis [mm]
u_z	Displacement along the Z axis [mm]
ξ	drop in the load-carrying capacity
ξ_k	drop in the load-carrying capacity given by the kth vibration mode

List of Acronyms

AISI	American Iron and Steel Institute
AR	Aspect Ratio
ATOS	Advanced Topometric Optical Sensor
CAD	Computer Aided Design
CFRP	Carbon Fibre Reinforced Plastic
DAAD	Deutscher Akademischer Austauschdienst
DIC	Digital Image Correlation

ERDF	European Regional Development Fund
FE	Finite Element
IP	In-Plane
KDF	Knock-Down Factor
HS	HemiSpherical joint
LC	Load Case
LVDT	Linear Variable Differential Transformer
MPC	Multi-Point Constraint
NASA	National Aeronautics and Space Administration
OoP	Out-of-Plane
PP	Parallel-Plates
RP	Reference Point
SP	Special Publication
UD	Uni-Directional
VCT	Vibration-Correlation Technique

1 Introduction

The buckling phenomenon, characterised by a change of a structure's equilibrium state as a result of a small increase in its loading, represents one of the most common aspects to be considered when designing load-bearing structures. For cylindrical shells, a robust estimation of the buckling load in service is both essential and particularly difficult, given their unstable post-buckling behaviour and high sensitivity to imperfections. This sensitivity was observed as early as 1914 by Southwell [5], in his work shape imperfections being considered the main source of discrepancy between the theoretical and measured load level at which a structure may lose its stability. Next to shape, loading, material, thickness and boundary conditions imperfections can all significantly reduce the experimental buckling load with respect to the theoretical value for a cylindrical shell under axial compression.

Owing to this high buckling load sensitivity to imperfections, to the complexity of include them in theoretical estimations, and to the high demand for these types of structures in the aerospace, marine, or energy sectors, to name a few, buckling research remains an active topic, despite its long history. Some of the most significant studies have been compiled in the NASA SP-8007 [6] guideline on buckling of thin-walled circular cylinders, where a comprehensive number of experimental results was used to provide lower bound Knock-Down Factors (KDFs, ratios between the measured and theoretical buckling values) for isotropic cylinders as a function of the ratio between their radius and thickness. The KDFs recommended for cylindrical shells with radius over thickness ratios lower than 1500 subjected to axial compression are within a 0.18-0.84 interval and are often found to be over-conservative, particularly for

composite cylinders, therefore decreasing the efficiency of these structures in service [2, 7, 8].

In recent years, finite element analysis has become an indispensable tool in designing and sizing any type of load-bearing structure, with a significant impact on improving their structural efficiency. For cylindrical shells in particular, it represents a powerful tool to study their sensitivities under various conditions, as it allows the inclusion of virtually any type of imperfection. While taking imperfections into account in numerical models can often yield robust buckling load estimations, validated by experimental tests, acquiring and implementing these in numerical models may require a significant time and effort and can therefore be costly as well. Imperfection types such as shape, thickness, and material are relatively easy to implement and often lead to great improvements in the accuracy of the buckling load estimation. However, imperfections related to loading and boundary conditions are more difficult to acquire and implement before testing or during service and can therefore be an important source of a poor correlation between the structure's theoretical and in-situ response under load. On the other hand, non-destructive methods can be successfully used to determine the in-situ buckling loads of cylindrical shells, as the aforementioned imperfections are inherently captured within the structure's response on which the estimation is based. Among these, the most relevant for cylindrical shells under axial compression are the probing technique [9] and the Vibration-Correlation Technique (VCT) [10].

In the probing technique, a dimple-like buckling shape, associated with the lowest energy barrier (as determined in [11]) that must be overcome to reach buckling, is reproduced by applying a displacement-based lateral point load with various magnitudes. As the lateral displacement is gradually increased, the lateral reaction force reaches a maximum, this peak value being inversely proportional to the axial load applied. Upon further increasing the applied lateral displacement, the lateral reaction load begins to drop, eventually yielding a zero reaction force, and the area under this load-displacement curve represents the energy barrier that must be exceeded for the cylinder to buckle under that axial load level. However, in practice, the point

at which the lateral reaction force decreases to zero might need to be extrapolated if there is no inner radial support at the probing location on the cylinder to prevent it from losing its stability and risking structural damage. As the peak lateral reaction force decreases with increasing the axial load level, the axial load at which the peak reaction force reaches zero (the buckling load) can be extrapolated based on measurements taken at several axial load levels. While this method was shown to give reliable buckling load estimations, the predictions were shown to be sensitive to the probing location [9, 12, 13]. In this regard, the path of least resistance, typically found near the most significant imperfection, should be probed for reliable buckling estimations, as probing at a near-perfect location might yield unconservative predictions.

The vibration-correlation technique makes use of the structure's change in vibration response as a function of the load applied to extrapolate the buckling load. This is often referred to as the direct use of VCT, while its indirect use is in determining in-situ boundary conditions [10], or fibre volume fractions of composite structures [14]. The experimental procedure requires an exciter to induce vibrations in the structure and measuring equipment to capture the structure's vibration response. Loudspeakers or harmonic hammers are typically used to induce vibrations, while the vibration modes and their corresponding frequencies are usually identified using either accelerometers, or laser vibrometers. When the combination of a loudspeaker and a laser vibrometer is used, direct contact with the structure is avoided, therefore the risk of the vibration response measurement equipment to influence the buckling load is minimal. Furthermore, the use of a laser vibrometer can provide well-defined vibration modes, which would otherwise require a significant number of accelerometers attached to the structure, therefore imposing a risk of influencing its buckling and vibration response. This, however, usually comes at the expense of a significantly larger measurement time, which might be prohibitive when the vibration response is measured for a large number of load levels and/or when measurement difficulties arise. These can be related to the surface measured, as the vibration response of a surface with imperfections, poor surface reflectivity, or speckled patterns may require more time to be accurately measured. Furthermore, large lateral movements during the

measurement may also increase the measurement time when using a laser vibrometer.

Even though both the aforementioned non-destructive methods to predict buckling loads of cylindrical shells were proven effective within the academic environment, interest from the industry in applying these methods in their validation tests remains limited. This thesis aims to expand the state of the art regarding VCT applied to cylindrical shells, primarily through numerical analyses, focusing on three key aspects of equal interest for both the academic and industrial environments. First of all, the influence of the maximum load level measured and the number of measurements on the VCT buckling load prediction is investigated. Secondly, the sensitivity of VCT towards shape and loading imperfections is assessed. Thirdly, the feasibility of using VCT to provide robust buckling predictions when additional loads, besides axial compression, are applied to cylindrical shells is explored. Then, the results of an experimental campaign that addresses the key aspects explored in the aforementioned three studies are presented. In this experimental campaign, VCT was applied to a real-scale launcher structure, tested under two uneven compression load cases, which induced significant bending components. Lastly, the knowledge gathered throughout the research conducted is summarised in a set of practical guidelines for optimising the application and outcome of VCT for predicting the axial load level at which cylindrical shells buckle.

2 Literature Review

The connection between a structure's vibration response and its load was initially documented more than a century ago [15, 16]. In this early investigation, the following relation between the applied axial load P and the frequency of a certain vibration mode k (F_k) was proposed for a beam:

$$f_k^2 + p = 1 \tag{2.1}$$

where p is the ratio between the applied axial load P and the critical buckling load P_{cr}, and f_k is the ratio between the loaded vibration mode frequency F_k and its unloaded counterpart $F_{0,k}$. This relation was analytically proven for a perfect beam with simply supported boundary conditions, provided that the buckling mode is identical to the vibration mode taken into consideration. Furthermore, other boundary conditions showed little variation from this linear relationship, making this VCT approach more feasible for practical testing conditions [17]. Using this relation, the buckling load can be found by extrapolating the load ratio p at which f_k^2 equals zero, as shown in Figure 2.1a, and then multiplying this extrapolated load ratio by P_{cr}. In the above relation, P_{cr} is the only quantity that must be determined before the measurement, an aspect that is valid for all VCT approaches. After these initial investigations at the beginning of the 20^{th} century, the level of interest in further investigating and exploiting the relation between a structure's vibration response and its loading slowly picked up, focusing mainly on beam structures, for which buckling load predictions and boundary conditions were estimated [17–22].

Further investigations in the 30s on columns [23] and in the 40s on circular plates [24, 25] concluded that this linear relationship does not hold true in the presence of

imperfections, shape in particular, the frequency response showing a sharp bend as the load approached the buckling load, as shown in Figure 2.1b. Other compression members like trusses and frames were shown in a study around the middle of the 20^{th} century to display a similar behaviour [26, 27]. Nevertheless, the linear relationship for perfect, simply supported columns and polygonal plates was analytically validated in [24–26].

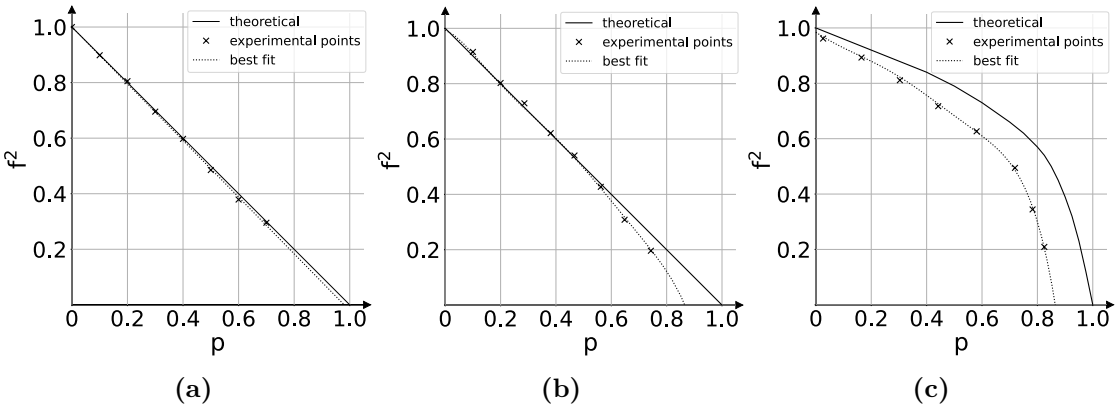

Figure 2.1 – a): load-frequency relation for beams under axial compression
b): load-frequency relation for cylindrical shells under axial compression
c): load-frequency relation for spherical shells under external pressure

An experimental study on buckling of cylindrical shells around the same period, but not directly related to VCT, showed that a linear relationship between the squared frequency and the load did exist, but that the frequency was far from zero at the buckling load [28]. Similarly, roughly a decade later another experimental study, again not related directly to VCT, concluded that the frequency of the monitored vibration mode tended to zero as the load approached the buckling load [29]. In a precursor to VCT for buckling load estimations for cylindrical shells under axial compression and external pressure [30] from the 60s, the linear relationship shown in 2.1 was analytically validated for both axial compression and external pressure loading. While for axial compression this relation was also experimentally validated, under external pressure the author reported deviations from linearity. Nevertheless, the author had the following recommendations on exploiting this relation [30]:

"If the concept of an equivalent freely-supported cylinder is valid for buckling results as well as for vibration frequencies, the linear approximation between the square of

the vibration frequency and axial load and external pressure may also be valid. If this is the case, vibration tests could be conducted in connection with static buckling tests to achieve non-destructive testing. By recording vibration frequencies at various increments of load it may be possible to extrapolate to the buckling values without damaging costly test specimens or actual hardware. Since the natural vibration frequencies for cylinders are sensitive to both boundary conditions and imperfections, it may be possible to obtain better correlation between buckling tests by using experimental vibration frequencies as an index of imperfection or support restraint."

which accurately describes both the direct and indirect uses of VCT as they are understood today.

One of the first actual applications of VCT to a shell structure came around the same time in the 60s, where the method was successfully used to predict the pressure at which the tested spherical shells would buckle under external pressure [31]. A schematic of the load-frequency behaviour found is shown in Figure 2.1c, where the quantity p on the horizontal axis refers to the ratio between the applied external pressure and the theoretical external pressure at which the shell would buckle. As it can be seen in this figure, the non-linearity observed earlier in [32] is present. Therefore, the VCT estimation was done in an empirical manner, namely by extrapolating the load at which the frequency would become zero via a curve fit.

For cylindrical shells under compression or external pressure, one of the earliest VCT applications for buckling load estimations was in the early 70s, where the linear relationship was used to predict the collapse load with an error within 1% [33], using vibration modes similar to the buckling ones. However, for the axial compression load case an artefact was employed to obtain a reliable buckling load prediction. This artefact implied using only the points after the bend in the load-frequency relation occurred to extrapolate the buckling load. Had the other points at lower load levels been used, where a quasi-linear behaviour was observed, the buckling load would have been severely overestimated. Furthermore, although a quasi-linear load-frequency relation was observed for the vibration modes dissimilar to the buckling mode, the VCT estimation using these modes would have resulted in a severe over-estimation

as well.

With the increasing number of experimental campaigns querying the feasibility of VCT to determine the buckling loads of plates and cylindrical shells, the aforementioned deviation from linearity in the load-frequency response was consistently found [34–40]. As this deviation from linearity implies a loss of analytical foundation of the initial VCT procedure when applied to imperfect structures, the motivation to find a different VCT procedure that would give robust buckling load predictions for imperfect structures increased.

Within this time period, a novel VCT procedure was proposed for columns and shells by Souza et al. [41], where the buckling load is found using the following relation:

$$(1-p)^2 + (1-\xi_k^2)(1-f_k^4) = 1 \tag{2.2}$$

by extrapolating the value of $(1\text{-}p)^2 = \xi_k^2$ at $(1\text{-}f_k^4) = 1$, where ξ_k represents the load drop due to imperfections. Therefore, the buckling load estimation is now found using the following equation:

$$P_{VCT,k} = P_{cr}\left(1 - \sqrt{\xi_k^2}\right) \tag{2.3}$$

where the value of ξ_k^2 must be positive for it to have a physical meaning. One important aspect to be mentioned here is that the procedure proposed by Souza shares two important characteristics with the initial procedure, namely the use of a linear extrapolation and its reliance on the vibration frequency to drop to 0 at buckling, as $(1\text{-}f_k^4) = 1$ implies that $F_k = 0$.

However, the above VCT method was found by Arbelo et al. in [10] to be unreliable for unstiffened composite cylindrical shells, as often the value of ξ_k^2 was negative. In this publication the authors also proposed a new approach, analytically verified in Franzoni et al. [42] at a later stage, based on the following quadratic relation between $(1\text{-}p)^2$ and $(1\text{-}f_k^2)$:

$$(1-p)^2 = [1-(1-f_k^2)]^2 \tag{2.4}$$

where ξ_k^2 now represents the minimum value of the quadratic equation best fitted to the points of the $(1\text{-}p)^2$ vs $(1\text{-}f_k^2)$ VCT characteristic chart, as shown in Figure 2.2,

while the buckling load estimation is found using Equation 2.3. One of the key differences of this procedure with respect to the previous ones is that it no longer relies on the loaded vibration frequency F_k to drop to 0, aspect consistent with previous observations for imperfect structures [26]. This recent development boosted the interest in VCT, with multiple experimental campaigns validating the aforementioned approach being published afterwards [1, 3, 4, 10, 42–51]. Furthermore, the approach proved to be robust regardless of the construction material of the structures tested, as for steel, aluminium, as well as for carbon and glass fibre reinforced plastics made cylinders, VCT was able to provide reliable buckling load estimations. Moreover, the procedure also proved applicable for stiffened cylinders [4, 48, 49], as well as for open-hole ones, provided that the structure underwent a global, rather than a local buckling [46].

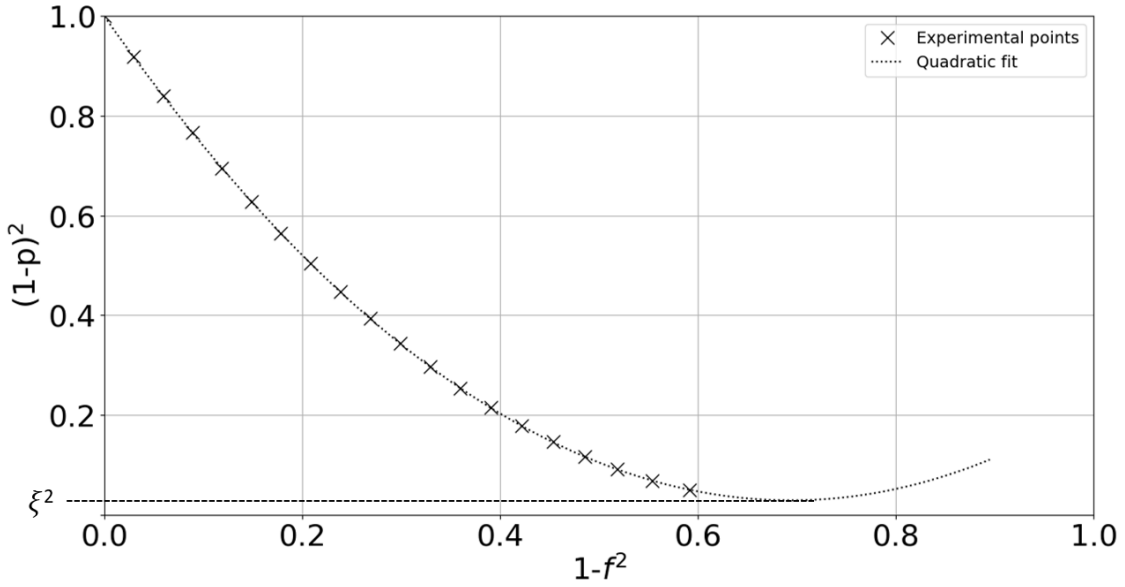

Figure 2.2 – Load-frequency relation according to Arbelo's procedure

The recent developments in reusable space structures also represent an important driver for further research on VCT, which can serve as a reliable tool to assess their potential loss of load-carrying capabilities upon reuse. This increased interest led to an empirical relation between the load applied and the structure's frequency response being proposed in [50], where $(1\text{-}p)^2$ is plotted against $(1\text{-}f)$, the rest of the procedure being identical to the one previously described. Throughout the thesis, this procedure is referred to as the **empirical** VCT procedure, while the one proposed by Arbelo

et al. in [10] and analytically verified by Franzoni et al. in [42] is referred to as the **analytical** VCT procedure.

Besides validating VCT for multiple cylindrical structures, research on this topic also addressed its numerical implementation, aiming to increase its efficiency. In doing so, focus was given to the frequency eigenvalue analysis, to avoid the repetition of this procedure for each VCT load step. In [52], the authors proposed a concurrent frequency eigenvalue analysis approach at multiple ratios of P/P_{cr} and used VCT to estimate the axial buckling loads P_{nl} obtained via Riks and/or dynamic explicit non-linear analysis procedures for a cylindrical shell subjected to combined loading. In these combined load cases, internal pressure, or torque, was introduced next to the main axial load. The outcome of this investigation was that their VCT implementation was able to accurately predict the numerical axial buckling load, at computational time lower by one order of magnitude compared to the Riks and dynamic explicit analysis procedures. Similarly, in [53] and [54] the authors used reduced order models to perform the frequency eigenvalue analyses required to perform VCT and compared the obtained buckling load estimations against those obtained by experiment and explicit dynamic analyses. Again, the agreement between the buckling load estimations provided by VCT and those obtained by experiment and explicit dynamic analyses was very good, both for the proper orthogonal decomposition [53] and for the combined approximation method [54] reduced order models, the computational time being also one order of magnitude lower when compared to the explicit dynamic analyses.

While VCT for buckling load estimations is a fairly old concept, little focus was given to its applicability range and the influence of its parameters over the obtained prediction. One of the earliest investigations over its parameters, namely the vibration frequencies measured at various degrees of loading, was published in [55], where for flat plates the authors concluded upon inspecting the equations used that any frequency measurement error would double its effect on the VCT buckling load estimation. This trend was also found for beams in [56], the authors reporting that frequency measurement errors between 2% and 6% led to VCT buckling prediction errors between 5% and 20%, depending on the beam's boundary conditions. In a more recent study on

a closely stiffened cylindrical shell under axial compression with and without internal pressure, a comparison has been made between the frequency measurements of two different laser vibrometers [4]. In this investigation, when the cylinder was subjected to axial compression for 2 out of the 6 load steps measured the frequencies retrieved were not identical. These deviations were 0.25Hz and 1.5Hz respectively, the ratios between these frequency measurements by the two equipment being 0.3% and 2.1% respectively. While the relative errors of the VCT buckling load estimations on the experimental buckling load using the frequency measurements of the two equipment were both within 10%, when performing progressive VCT estimations for the two sets of measurements, some differences were found between the obtained predictions. At the load level at which the initial deviation of 0.25Hz was seen, the difference in relative error with respect to the buckling load was around 3%, which then dropped to 1% when including the next measurement, and then increased to 11% at the final load step corresponding to the one at which the 1.5Hz deviation was recorded. A deviation between the frequency measurements was also seen for the combined loading case in which internal pressure was introduced next to compression, where for 1 out of 6 load steps a 0.25Hz difference was seen, the ratio between frequencies measured by the two equipment being 0.2%. This led to relative error differences from 5% to 8% between the two different frequency measurements, despite the lower number of deviations when compared to the axial compression load case. While the number of load steps used was relatively low for both the aforementioned load cases, and given that for the combined load case the frequencies were measured predominantly at relatively high load ratios, the differences between the VCT predictions obtained using the measurements taken by different equipment represent a clear sign that the VCT buckling load estimations are also relatively sensitive to frequency measurement errors.

Regarding the number of vibration measurements/load steps and the maximum load level at which these should be taken, the existing recommendations are not only scarce, but also not entirely in agreement. Concerning the number of vibration measurements sufficient for a reliable VCT buckling load estimation, in [57] the authors

reported that 6 load steps were sufficient, while in [47] the authors reported that at least 15 load steps were required to obtain a reliable VCT buckling load estimation. Similarly, in [1] load levels of at least 50% with respect to the buckling load were required to achieve robust predictions, while in [3] the authors reported that the desired accuracy was only achieved when using measurements at load ratios beyond 80% with respect to the experimental buckling load.

The significant number of experimental tests in which VCT provided robust buckling load estimations suggests that the method is relatively insensitive to minor boundary conditions and loading imperfections, which are inherent to each test and structure, as well as to different shape imperfections. Nevertheless, the only study in which this aspect was generally addressed was aimed at investigating the robustness of VCT for nominally identical cylinders and for two load introduction methods [50]. In this study, besides showing the robustness of the method, the authors also reported cases in which VCT was not able to provide reliable buckling load predictions, despite doing so for other, nominally identical cylinders, and for the same load introduction method. Even though the authors did not report the reason why VCT was not able to provide robust buckling load estimations in some cases, given their research methodology, this was likely due to particularities related to boundary conditions, loading and/or shape imperfections.

The vast majority of VCT usage for buckling load estimation was done for an axial compression load case, given that the analytical base of the VCT procedures proposed throughout the years was formulated focusing on this load case in particular. This represents a limiting factor in the use of VCT for buckling load estimations outside the academic environment, since often additional loads are applied to cylindrical shells next to compression during their design validation phase. To this date, there are few studies regarding the feasibility of using VCT to predict the axial buckling loads of cylindrical shells under combined loading. In [42], it was shown analytically that the VCT method also holds true when internal/external pressure is applied in addition to axial compression, providing also experimental evidence. In a more recent numerical investigation, the same relation was also shown to hold true in the presence of a

constant torque load [52].

Besides the aforementioned unknowns, all experimental validations of VCT were done in an academic environment, employing exclusively small-scale cylinders. Therefore, whether VCT is applicable to real-scale structures and, if so, the influence of possible size-effects over the accuracy of the method remains to be investigated.

3 Scope and Outline of the thesis

In this chapter, an overview of the research conducted throughout the thesis is presented. The motivation for the undergone research and the working hypotheses are shown in Section 3.1, while the outline of the thesis is presented in Section 3.2.

3.1 Scope

The literature survey shown in Chapter 2 highlights the rapid development of VCT for buckling load estimations of cylindrical shells. Nevertheless, there are still key aspects regarding its practical implementation, sensitivities, and limitations that are not yet well understood and are thus hampering its adoption beyond the academic environment. To begin with, there is no consensus regarding the number of measurements needed in order to obtain a robust buckling load estimation via VCT, nor regarding the maximum load level with respect to the expected buckling load at which the last measurement should be taken regarding the actual experimental procedure. While the academic environment might provide enough freedom to adjust both the number of load steps and the maximum load level at which the last measurement is taken, outside the academic level the same approach is likely not acceptable, owing to the more stringent restrictions concerning time, costs, and the acceptable risk of damaging the structure tested.

Secondly, although not very common, there were also cases in which VCT failed to provide reliable buckling load estimations. This behaviour was seen even within a set

of nominally identical cylinders and testing environments, where VCT provided reliable buckling load estimations for the majority of articles tested. While the relatively large number of experimental campaigns in which this non-destructive method was validated suggests that VCT is not particularly sensitive to the various imperfections inherent to each cylindrical structure and testing environment, the aforementioned unreliable predictions suggest that there are certain imperfection types that, be it individually, or lumped together, can compromise the robustness of the method.

Thirdly, while buckling under axial compression represents one of the main sizing criteria for cylindrical shells, in service significant additional loads are often also present (be it by design, or unintended). Therefore, during the development phase of such structures, their experimental campaigns often contain load cases in which these additional loads are applied next to compression. Initially, the VCT formulations were developed exclusively for the axial compression load case. Later, these VCT procedures were shown analytically and experimentally to be valid when internal or external pressure is applied, as well as numerically valid under a constant torque load applied next to compression. However, applying VCT to other combined load cases falls outside its traditional applicability. Nevertheless, given that these additional loads applied next to compression are generally of a lower magnitude, their influence on a cylinder's vibration response may not be large enough to the extent that VCT becomes unreliable. This may be the case especially if the additional loads are introduced before compression and the frequency response is measured at different magnitudes of compression loading while keeping the additional load constant, as the change in the frequency response would primarily come as a consequence of different magnitudes of compression load applied to the structure.

Lastly, the robustness of the method has thus far only been validated experimentally on small-scale cylinders. Therefore, the sensitivity of the method to potential size-effects and the feasibility of VCT to predict the buckling loads for real-scale structures remain unknown.

3.1.1 Research hypothesis

Aimed at exploring the range of applicability of VCT within industrial applications, the research conducted in this thesis is founded on the following research hypothesis:

"It is possible that the use of advanced stochastic analysis, together with industrial-scale experimental validation, will improve the accuracy of predicting buckling in cylindrical shells subjected to combined loading and structural imperfections using vibration-correlation techniques."

Furthermore, the following work hypotheses are defined to investigate the research hypotheses:

- It is possible to establish practical guidelines regarding the number of vibration measurements and the maximum load level taken into account for the experimental implementation of VCT, including the influence of potential frequency measurement errors.
- It is possible to verify numerically the relatively low sensitivity of VCT regarding shape and loading imperfections.
- It is possible to verify numerically that the applicability range of VCT can be extended to combined load cases.
- It is possible to validate experimentally that VCT is applicable to cylinders representative to real-scale launcher structures under bending-compression combined load cases.
- It is possible to define practical guidelines relevant to industrial applications of VCT for determining the axial load at which cylindrical shells buckle.

3.2 Outline

The thesis is structured in 8 chapters, with the following layout:

- Chapter 1 - Introduction: provides the motivation for the research conducted
- Chapter 2 - Literature review: covers the state-of-the-art of non-destructive methods to predict buckling loads of cylindrical shells, focusing on VCT and the aspects investigated in this research thesis
- Chapter 3 - Scope and outline: portrays the scope, research, working hypotheses, and provides an outline of the thesis
- Chapter 4 - VCT sensitivity towards the number of measurements and load level: introduces the methodology to partially decouple the number of measurements from the load level in the VCT estimations and to introduce frequency deviations in the measurement data. Then, the methodology is applied to the numerical results belonging to a family of nominally identical cylinders, and the significance of the number of measurements, maximum load level measured, and of the frequency deviations over the VCT predictions is evaluated. Afterwards, a similar investigation is performed using multiple sets of experimental results gathered from the available literature.
- Chapter 5 - VCT sensitivity towards shape and loading imperfections: provides the motivation for the chosen structure based on which the numerical investigation is performed, and introduces the procedures to introduce shape and loading imperfections in the finite element analysis. Describes the procedure to request the vibration response in the event that local buckling occurs at a significantly lower load level than the one at which global buckling occurs. Then, the influence of loading and shape imperfections over the buckling behaviour and robustness of the VCT predictions is assessed. Afterwards, for the cases where local buckling occurs, the possibility of using the vibration response exclusively beyond this local event to predict the global buckling load is motivated using

numerical and experimental results. Last, the results of a parametric study focusing on determining the optimum combination of VCT procedure and type of critical buckling load for reliable VCT buckling load predictions are shown. In this study, the analytical and empirical VCT procedures, together with the critical buckling loads obtained for the perfect and imperfect structure, were used to determine whether a certain combination of these yields better global buckling load estimation than the established procedure.

- Chapter 6 - VCT sensitivity towards combined loading: describes the numerical models of the cylinders used, together with the boundary conditions and load introduction procedures. In addition, the cylinder configurations and load cases under which the various critical axial buckling loads were determined are introduced. It presents the influence of the additional loads applied alongside axial compression over the axial buckling load, after which the robustness of the VCT predictions as a function of the type of additional load applied, its magnitude, the load introduction procedure and type of critical axial buckling load used in the VCT procedure is shown.

- Chapter 7 - Experimental validation of VCT for compression-bending load cases: provides experimental proof to the topics addressed in the previous chapters, especially for the one shown in Chapter 6, using the VCT results of a cylinder representative to a real-scale launcher structure subjected to combined loading. Details the structure and load cases tested, together with the experimental set-up and boundary conditions. Details the preliminary numerical investigation performed to assess the feasibility of VCT for the load cases tested, and to provide support in preparing the experimental test. Finally, the experimental results are shown and discussed.

- Chapter 8 - Guidelines: summarises the aspects observed throughout the conducted research that can be useful in the application of the VCT procedure in a set of guidelines/recommendations.

- Chapter 9 - Final remarks: outlines the main findings and conclusions of the

thesis, exposes some of the limitations of the conducted study and provides topics needing further research for a better understanding of the VCT method's capabilities and limitations.

4 VCT sensitivity towards the number of measurements and load level

The lack of consensus regarding the number of measurements and the load levels at which these should be taken with respect to the expected buckling load can raise confusion regarding the experimental procedure to determine the in-situ buckling load of cylindrical shells under axial compression via VCT. This section addresses this issue using both numerical and experimental data, taking into account possible frequency measurement errors as well.

Section 4.1 introduces the methodology used to study the influence of the vibration measurements number and their corresponding load level with respect to the VCT buckling load predictions. Then, in Section 4.2 this methodology is used to initially assess these dependencies using numerical data obtained from the FE models of a set of nominally identical cylinders. Next, in Section 4.3 the outcome from the investigation based on numerical data from Section 4.2 is verified using experimental data. Finally, a discussion and the conclusions drawn from this study are shown in sections 4.4 and 4.5, respectively.

4.1 Methodology

The general approach to determine the buckling load of a structure using VCT is to perform successive predictions with each new measurement taken, once at least three measurements are available, owing to the minimum number of points needed to determine the best-fitted quadratic curve. However, given that there is a strong coupling between the number of measurements taken and their corresponding load level, increasing the number of measurements implies raising the load level as well. Thus, an independent assessment of the influence of these two parameters over the VCT buckling load prediction is not possible in this manner. Therefore, an artefact is needed to at least decrease this strong coupling between the number of measurements and the maximum load level used. In this study, this was done by taking combinations of r measurements from a total of n employing the combination formula:

$$C(n,r) = \frac{n!}{(n,r)!r!}, r = 3,4,5....n \tag{4.1}$$

to perform multiple VCT predictions using the analytical VCT formulation, therefore allowing the VCT predictions to be grouped by the same number of measurements or maximum load level for further assessment. This approach does not fully decouple the number of measurements from the maximum load level, with limitations particularly noticeable at extreme values of r. These limitations come due to the nature of the combination formula, since the maximum load level for any r value would be at least that of the r^{th} measurement. For example, at the lowest spectrum (r=3), while the maximum load level can be any starting from the one of the r^{th} measurement on, the number of measurements cannot be varied when the maximum load level considered is the one of the r^{th} measurement. Conversely, for r values towards the higher extreme, for example r=n-1, the maximum load level would be either the one of the last frequency measurement, or the one before it. Nevertheless, this residual coupling is small enough to provide insight into the sensitivity of the VCT buckling load prediction with respect to the number of measurements taken and the maximum load level used in making these predictions.

For the study based on numerical results, the FE models of a set of nominally identical cylinders were used, their frequency response being determined for a number of 20 load levels, in steps of 5% load ratios with respect to their buckling loads determined via non-linear analyses. Then, the combination formula was used to generate load step combinations and perform VCT buckling load estimations, so that these predictions could be represented as individual distributions for each number of measurements and maximum load level considered and compared to a baseline prediction. This baseline represents the estimation obtained using all available measurements, hence, also the maximum load level available, and was used to normalise the obtained VCT predictions for an easier interpretation of the results. Furthermore, given the existence of some unfeasible load step combinations with respect to the maximum and minimum load levels, several load criteria were also applied to keep only reasonable combinations for practical applications, such that, for example, VCT estimations based on measurements at [0%, 5%, 10%], or [85%, 90%, 95%] load ratios with respect to the buckling load would be avoided. In doing so, it was also verified by comparing the distributions with and without load criteria applied that there were no major differences between the two, thus the general behaviour of the VCT predictions when varying the number of measurements, and the maximum load level was retained when applying these criteria.

Besides the visual interpretation based on the VCT predictions distributions for different numbers of measurements and maximum load levels, a correlation analysis was also performed for an easier assessment of the influence of these two parameters over the VCT predictions. In this regard, Kendall's correlation coefficient τ was chosen as best suited, given its low sensitivity to outliers and applicability when working with ordinal data, aspects not entirely satisfied by other commonly used correlation coefficients like Pearson's r, or Spearman's r_s [58–60]. Kendall's correlation coefficient τ describes the strength of the monotonic relation between two parameters and ranges between -1, for a monotonic decrease, and 1, for a monotonic increase, while a value of 0 shows the lack of a monotonic relation between the two parameters analysed. Regarding the assessment of the correlation strength given by the value

of this coefficient, there is no general consensus on the intervals between which this coefficient describes a strong, moderate, or a weak correlation. For this investigation, the following τ size effect magnitudes are considered [61]:

- $|\tau|$ = 0.07-0.21, weak correlation
- $|\tau|$ = 0.21-0.35, moderate correlation
- $|\tau| > 0.35$, strong correlation

The influence of frequency measurement errors was investigated by randomly altering the frequencies by magnitudes within ±0.1Hz, ±0.25Hz, and ±0.5Hz intervals, these magnitudes being chosen considering the accuracy of modern frequency measurement equipment and the reported measurement differences mentioned in chapter 2. Then, in order to increase the statistical relevance and decrease the influence of possible outliers given by particular combinations of measurements, 50 sets with altered frequencies within the aforementioned limits were generated from the nominal data sets.

Regarding the investigation based on experimental data, a very similar procedure to the one previously described was used for multiple VCT experimental data sets gathered from the available literature. Given the scarcity of available experimental data, as well as due to the differences in the number of measurements taken and the maximum load level measured in each experimental test, using the exact same procedure as in the study based on numerical data was no longer feasible. In this case, applying load criteria would have either rendered the data from some cylinders unusable, or heavily decreased its overall relevance within the study, given the low number of combinations satisfying the load criteria used. Additionally, the different rates at which the normalised VCT predictions converge towards the baseline prediction as a function of the number of measurements or the maximum load level considered between different cylinders would have likely resulted in an apparent lack of correlation when performing the correlation analysis over a combined data set. Therefore, in the study based on experimental results, the correlation was performed for each data set individually, after which the obtained correlation coefficients were averaged.

4.2 Investigation based on numerical data

The study based on numerical data is aimed at assessing the influence of the number of measurements and the maximum load level taken into account over the robustness of the VCT predictions in an ideal scenario, exempt from any unintended measurement errors that may arise during an experimental test, providing at the same time a baseline for the investigation based on experimental data.

4.2.1 FE models

The nominal geometry of the FE models used in this study is the one belonging to a family of nominally identical monocoque cylinders tested at the DLR Institute of Lightweight Systems featured in [2]. At this test facility, the load was introduced by a hydraulic actuator acting on the lower loading plate, while the load was measured by 3 load cells evenly distributed along the cylinder's circumference and connected to the upper load introduction surface. Furthermore, any potential uneven load distribution across the cylinder's circumference due to uneven lengths was minimised by placing a robust cylindrical structure between the top edge of the cylinders and the 3 loading cells. Additionally, the top and bottom outer surfaces of the cylinders were cast in epoxy resin rings over a length of 20mm to further promote a uniform load introduction, as well as to provide lateral support.

These nominally identical cylinders were made out of carbon fibre reinforced plastic (CFRP), with a nominal wall thickness of 0.5mm, free length of 500mm, 20mm overhang, a 250mm radius, and with a [$\pm 24°$, $\pm 41°$] layup. The material properties of the uni-directional (UD) Hexcel IM7/8552 ply used to manufacture the cylinders are shown in Table 4.1, while the epoxy resin had an elastic modulus of 2.45GPa, a Poisson ratio of 0.3, and a density of 2.09g/cm^3.

The imperfection patterns used are the ones of the Z15, Z17, Z18, and Z20-26 cylinders, the shape imperfections being measured on their outer surface using the ATOS photographic profilometer system, while their thickness imperfections were measured

by an ultrasonic tester. The shape imperfections were introduced in the FE model using an inverse interpolation method that takes into account the distance between the FE nodes and the measurement points acquired by the photographic profilometer system to adjust the radial coordinate of the former, approach commonly used to include measured shape imperfections for cylindrical shells [1, 7, 10, 62–66].

E_1 [GPa]	E_2 [GPa]	G_{12} [GPa]	ν_{12}	ρ $[g/cm^3]$
142.5	8.7	5.1	0.28	1.58

Table 4.1 – Hexcel IM7/8552 ply material properties

On the other hand, the thickness imperfections were implemented in the model according to the procedure described in [67]. In this approach, the differences between the nominal thickness and the measured values are assumed to be due to different fibre volume ratios in the laminate, given by either a lack, or an excess in resin with respect to the nominal value. Based on this assumption, the material properties are recalculated for the different thicknesses using the composition rule. Then, these recalculated material properties are assigned to the FE elements in a discretised manner to keep the complexity of the FE model reasonable, since otherwise it would have implied defining a very high number of different material properties and element sets.

The models were built using the Abaqus FE analysis package, in which linear buckling analyses using a Lanczos procedure were used to determine the values of P_{cr} and non-linear analyses using a Newton-Raphson procedure were used to determine the values of P_{nl}. The cylindrical shells were meshed with 2D quadratic quadrilateral shell elements with 8 nodes and reduced integration (S8R), while the resin rings were meshed with 3D brick elements with 20 nodes and reduced integration (C3D20R). Figure 4.1 provides a visual interpretation of the FE models, where in Figure 4.1a the mesh of the cylinder with highlighted regions over which boundary conditions were applied is shown, while a schematic of the boundary conditions used to restrain the model is shown in Figure 4.1b.

The mesh convergence analysis showed that 120 elements along the circumference of the cylinders were sufficient to accurately capture their compressive response, with

the number of elements along the axial direction chosen to ensure an element aspect ratio close to 1. The mesh of the resin rings and the cylinders was defined such that, in a reference cylindrical coordinate system RθZ, the Z and θ coordinates were identical, while the radial coordinates of the resin rings were adjusted as a function of the cylinder's thickness. Then, constraint equations were used to connect the translations of the nodes at the top and bottom edges of the cylinder with their resin rings counterparts, except for the ones at the very edge, where boundary conditions for load introduction were specified.

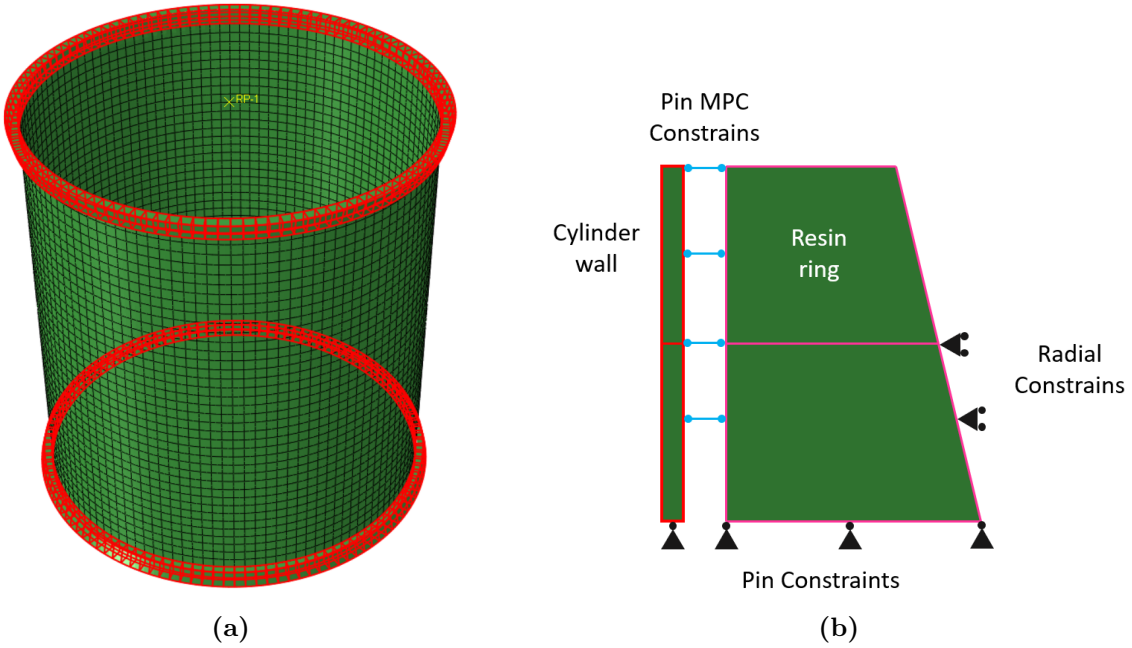

Figure 4.1 – Z cylinders FE mesh with highlighted resin rings (a) and the boundary conditions applied at the top and bottom edges (b)

Additionally, at the outer edges of the resin rings, roller constraints were specified to restrict their radial movement. In order to introduce the load in the FE models, the nodes at the bottom of the cylinder had constrained translations, while at the top, these were connected to a Reference Point (RP) for which the radial displacement was restrained and an axial displacement was applied. The aforementioned RP served only as a modelling artefact, allowing for an easier post-processing of the axial load and displacement of the models. Lastly, the translational degrees of freedom at the top and bottom surfaces of the resin rings were locked via Pin constraints.

4.2.2 Results

Table 4.2 shows the buckling values obtained via linear analysis P_{cr}, non-linear analysis P_{nl}, experiment P_{exp}, as well as the relative error between the numerical results and experiments ε_{nl-exp}, and the relative error of the baseline numerical VCT predictions with respect to the numerical results ε_{VCT-nl}. The variation in the P_{cr} values among the different cylinders is due to the use of averaged measurements for radius and length in the FE models, as well as due to using material properties corresponding to the average measured thickness, instead of the nominal one. As it can be seen from this table, for several cylinders the experimental buckling load was not closely matched in the numerical analysis, owing to possible material inhomogeneities or residual loading imperfections. Similarly, the numerical predictions provided by VCT, although excellent for most cylinders, for Z17 and Z18 these were relatively poor, owing to their imperfection signatures. Nevertheless, these numerical models were used in this study since the aspect investigated is the influence of the number of measurements and maximum load level over the VCT prediction, not its actual accuracy.

	Z15	Z17	Z18	Z20	Z21	Z22	Z23	Z24	Z25	Z26
P_{cr} [kN]	30.41	30.25	31.59	32.52	32.18	32.25	31.59	33.02	30.79	31.59
P_{nl} [kN]	24.52	21.24	20.32	26.42	25.86	26.39	26.10	26.83	24.76	25.90
P_{exp} [kN]	23.36	24.63	21.32	23.08	22.63	23.99	25.02	23.62	25.69	22.43
ε_{nl-exp} [%]	4.97	-13.76	-4.69	14.47	14.27	10.0	4.32	13.59	-3.62	15.47
ε_{VCT-nl} [%]	1.26	9.88	16.68	1.44	1.43	0.71	0.80	2.59	3.07	1.38

Table 4.2 – Z cylinders buckling loads

As mentioned in section 4.1, for the investigation based on numerical data some load criteria were imposed over the combinations of load steps to filter out the VCT prediction using unrealistic combinations, these criteria being shown below:

1. Maximum load ratio within a 50%-85% interval
2. Bias towards higher load levels
3. Minimum load ratio within 15%

4. Maximum load ratio gap of 20%

The higher limit on the maximum load ratio was imposed given that, although typically high maximum load ratios are desired, in practical applications of VCT, holding the load constant at levels near the buckling load may be too high of a risk, particularly when the load introduction is force-based.

On the other hand, the lower limit at 50% was imposed as a bare minimum, given that even for cylindrical shells highly sensitive to imperfections, a diligent numerical analysis using current FE tools should not overestimate the experimental buckling load by such a high degree. The second criterion was introduced due to the non-linear decrease of the vibration mode frequency as the load increases. Since the frequency difference between consecutive measurements performed between equal load ratio differences increases as the load level increases, the measurements taken at higher load ratios are more relevant in accurately describing the quadratic curve to be fitted to the points of the VCT characteristic chart. To impose this criterion, the load combinations for which less than half of their entries were above the mean load ratio of that combination were left out, avoiding thus unrealistic load step combinations such as [0%, 5%, 10%, 30%, 50%].

The third load criterion was implemented to ensure that the VCT predictions account for the lower load levels as well, since it was observed that when failing to do so, the quadratic curve fit can miss the points at lower load levels by large amounts, representing thus an unrealistic behaviour. Lastly, a maximum load ratio gap was imposed to keep the load steps relatively evenly distributed between their minimum and maximum load levels, avoiding thus unrealistic load step combinations such as [0%, 75%, 80%, 85%].

Figure 4.2 shows the distributions, in violin plots, of the VCT predictions for the first vibration mode as a function of the number of load steps used, with and without load criteria applied in orange and blue, respectively. Here, for each number of load steps a distribution is plotted, the horizontal bars at their ends representing the extreme points, giving thus their amplitude. Furthermore, median lines are also plotted for

each violin plot to provide additional information on the distributions of the VCT predictions shown.

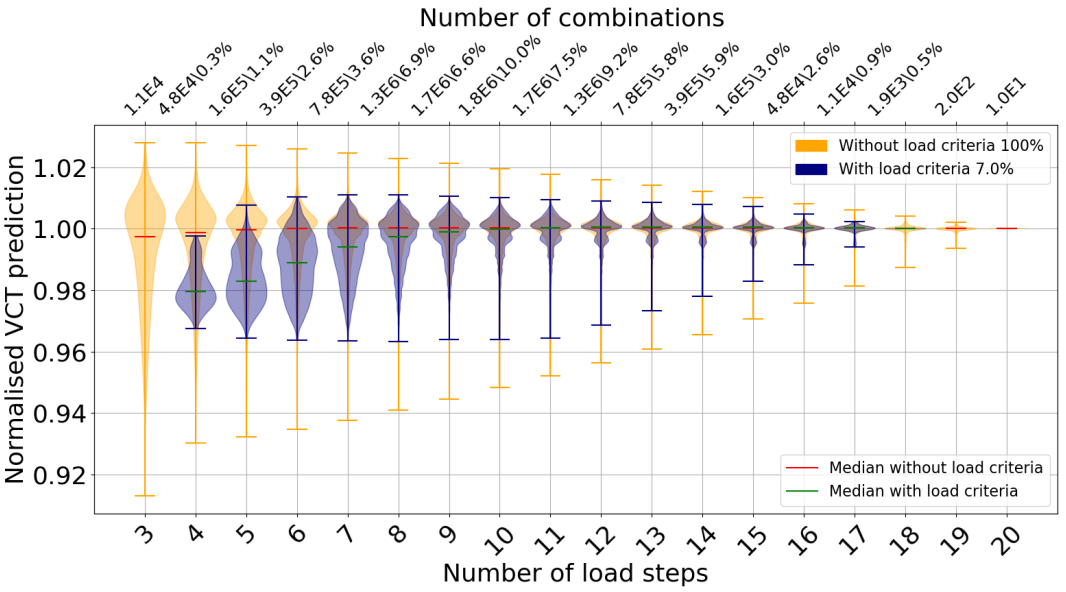

Figure 4.2 – VCT predictions as a function of the number of measurements

In this figure, besides the number of load steps on the bottom horizontal axis and the normalised VCT prediction on the vertical axis, an additional top horizontal axis was included, in which information regarding the number of VCT predictions within each distribution is provided. For the distributions with unfiltered load steps, the total number of predictions is given, while for the distributions with filtered load steps, the number of predictions is shown in percentages with respect to the number of predictions without load criteria applied. This secondary top horizontal axis was added to better understand the number of predictions in each distribution and the impact of applying load criteria on the number of predictions. Following this secondary axis, it can be seen that when applying load criteria, the centre of quasi-symmetry shifts forward by one load step, in the case without load criteria this being at 10 load steps, while in the case with load criteria applied, it moves to 11 load steps. On the other hand, the largest number of predictions in both cases remains in the distribution with 10 load steps. Overall, the percentage of predictions retained when applying load criteria is 7%, aspect also highlighted in the figure's legend.

Taking into consideration that the locations where the vast majority of the predic-

tions lie within the shown distributions are more relevant than the amplitudes, these intervals are defined here as the spans of the distributions, and their upper and lower limits are considered the points where the widths of the distributions become different from zero. As an example, for the distribution of the VCT predictions where 3 load steps were used, while the amplitude of this distribution is 0.12, given that all VCT predictions lie within a (0.91, 1.03) interval, the span is 0.09, as the width of the violin plot is different than 0 only between a (0.94, 1.03) interval.

Upon analysing the above figure it can be seen that, while there are changes in the amplitudes and spans of the distributions depending on the number of load steps used, these are quantitatively insignificant, given that all the obtained predictions are contained within a (0.91, 1.03) interval. This outcome is due to both the numerical nature of the results, as well as due to the low variation of the VCT predictions as a function of the number of load steps and maximum load level used. Such behaviour represents the ideal scenario for VCT, given that the points in the VCT characteristic chart describe accurately a quadratic behaviour and robust predictions are provided regardless of the number of load steps or the maximum load level used. Nevertheless, this behaviour is not often seen in practice, since any measurement errors might induce significant differences in the obtained VCT prediction.

Regarding the evolution of the VCT predictions as a function of the number of load steps, it can be seen that when increasing the number of load steps, not only do the amplitudes of the distributions decrease, but their span is also increasingly smaller, although this aspect is not as pronounced initially when load criteria are applied. This behaviour is likely due to the large variation of maximum load levels within the predictions from combinations with a low number of load steps, maximum load level which becomes progressively restricted when increasing the number of load steps. Another observation is that the median of the distributions stabilises after a certain number of load steps, around 5-6 load steps for the unfiltered predictions, while for the filtered predictions, this happens around 9-10 load steps. Furthermore, after the number of load steps used exceeds a certain level, significant changes are not seen in the spans of the distributions. This suggests the existence of a threshold regarding the

number of load steps, after which a significant change in the obtained VCT prediction is not seen when further increasing the number of load steps.

Figure 4.3 shows the distributions of the same predictions as the ones from Figure 4.2, in which now the predictions are rearranged as a function of their maximum load ratio.

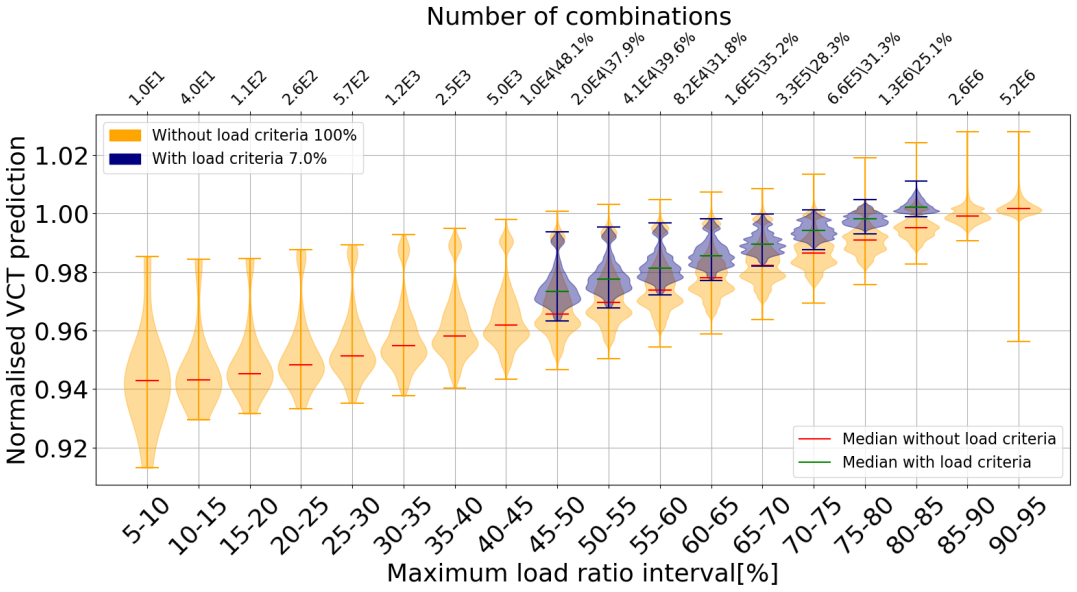

Figure 4.3 – VCT predictions as a function of the maximum load level

Although in numerical analyses it is relatively easy to determine the frequency response at a specific load ratio, here, the predictions are shown for intervals of load ratios. This choice has been made as it allows for a consistent comparison with the results obtained based on experimental data, since retrieving the frequency response at predefined load ratios during an experiment is not as straightforward as in a numerical analysis. While also present in Figure 4.2, here, a pronounced waviness can be seen in some of the distributions, a behaviour resulting from the inclusion of data sets belonging to different cylinders. The most important aspect to retain from this figure is that the VCT predictions seem proportional with the maximum load ratio used, regardless of the number of load steps. Furthermore, the amplitudes of the distributions, as well as their spans, tend to decrease as the load level increases, suggesting that larger load levels can also help reduce the variations induced by load

steps at lower load levels.

When considering both figures, it can be observed that for the unfiltered data, the extreme predictions are generally given by the combinations with the lowest number of load steps, the lowest maximum load level providing the lowest predictions, while the highest provides the highest predictions. Upon applying load criteria, the same aspect regarding the number of load steps is no longer valid, given that the predictions with extreme load ratios, be it at the lowest or at the highest spectrum, are filtered out.

The relative insensitivity of the VCT prediction with respect to the number of measurements and its sensitivity towards the maximum load ratio used were also seen in the correlation analysis. Figure 4.4 shows the outcome of the Kendall correlation analysis, the values in each cell representing the correlation coefficient between the parameters corresponding to its line and column. Here, it can be seen that for the unfiltered load steps, the correlation between the number of load steps and the VCT predictions is basically non-existent, given that the correlation coefficient is close to 0. Similarly, for the filtered load steps the correlation coefficient of τ=0.13 describes a weak correlation and can be considered as 'artificial', given that the load criteria applied do not allow many predictions with the highest load ratio available when few load steps are used. On the other hand, the correlation coefficients between the VCT predictions and the maximum load level used are strong in both cases, the influence of the applied load criteria being also noticed in the higher coefficient for the filtered predictions. This correlation increase was expected, given that the load criteria applied favour larger load ratios and have limitations on the maximum load ratios used. As previously mentioned in section 4.1, a residual coupling between the number of measurements and the maximum load level when generating VCT predictions using combinations of load steps remains, given that τ=0.22 when no load criteria were applied and that τ=0.33 when load criteria were applied, this increase being also expected given the nature of the aforementioned criteria. Nevertheless, the non-existent correlation between the number of load steps and the VCT predictions and the monotonic relation between the VCT predictions and the maximum load

level observed were not bound by this residual coupling. Therefore, this approach was further used in the study based on numerical data.

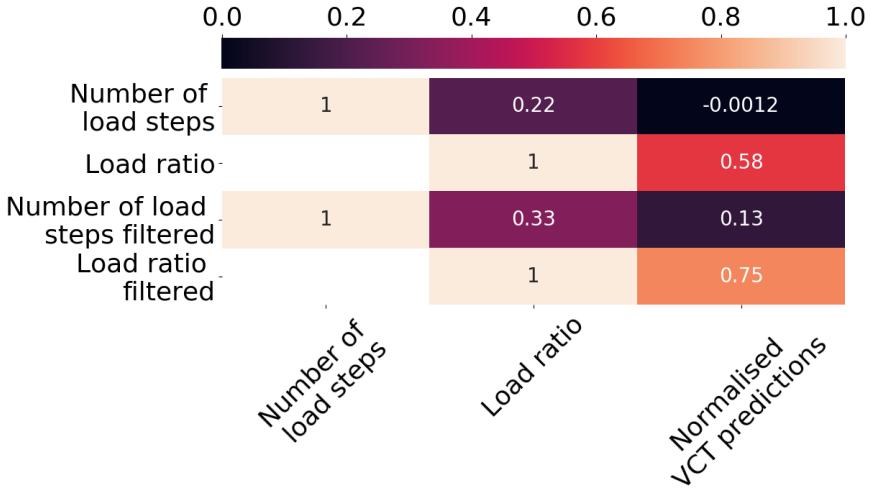

Figure 4.4 – Kendall correlation analysis

Influence of frequency measurement errors

The investigation based on pristine numerical data revealed that the number of measurements taken has a relatively small influence over the VCT prediction and that there seems to be a certain number of measurements beyond which a significant change in the VCT predictions obtained upon increasing this number is not observed. On the other hand, the maximum load level used seemed to have a significant influence over the VCT predictions, regardless of the number of load steps used. However, in practical applications, frequency measurement errors may arise, causing the points in the VCT characteristic chart to deviate from a quadratic behaviour and introducing uncertainties in the buckling load prediction. Therefore, the sensitivity of the VCT predictions with respect to these two parameters was also investigated in the presence of various magnitudes of frequency deviations. As described in Section 4.1, 50 data sets based on the reference numerical results were generated for each cylinder, in which each frequency was altered by a random amount within ± 0.1Hz, ± 0.25Hz, and ± 0.5Hz. Furthermore, given that the load criteria applied did not significantly alter the behaviour of the predictions with respect to the number of load steps used and their maximum load level, and that they were applied to filter out unrealistic load

step combinations, the influence of frequency measurement errors was investigated with these criteria applied.

Influence of ±0.1Hz frequency deviations

Figure 4.5 shows the distributions of the VCT predictions in the presence of random frequency deviations within ±0.1Hz, grouped by the number of load steps used.

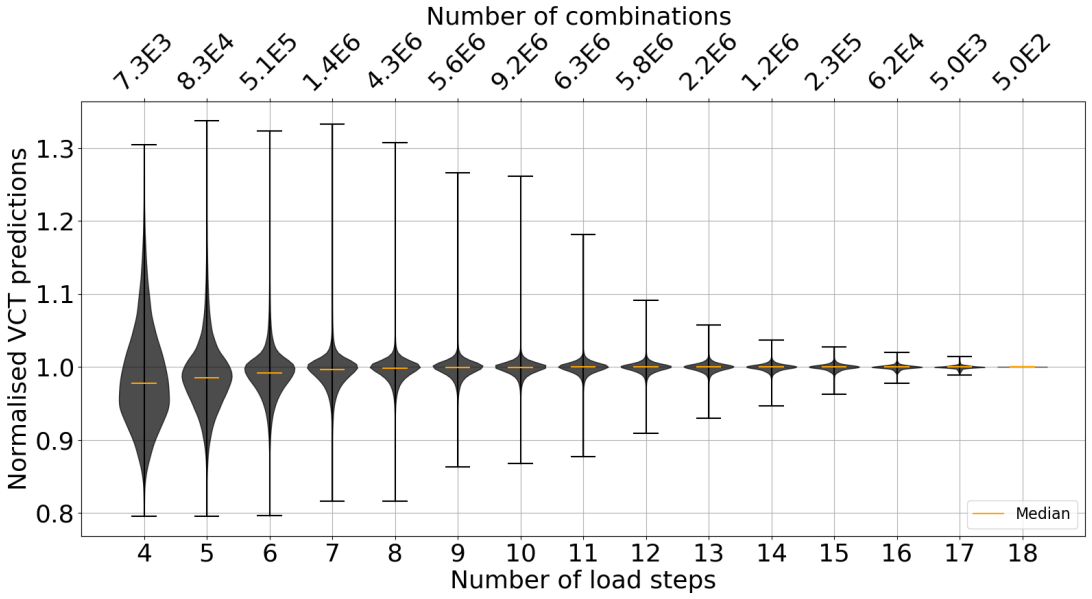

Figure 4.5 – VCT predictions as a function of the number of measurements with random frequency deviations within ±0.1Hz

When comparing this figure with Figure 4.2 for the reference data set, some clear differences can be seen. Firstly, it can be clearly seen that the frequency deviations introduced had a large impact over the amplitudes of the distributions, given that for the reference set all predictions were within a (0.91-1.03) interval, whereas here they are within a (0.8-1.35) interval. Next, the relatively constant drop in the amplitudes of the distributions is not seen starting from the lowest number of load steps. In this case, the amplitudes start to decrease slowly after a number of 7 load steps, and more pronounced for a number of load steps higher than 10.

On the other hand, when the extreme predictions are disregarded, it can also be seen that there is a rapid initial decrease in the span of the distributions until a

certain number of load steps is reached, beyond which large changes are not observed upon further increasing the number of load steps. For this magnitude of frequency deviations, the majority of the predictions using 6, or more, load steps seem to be within ±10% with respect to the baseline predictions. In what follows, this interval of ±10% is used as a threshold to describe robust predictions and to determine the number of load steps, or maximum load level, beyond which significant changes in the VCT predictions are not observed upon gradually increasing the values of these parameters.

Figure 4.6 shows the distributions of the VCT predictions in the presence of random frequency deviations within ±0.1Hz, grouped by the maximum load level used.

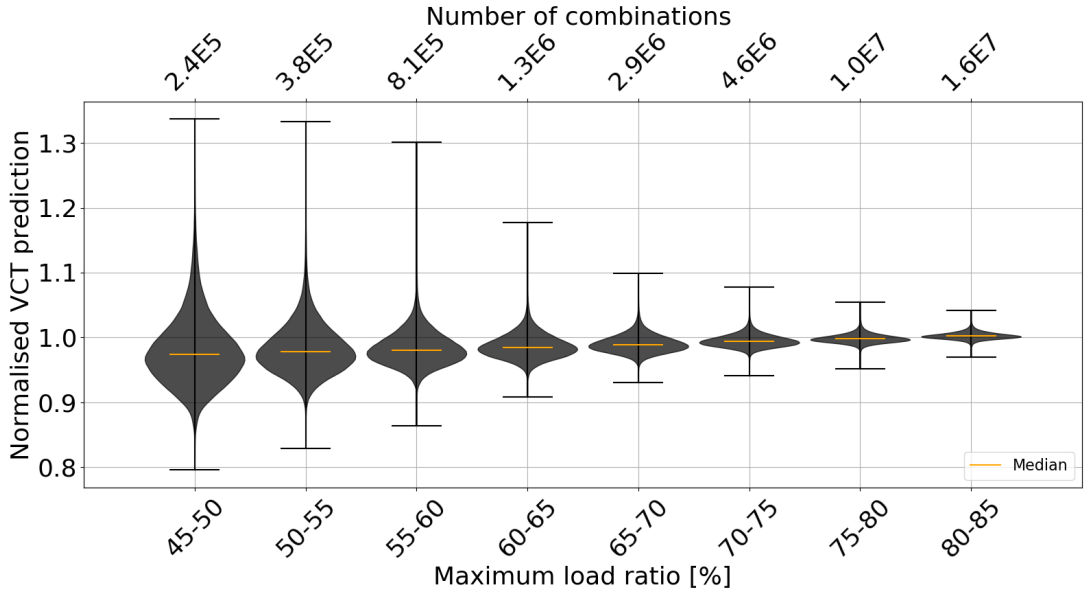

Figure 4.6 – VCT predictions as a function of the maximum load level with random frequency deviations within ±0.1Hz

The significant influence of the introduced deviations can also be seen when comparing this figure with its analogue figure 4.3, as in this case both the lowest and the highest predictions are obtained for the lowest maximum load level. Furthermore, although the same trend regarding the amplitudes of the distributions and their spans is still valid, the influence of the maximum load level in the presence of frequency deviations appears less pronounced. For this magnitude of frequency deviations, a maximum

load ratio as low as 55% would likely provide a prediction well within 10% with respect to the one when all the load steps are used.

The drop in strength of the monotonic relation between the maximum load level used and the VCT predictions was also captured in the correlation analysis, as shown in Figure 4.7. The correlation coefficient between these two parameters roughly halved and while a value of τ=0.38 still denotes a strong relation, given the considered coefficient effect sizes, it is now at the threshold between a strong and a moderate correlation. Conversely, the correlation between the number of load steps and the VCT predictions went from weak to non-existent in the presence of the aforementioned frequency deviations.

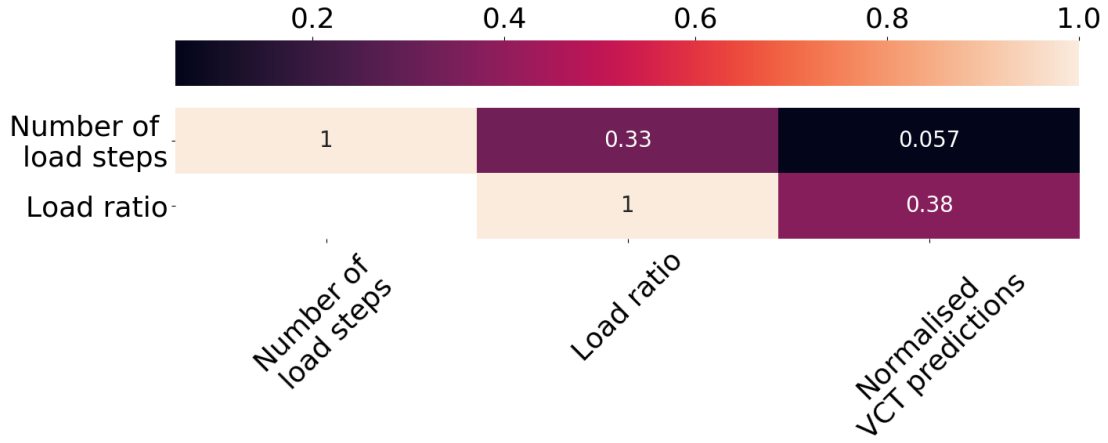

Figure 4.7 – Kendall correlation analysis with random frequency deviations within ±0.1Hz

Influence of ±0.25Hz frequency deviations

Figure 4.8 shows the distributions of the VCT predictions in the presence of random frequency deviations within ±0.25Hz, grouped by the number of load steps used. Here, most of the aspects observed when random frequency deviations within ±0.1Hz were introduced remain valid. The only important aspect to be mentioned is that increasing the magnitude of the frequency deviations further increased the amplitudes of the distributions and moved forward the threshold number of load steps after which the majority of the predictions are within 10% with respect to the baseline. This threshold is now at 7 load steps, one more than for the previous case.

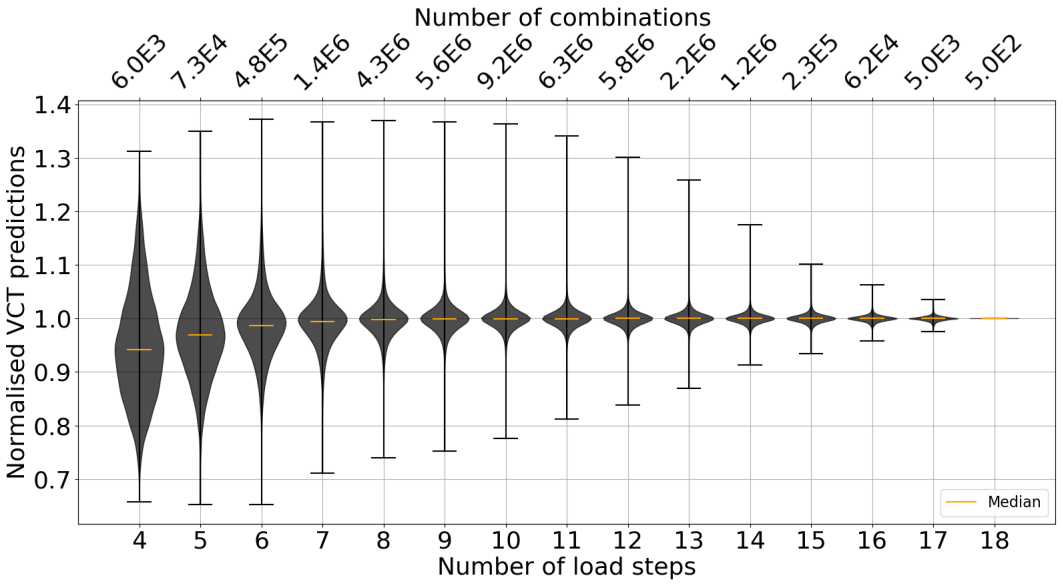

Figure 4.8 – VCT predictions as a function of the number of measurements with random frequency deviations within ±0.25Hz

Similarly, when looking at the prediction distributions grouped together by the maximum load level used from Figure 4.9, major differences upon increasing further the magnitude of the introduced frequency deviations are not seen either. As expected, the maximum load level needed to reach a prediction within 10% with respect to the baseline is slightly higher, now being at least 60%.

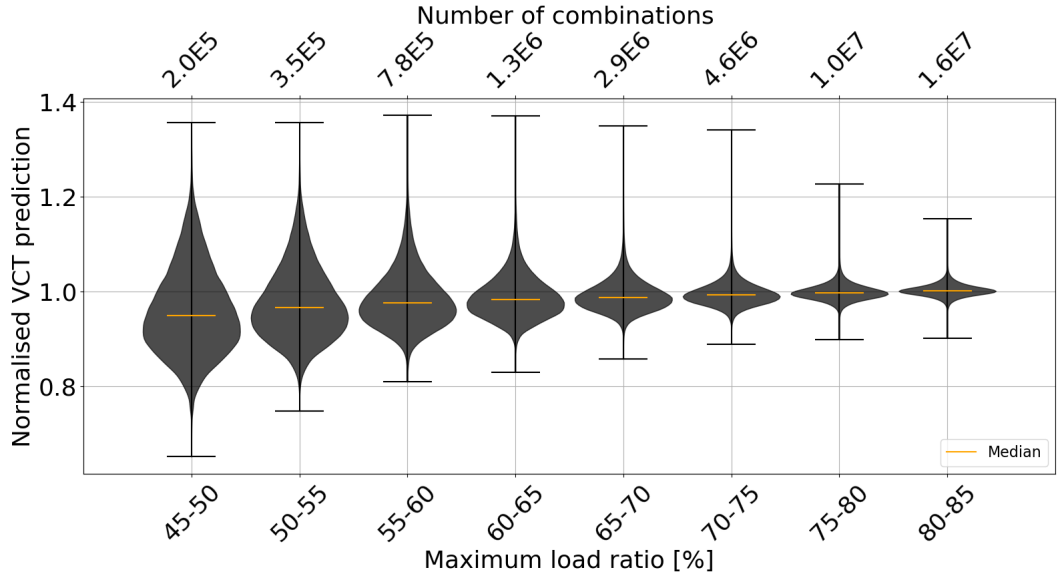

Figure 4.9 – VCT predictions as a function of the maximum load level with random frequency deviations within ±0.25Hz

While an increase in the magnitude of the frequency deviations introduced did not seem to greatly influence the strength of the monotonic relation between the maximum load level used and the VCT predictions, the correlation analysis revealed that this coefficient roughly halved again, as seen in Figure 4.10. The value of this coefficient now indicates a moderate strength of the monotonic relation between the two parameters. This significant decrease was likely influenced by the combinations having a low number of load steps with lower maximum load ratios, which provided predictions higher than those using higher maximum load ratios. On the other hand, increasing the magnitude of the introduced frequency deviations had no influence over the correlation between the number of load steps and the VCT predictions, this correlation remaining non-existent, as expected.

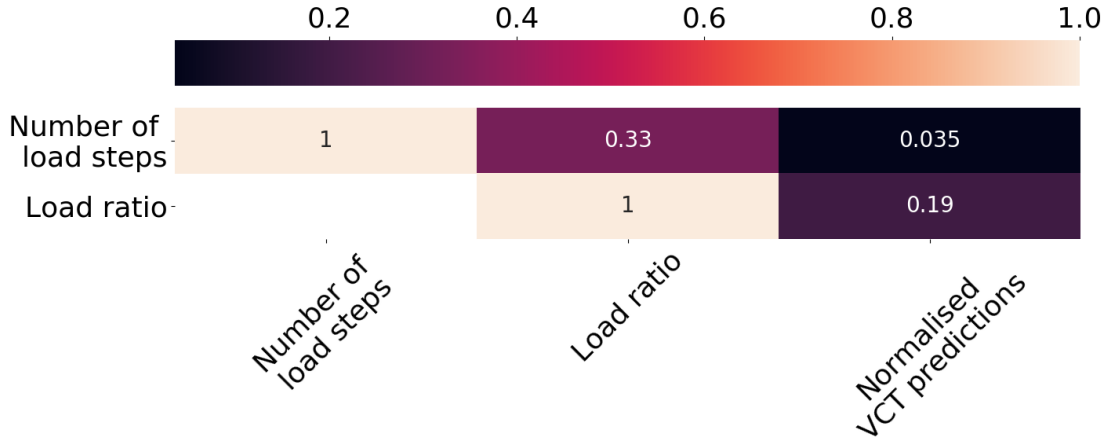

Figure 4.10 – Kendall correlation analysis with random frequency deviations within ±0.25Hz

Influence of ±0.5Hz frequency deviations

Increasing further the magnitude of the introduced frequency deviations revealed no changes with regard to the trends observed for the lower frequency deviations magnitudes. Figure 4.11 reveals that for this frequency deviation magnitude, using 9, or more, load steps would likely yield a prediction within 10% with respect to the baseline, while Figure 4.12 shows that the maximum load level used should be now at a load ratio of at least 75%.

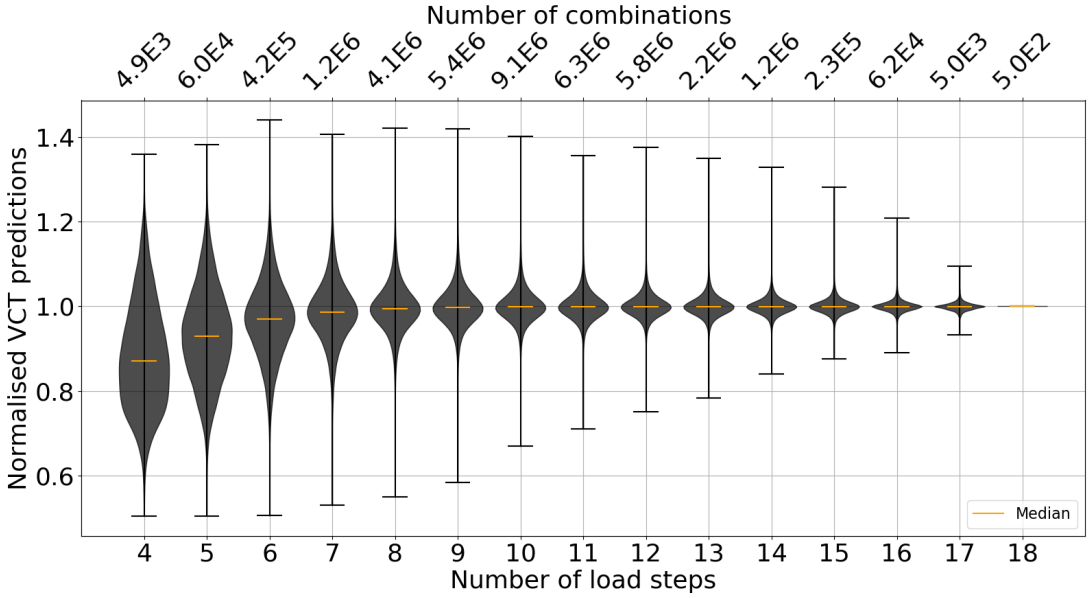

Figure 4.11 – VCT predictions as a function of the number of measurements with random frequency deviations within ±0.5Hz

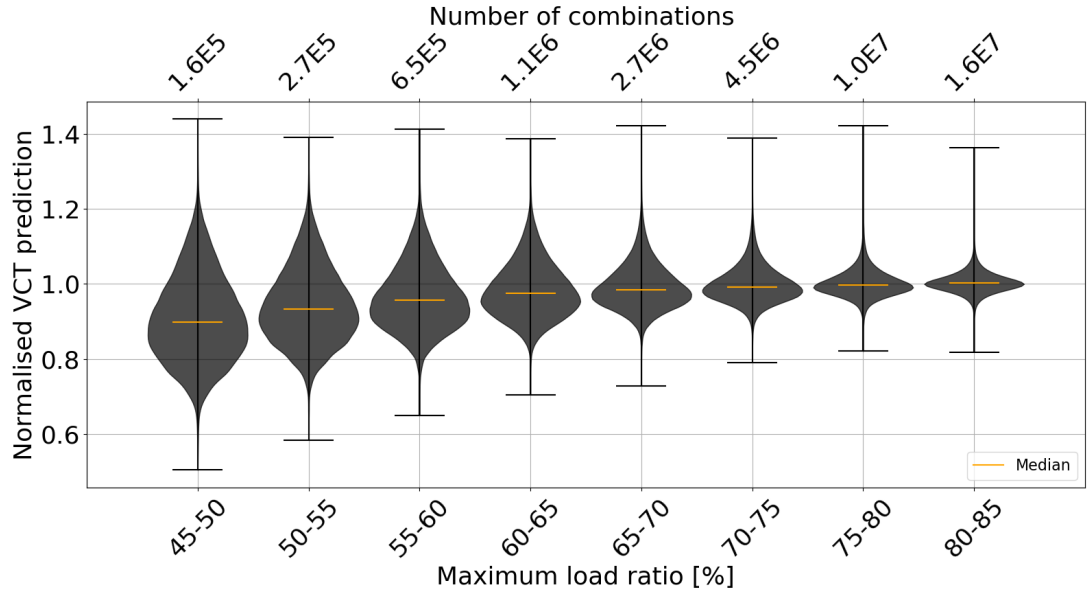

Figure 4.12 – VCT predictions as a function of the maximum load level with random frequency deviations within ±0.5Hz

As expected and shown in Figure 4.13, the correlation between the VCT predictions and the number of load steps remained non-existent, while the strength of the correlation with respect to the maximum load level used roughly halved again, describing

this time a weak correlation, due to the same reason as previously mentioned.

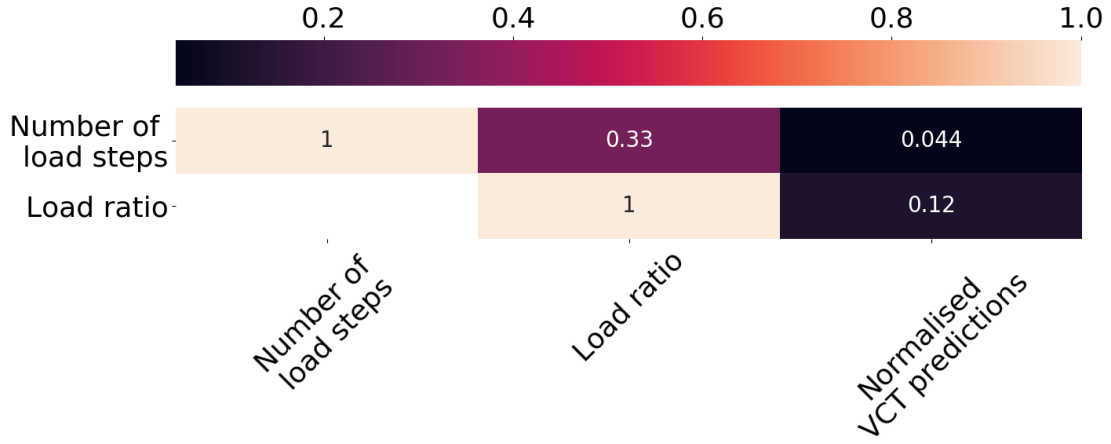

Figure 4.13 – Kendall correlation analysis with random frequency deviations within ±0.5Hz

4.3 Investigation based on experimental data

The investigation based on numerical results has revealed that there is no correlation between the number of load steps used and the VCT predictions, while the maximum load level used in the VCT predictions has a strong influence over the obtained results. Furthermore, the strength of the relation between the VCT predictions and the maximum load level used in obtaining them was shown to significantly decrease when frequency measurement errors occur. The existence of frequency deviations also increased the relevance of the number of load steps used, given that increasing this number would further limit the paths that the best-fitted quadratic curve could take.

Nevertheless, the investigation based on numerical data was performed for a set of nominally identical cylinders and can therefore also reflect aspects given by possible particularities implicit to this nominal design. Hence, an investigation was also performed using experimental data gathered for a plethora of different cylinders during a thorough literature review.

4.3.1 Structures investigated

Table 4.3 shows the cylinders from which the data sets used in the investigation based on experimental results were taken, where '*' denotes stiffened cylinders and '**' denotes cylinders tested under combined loading with internal pressure applied next to compression. Furthermore, the numbers in the round parentheses represent the assigned cylinder IDs, given that some belong to sets of nominally identical cylinders. When the same cylinder was tested under multiple loading scenarios, or for cylinders of the same nominal configuration, the P_{cr} and ε_{VCT} values are either shown in intervals, or in the order of their IDs for the cases where the number of nominally identical structures tested was two. The 'HS' or 'PP' suffixes denote the load introduction method, the former for hemispherical joints connected to the load introduction plates and the latter for the cases where the load was introduced by parallel plates.

As it can be seen from this table, there is a large variation between these cylinders regarding their construction material, dimensions, testing environment, and stiffening, therefore providing enough variety to compensate for any particular behaviour given by a certain cylinder. The actual number of VCT data sets was 48, the difference between this number and the number of cylinder names from Table 4.3 being due to the multiple nominally identical cylinders tested, and since some cylinders have been also tested with various degrees of internal pressure. Given the variation in the number of vibration modes and load steps for which experimental data was published, an identical approach as for the study based on numerical data would be unreliable. For instance, in [47] data for 4 vibration modes over 16-17 load steps was published for two cylinders, while for R09, data was available for only the first vibration mode, over just 7 load steps. Had the same approach been used, it would have induced a high bias towards the former, with more than 80% of the total number of generated predictions belonging to these two cylinders alone. Therefore, the VCT predictions were only performed for the first vibration mode for all these cylinders, while the number of load steps was reduced to 14, where applicable.

Name	Material	L [mm]	D [mm]	t [mm]	R/t	AR	P_{cr} [kN]	P_{exp} [kN]	$\varepsilon_{VCT-exp}$ [%]
Ghahfarokhi grid* [48]	GFRP	300	160	1.2	66	1.9	29.3	22.1	-3.1
Ghahfarokhi grid 2* [49]	GFRP	300	160	1.5	32	1.9	50.1	40.3	+2.36
Labans classic tow [47]	CFRP	790	600	1.45	207	1.3	420	303	-3.96
Labans variable tow [47]	CFRP	835	600	1.45	207	1.4	260	208	-1.44
R07 [1]	CFRP	500	500	0.63	399	1	34.2	22.4	-5.1
R08 [1]	CFRP	500	500	0.63	399	1	34.2	22.7	+7
R09 [1]	CFRP	500	500	0.63	399	1	34.2	21.6	-2.3
R15 [3]	CFRP	500	500	0.52	478	1	35.1	24.2	+10
D100H200L1-HS (1, 2) [50, 51]	CFRP	200	100	0.29	170	2	6.7	3.2, 2.9	-12.9, -9.3
D100H200L1-PP (3-9) [50, 51]	CFRP	200	100	0.29	170	2	6.7	(3.2, 4.4)	(-19.3, 10,5)
D100H200L2 (1-3, 3a, 5) [51]	CFRP	200	100	0.27	183	2	15.6	(8, 8.7)	(-12.2, 12.8)
D100H400L1-HS (1-3) [50, 51]	CFRP	400	100	0.3	168	4	6.7	(2.5, 3.2)	(-29.4, -6.3)
D100H400L1N-PP (4-6) [50, 51]	CFRP	400	100	0.3	168	4	6.7	(4.7, 5.26)	(-1.9, 6.8)
D100H400L2 (2) [51]	CFRP	400	100	0.36	141	4	13.4	7	-3.6
D300H150L1 (1, 3) [51]	CFRP	150	300	0.36	418	0.5	7	2.4, 3.5	15.7, 4.2
D300H150L1-HS (2) [50, 51]	CFRP	150	300	0.36	418	0.5	8.3	5.6	14.4
D300H150L2 (1) [51]	CFRP	150	300	0.36	418	0.5	18.8	7	37.99
D300H150L2N (3) [51]	CFRP	150	300	0.36	418	0.5	18.8	12.7	-0.7
D300H150L1N-PP (5) [50, 51]	CFRP	150	300	0.36	418	0.5	9.6	5.4	-10.4
D300H300L1-PP (3) [50, 51]	CFRP	300	300	0.34	446	1	5.6	3.3	34.9
D300H300L1N-PP (4, 5) [50, 51]	CFRP	300	300	0.34	446	1	8.9,	4.2, 4.1	-8, 6.5
SST1 [3]	Steel	500	500	0.5	500	1	183.1	70.2	0
SST2 [3]	Steel	800	800	0.5	800	1	183.1	49.9	+5
Z37 [3]	CFRP	800	500	0.79	318	1.6	89.8	59	-1
Z38*, ** [4]	Al	1000	801	2.18	183	1.2	(109, 139.7)	(86.5, 127.9)	(-5.4, -2.6)
ZD27 [57]	CFRP	560	502	0.58	432	1.1	27.4	15.9	-4.35
ZD28 [57]	CFRP	560	502	0.48	523	1.1	22.46	21.49	-8.3
ZD29 [57]	CFRP	560	502	0.52	482	1.1	24.33	21.86	-6.28

Table 4.3 – Cylinders used for the experimental-based investigation

When reducing the number of load steps, the frequencies at the minimum and maximum load levels were retained, while ensuring that consecutive measurements were not discarded. In doing so, the largest contribution for any cylinder was reduced to around 10% and given that there were 7 such sets with 14 load steps, it meant that 7/48 cylinders (≈15%) provided roughly 70% of the predictions. While a significant bias towards data from a few cylinders remained, the number of load steps of these data sets was not further reduced in order to generate a relatively large number of VCT predictions with different maximum load ratios and number of load steps, such that the correlation between these two parameters and the VCT predictions, together

with the influence of introducing frequency errors would be better assessed. Furthermore, as previously mentioned in section 4.1, load criteria were not applied in this case, given the experimental nature of this data, as well as to avoid a further reduction in the number of load steps for the cylinders that already had relatively few load steps.

4.3.2 Results

Figure 4.14 shows the VCT predictions based on the reference experimental data, grouped by the number of load steps. When comparing this figure with its numerical counterparts, one can observe that the same trends hold true in this case as well. As in the numerical-based analysis with unfiltered load steps, the amplitudes of the predictions tend to decrease with increasing the number of load steps and the extreme predictions are found when using the minimum number of load steps. Furthermore, the spans of these distributions are also getting increasingly smaller as the number of load steps is increased, the majority of the predictions being within 10% with respect to the baseline when 8, or more, load steps are used. Perhaps the most striking difference with respect to the numerical cases is given by the large amplitude of these distributions and especially the existence of large overestimates of the baseline prediction. A more detailed investigation revealed that these extreme overestimates are given exclusively by the data set of the SST2 cylinder and are possible due to two particular conditions satisfied by the experimental data of this cylinder.

Firstly, an extremely low knock-factor is needed, which for this cylinder is 0.29. Secondly, the existence of either measurement errors, which would highly increase the variation of the VCT predictions when combinations of load steps are used (current case), or a strong, negative monotonic relation between the maximum load level and the VCT predictions. Although the latter is less common, this behaviour has been observed for several cylinders, an aspect entirely absent in the predictions based on numerical data. Regardless of these large overestimates, the data set of this cylinder was kept in this study, given the excellent VCT prediction during the experimental

test, as reported in [3].

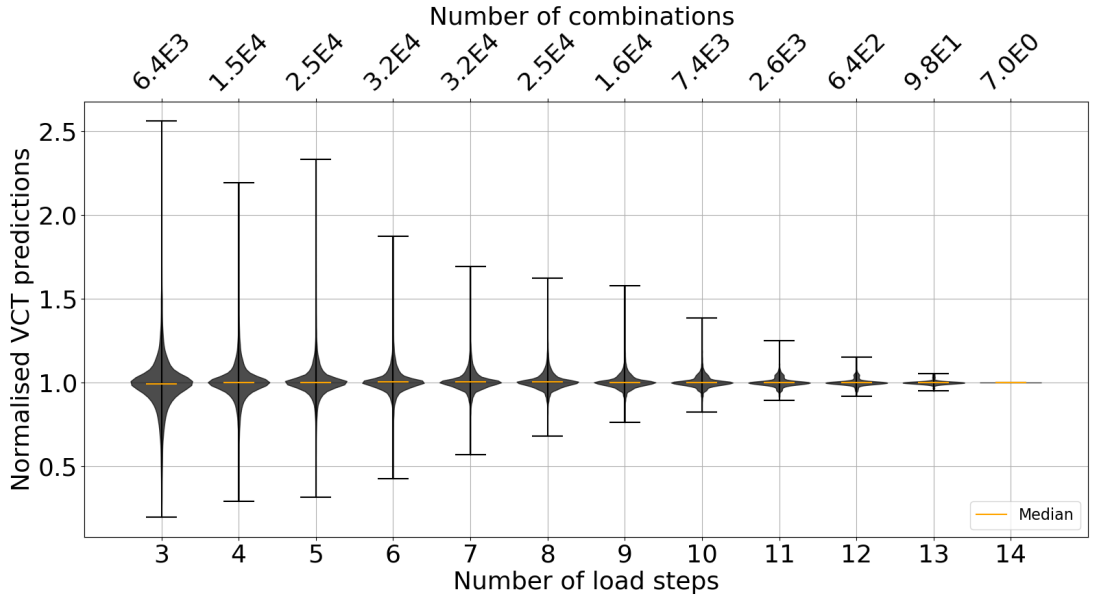

Figure 4.14 – VCT predictions as a function of the number of measurements

Figure 4.15 shows the VCT predictions from Figure 4.14, rearranged as a function of the maximum load ratio. Similarly, just as for the numerical results with frequency deviations taken into account, the maximum load level used seems more significant at lower load levels. Here, significant differences between the distributions can be seen at maximum load ratios lower than 70%-75%, point beyond which the predictions tend to stabilise. This maximum load ratio also represents the threshold after which the majority of the predictions obtained lie within 10% with respect to the baseline predictions.

Given the large variety in nominal geometry, number of load steps, and their load ratios between the different cylinders experimentally tested, a correlation analysis over a combined data set including all these cylinders would be misleading. As the normalised VCT predictions would converge towards 1 with different rates, it would likely result in an apparent lack of correlation between the number of load steps, or maximum load level, and the VCT predictions. Therefore, the correlation analysis was performed for each data set individually, and the resulting coefficients were averaged and displayed in a heatmap consistent in layout with the ones previously shown.

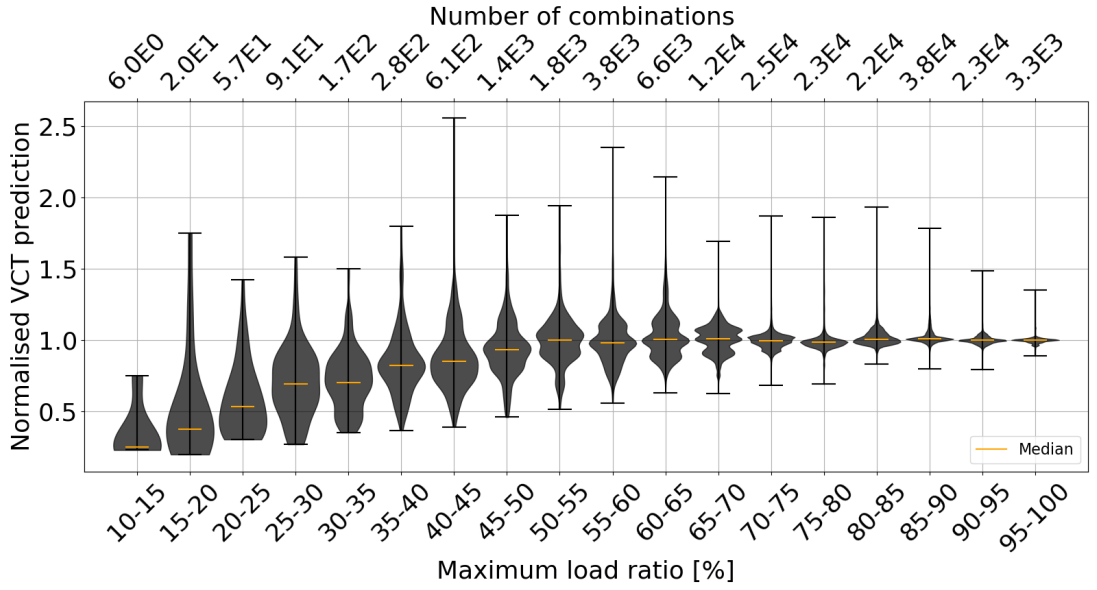

Figure 4.15 – VCT predictions as a function of the maximum load level

Figure 4.16 shows the heatmap with the correlation coefficients for the investigation based on the reference experimental results. The most notable aspect with respect to the numerical investigation is that now the strength of the monotonic relation between the maximum load level used and the VCT predictions appears to be weak. In this case, a weaker correlation is not totally unexpected, since the study based on numerical results already showed that frequency deviations can alter this strength, and some level of measurement error is present in any experimental test.

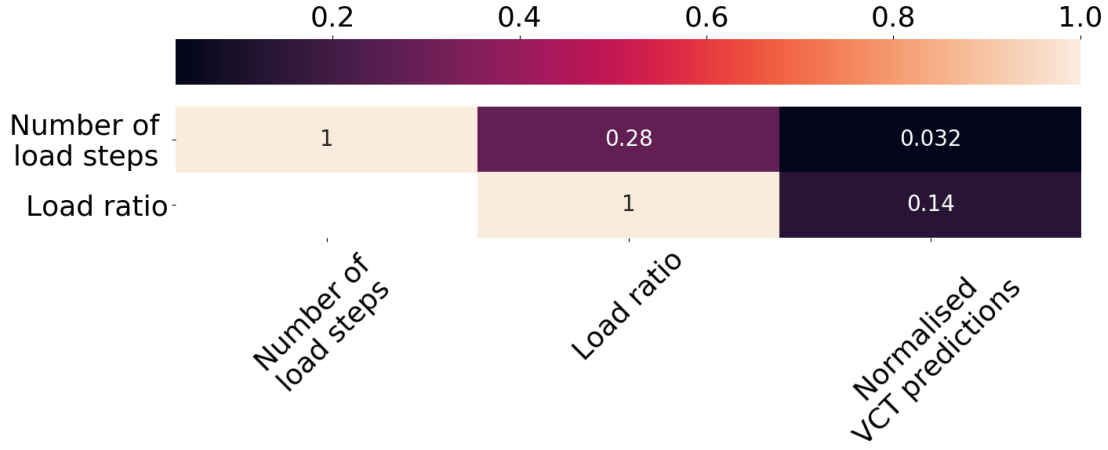

Figure 4.16 – Kendall correlation analysis

Influence of frequency measurement errors

Identically to the investigation based on numerical results, and despite the high likelihood that some frequency measurement errors are already present, here the measured reference frequencies were also altered by random values within ±0.1Hz, ±0.25Hz, and ±0.5Hz intervals, and 50 such sets were generated for each set of experimental data. Given the likely existing measurement errors in the experimental data, and due to the aforementioned cases where the VCT predictions decreased with increasing the load level, there were only minor differences between the results obtained using the reference experimental data and the ones with various magnitudes of such deviations introduced. Therefore, here only the results obtained when frequency deviations within ±0.5Hz have been applied are shown.

Figure 4.17 shows the distributions of the VCT predictions as a function of the number of load steps when frequency deviations within ±0.5Hz have been applied to the reference experimental data.

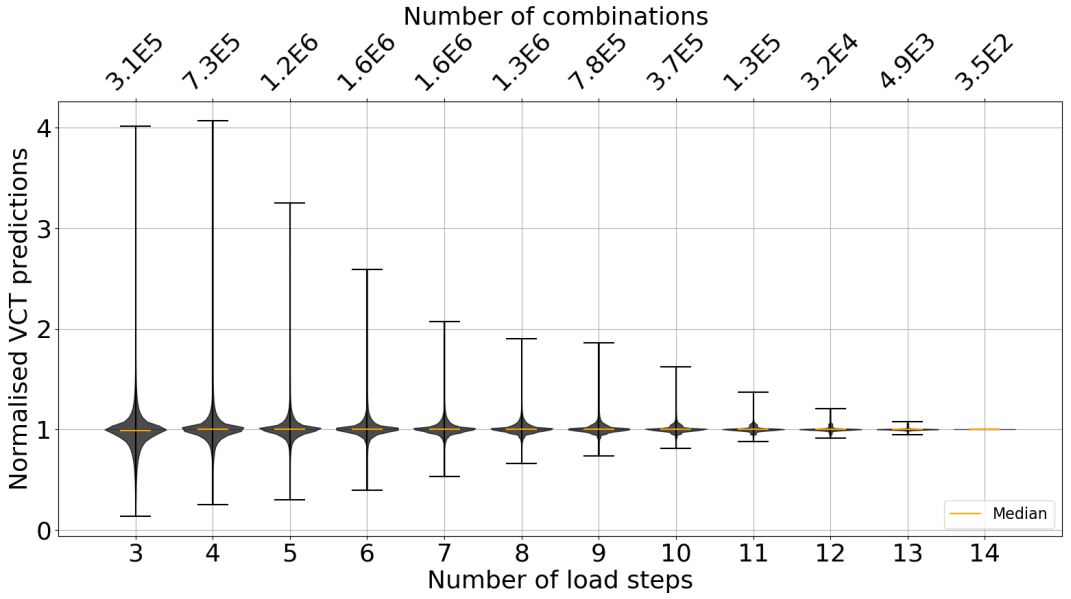

Figure 4.17 – VCT predictions as a function of the number of measurements with random frequency deviations within ±0.5Hz

When comparing this figure with its analogue Figure 4.14 based on the reference experimental data, one can notice the similarity between the two, the only significant

difference being the larger prediction amplitudes due to the introduced frequency deviations. This aspect remains valid also when these predictions are arranged as a function of the maximum load level used, as shown in Figure 4.18.

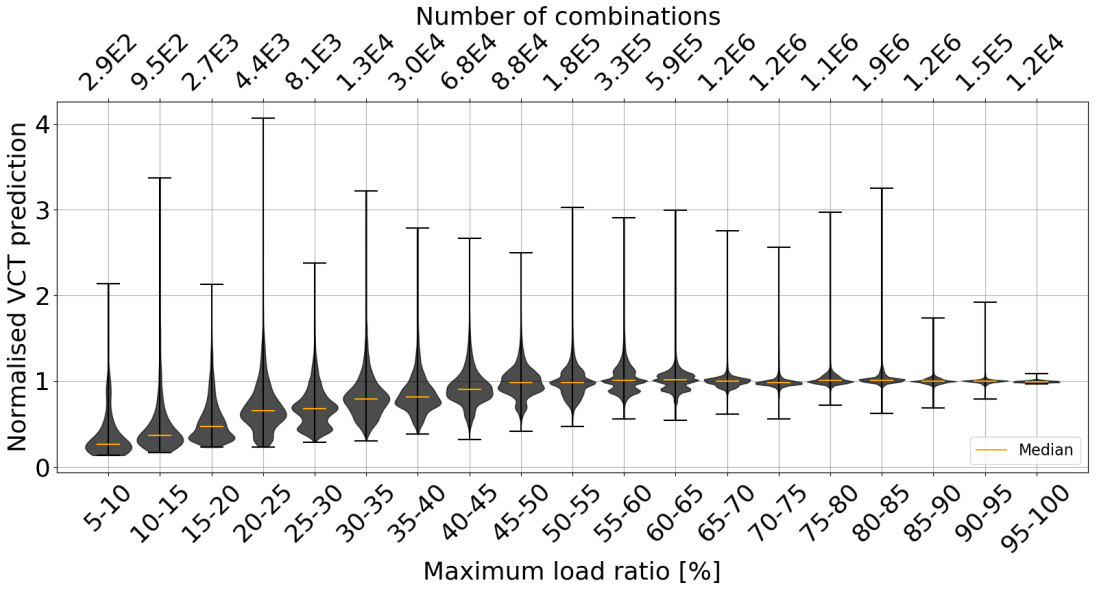

Figure 4.18 – VCT predictions as a function of the maximum load level with random frequency deviations within ±0.5Hz

For this frequency deviation magnitude applied to the reference experimental data, it seems that a robust prediction would require at least 9 load steps, with a maximum load ratio of at least 70%, given that the spans of the distributions when these conditions are satisfied are within 10% of the baseline predictions where all available load steps are used.

While the similarity between the distributions of VCT predictions as a function of the number of load steps, or the maximum load ratio for the data generated from numerical results and for the one generated from experimental data is strong, the correlation analysis in the presence of measurement deviations appeared to evolve differently when increasing the magnitude of the introduced deviations. As it can be seen when comparing Figure 4.19, for the case where ±0.5Hz frequency deviations were applied to the experimental data, with Figure 4.16, where no such deviations were applied, one can notice that, although in both cases the correlation appears to be weak, there is an apparent increase in the strength of the positive monotonic

relation between the VCT predictions and the maximum load ratio. This seems to be in contradiction with the observations drawn from the numerical-based investigation, where the correlation decreased with increasing the magnitude of the frequency deviations.

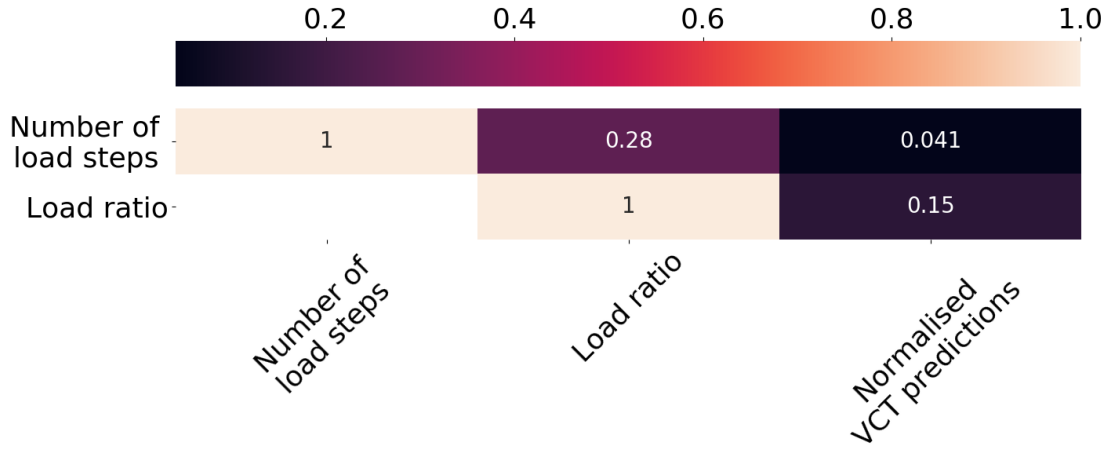

Figure 4.19 – Kendall correlation analysis with random frequency deviations within ±0.5Hz

4.4 Discussion

The investigation using numerical results revealed that a monotonic relation between the number of load steps used and the obtained VCT prediction does not exist. Nevertheless, the number of load steps can be relevant in the presence of measurement errors, since increasing this number restrains the possible paths that the fitted quadratic curve can take. In contrast, a strong, positive, monotonic relation was observed between the maximum load ratio and the VCT predictions, the strength of this relation decreasing as the magnitude of the frequency deviations introduced increased. Furthermore, threshold values regarding the number of load steps and the maximum load ratio were identified, given that the distributions of the VCT predictions obtained beyond these threshold values did not significantly change and were within 10% of the baseline prediction. For the largest magnitude of the frequency deviations introduced, these conditions were satisfied when the predictions were performed using at least 9 load steps, with a maximum load ratio of at least 70%.

The trends observed in the sensitivity study based on numerical data were also generally confirmed when performing the sensitivity study based on experimental data. The only exception was regarding the correlation analysis between the maximum load ratio and the VCT predictions, where for the investigation based on numerical data, it was initially strong and decreased with increasing the magnitude of the introduced frequency deviations. On the other hand, in the investigation based on experimental data, this coefficient based on the reference experimental data depicted a weak, positive, monotonic relation, which slightly increased when increasing the magnitude of the introduced frequency deviations. However, while the correlation coefficient for the analysis based on the numerical data was performed using a combined data set containing the results from all FE models, same was not the case for the study based on experimental data, given the different number of load steps measured and their corresponding load ratios, as well as the different rates at which the predictions converge towards the baseline predictions as a function of the number of load steps and maximum load level used. Therefore, the correlation analyses were performed for each set of experimental data individually, after which an averaged coefficient was determined. With this in mind, and given the low average correlation coefficient suggesting a weak, positive, monotonic relation between the maximum load ratio used and the VCT prediction, the correlation coefficients used to compute this average were also individually inspected.

For the reference experimental data, it was found that, while a strong, positive, relation between the maximum load level used and the VCT predictions was present for the majority of the cylinders, there were also cylinders for which this was not the case. For some of the cylinders, the predictions decreased with increasing the load ratio, be it overall, or only before/after a certain load level, rendering significantly lower values of the correlation coefficients, in some cases to the extent in which an apparent strong, negative, monotonic relation was suggested by the correlation analysis. The decreases in the VCT predictions were observed predominantly for a maximum load ratio higher than 50%, given the higher number of load step combinations at higher load ratios. The correlation analysis also reflected the influence of this bias, despite

the general VCT prediction increase with the maximum load level up to load ratios of 50%. The individual correlation coefficients describing the strength of the monotonic relation between the VCT predictions and the maximum load level used had therefore also negative values, these being contained within a (-0.64, 0.77) interval, therefore yielding the unexpectedly low value of τ=0.14 when averaged. The cases where the VCT predictions decreased with increasing the load levels were also the source of the minor increase in apparent correlation strength when frequency deviations were introduced in the experimental data. The correlation coefficients between the VCT predictions and the maximum load level used, be they positive or negative, decreased in magnitude when increasing the magnitude of the frequency deviations introduced. However, for the cases where these coefficients were negative, the decrease in magnitude was significantly larger than for the cases where these coefficients were positive, giving thus an apparent increase in the correlation between the VCT predictions and the maximum load level used.

Overall, the frequency deviations introduced in the experimental data seemed to have a lower influence over the correlation between the obtained VCT predictions and the maximum load level used than observed in the study based on numerical data. While one of the possible reasons why this happened might be due to the already existent measurement errors within the experimental data, it is more likely that this occurred due to a favourable combination of factors related to the magnitude of the introduced frequency deviations, the vibration response of the cylinders tested experimentally, and to the number of load steps measured. For example, for the numerical investigation the frequency response of the models run was requested for 20 load levels and the average frequency difference between 2 consecutive load steps was around 3Hz, which when considering the largest magnitude of the frequency deviations introduced of $\pm$0.5Hz, it meant that the difference in frequency between two consecutive load steps could change by as much as one third with respect to the reference one. While similar differences between consecutive load steps were also observed in some experimental results, these differences were generally significantly larger, meaning that the maximum magnitude of the introduced frequency deviations was bound to bring smaller

changes to the frequency differences between consecutive load steps. Additionally, while this difference between the frequencies of consecutive steps is implicitly related to the vibration response of the structure analysed, minor adjustments can also be made when defining the number of load steps. In this regard, the larger number of load steps used in the numerical investigation favoured the lower frequency difference between consecutive load steps when compared to the experimental results, ultimately increasing the sensitivity of the correlation between VCT predictions and the maximum load level to the magnitude of the introduced frequency deviations.

4.5 Conclusions

In this chapter, a sensitivity study on the influence of the number of measurements and maximum load level measured over the buckling load prediction obtained by VCT was conducted, based on both numerical and experimental results. Given that when performing VCT, the number of load steps is normally directly linked with the maximum load level used, here multiple VCT predictions were performed using combinations of load steps, such that the number of load steps was no longer perfectly coupled with the maximum load level used to obtain the prediction. Furthermore, given that errors might arise during an experiment, the influence of frequency measurement errors was also taken into account by generating 50 data sets based on the reference numerical/experimental results, in which each frequency was modified by a random amount within three different magnitudes, namely $\pm$0.1Hz, $\pm$0.25Hz, and $\pm$0.5Hz.

The investigation based on the reference numerical results revealed that there is no monotonic relation between the VCT predictions and the number of load steps, while between the VCT predictions and the maximum load ratio a strong, positive, monotonic relation was found. Furthermore, while a monotonic relation between the number of points and the VCT predictions was not identified, it was found that increasing the number of load steps can lower the variation of the VCT predictions, given that it restrains the space where the best quadratic curve can be fitted to the points in

the VCT characteristic chart, aspect also valid when increasing the maximum load level considered. In this regard, threshold values regarding the number of load steps and maximum load ratio were also identified, beyond which further increases in either the number of points or the maximum load level would result in differences of less than 10% compared to the baseline prediction using all available load steps. In the numerical study, these threshold values were proportional to the magnitude of the introduced frequency deviations, since these increased the variation of the predictions, and therefore a larger number of points and higher load ratios were needed to provide enough restraints on the possible paths the quadratic fits could take. Additionally, the strength of the positive monotonic relation between the maximum load level used and the VCT predictions decreased with increasing the magnitude of the frequency deviations applied.

The general observations drawn from the investigation based on numerical results were also aligned with those resulting from the investigation based on experimental data. Due to the variations in the number of load steps and load levels measured during the experimental applications of VCT, and the different rates at which the VCT predictions converged to the baseline prediction, the correlation analysis was performed for each cylinder individually, and an average coefficient was then computed. Although the average correlation coefficient describing the strength of the monotonic relation between the maximum load level and the VCT predictions showed a weak correlation, an in-depth inspection of the individual coefficients revealed that the unexpected low magnitude of the average one was given by the measurements of a few cylinders displaying a relatively uncommon behaviour. For these cylinders, within load ratios specific to each cylinder, the VCT predictions decreased with increasing the maximum load ratio, this behaviour being generally observed for maximum load ratios higher than 50%. Given that using combinations of load steps to partially decouple the number of load steps from the maximum load ratios had a residual bias towards higher load ratios, providing more predictions as the maximum load level increases, the correlation coefficient describing the strength of the monotonic relation between the maximum load level and the VCT prediction for these cases was often

negative, its magnitude describing a strong correlation. This happened despite the clear increase of the VCT predictions with increasing the maximum load level up to load ratios of 50%, and resulted in the low magnitude of the averaged correlation coefficient.

In the investigation based on experimental results, the magnitude of the frequency deviation introduced seemed to alter the correlation between the VCT predictions and the maximum load level used by a lower degree than observed in the investigation based on numerical results. The source of this discrepancy was most likely given by the larger relative changes in the frequency differences between consecutive load steps considered in the numerical results, this effect being also favoured by the larger number of load steps used.

For the largest magnitude of random frequency deviations introduced, up to ± 0.5Hz, the majority of the VCT predictions were within 10% from the baseline prediction when at least 9 load steps at a maximum load ratio of at least 70% were used to perform the prediction, aspect valid in both the study based on numerical results, and on the one based on experimental results. While the study based on experimental results raises the confidence in these threshold values, given the large variety of structures, number of load steps, and maximum load levels measured, particular cases in which a satisfactory VCT prediction might not be achieved when satisfying these conditions might still exist. Nevertheless, the methodology applied here can still be deployed to perform a sensitivity study specific to the structure in question and determine its specific threshold values regarding the number of measurements to be taken and the maximum load level.

5 VCT sensitivity towards shape and loading imperfections

The significant number of various cylinders for which VCT was able to provide a reliable buckling load prediction under axial compression implicitly suggests that this method is not particularly sensitive to different imperfection signatures inherent to each of those structures. Nevertheless, although low in number, there were also cases in which VCT was not able to provide robust estimates of the buckling loads determined by experiments, some of which have been reported in [50]. Furthermore, in the investigation on the influence of the number of measurements and maximum load ratio over the VCT predictions shown in Chapter 4, this aspect was also found in numerical analyses for two imperfection signatures belonging to a family of nominally identical cylinders, namely the ones of cylinders Z17 and Z18. While this uncommon behaviour is clearly tied to the imperfection signatures of the tested structure and equipment, the source of this behaviour could not be isolated within the different types of imperfections, given that investigations focusing explicitly on the sensitivity of VCT to different imperfection types have not been published. In addressing this aspect, as well as to increase the method's appeal for industrial applications, a numerical sensitivity study focusing on the influence of various loading and shape imperfection magnitudes is conducted in this chapter.

5.1 Methodology

The numerical model used in this study belongs to the SST1 cylinder tested at Riga Technical University, the buckling and VCT results being published in [3]. This particular cylinder was chosen here due to its high imperfection sensitivity, knockdown factor of 0.38, as well as due to the reliable experimental VCT predictions with a relatively low sensitivity towards the maximum load level. The cylinder was manufactured by rolling up an AISI 304 steel plate to the desired curvature and laser welding its edges, the geometry and material properties being shown in Table 5.1. The self-alignment between the structure and loading plates was enhanced by placing a hemispherical joint between the machine's crosshead and the loading plate, minimising thus the bending effects due to an uneven load distribution along the cylinder's circumference. Additionally, the top and bottom edges were cast in resin over a 25mm length which, together with steel rings placed at their inner side, provided radial support and ensured a uniform load introduction.

ρ $[g/cm^3]$	7.8	L_{tot} [mm]	550
ν_{12}	0.29	L_{free} [mm]	500
E [GPa]	193	R [mm]	250
G [GPa]	77	t [mm]	0.5

Table 5.1 – SST1 cylinder geometry and material properties

The FE model of the structure was built in the Abaqus FE software, the mesh convergence analysis showing that 120 S8R elements across its circumference are sufficient to capture the influence of the applied shape imperfections. In order to constrain the model, boundary conditions were applied over the areas in contact with the resin and inner steel rings, restraining all degrees of freedom except axial translations, while the load was introduced by applying axial displacements on the top and bottom nodes. Figure 5.1 shows the mesh of the FE models used, where the areas highlighted in red correspond to the nodes on which boundary conditions were specified.

The cylinder's out-of-plane (OoP) imperfection, shown in Figure 5.2, was measured on the inner side of the structure and was implemented in the model using the same procedure mentioned earlier in Section 4. This shape imperfection pattern was applied in amplitudes from 0.01 to 3 times the measured magnitude to study the sensitivity of VCT towards shape imperfections.

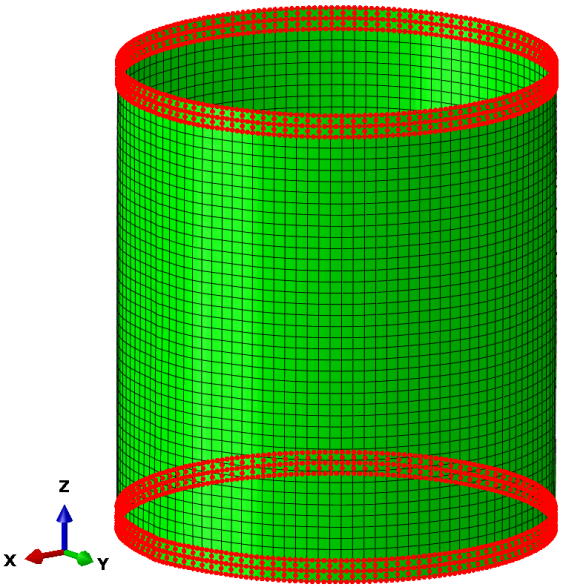

Figure 5.1 – SST1 cylinder FE model

Given that the in-plane (IP) imperfections of the cylinder's edges (different cylinder lengths across its circumference) were not measured, the IP imperfection signature published in the NASA SP 8007 guideline [6] was used to model loading imperfections. Figure 5.3 shows the aforementioned patterns in normalised form, such that the measurements taken lie between 0 and 1mm.

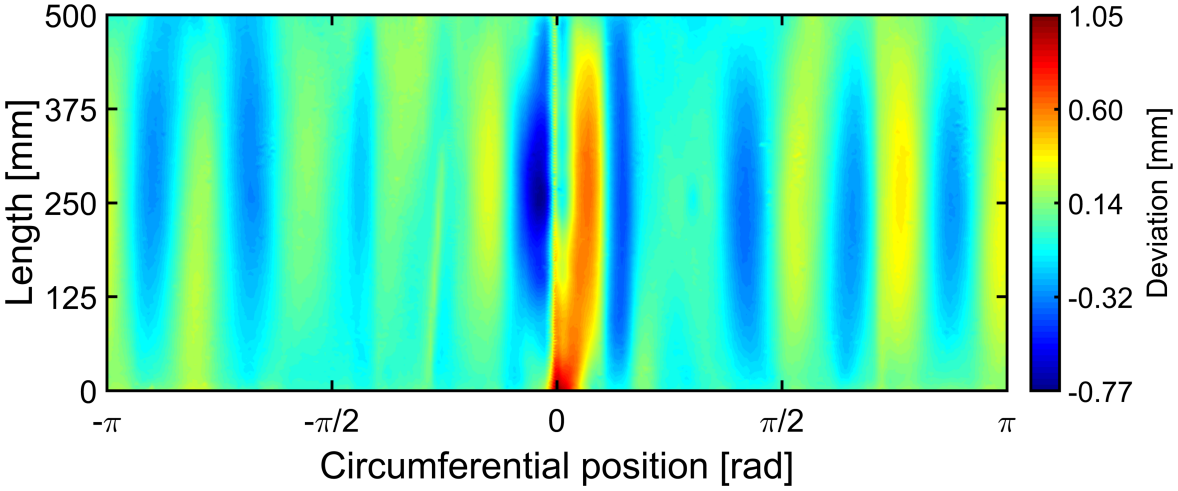

Figure 5.2 – SST1 OoP imperfection pattern [3]

Similarly as for the shape imperfections, these patterns were used to introduce load imperfections of various magnitudes, starting from 0.01 to 0.25 with respect to the magnitude shown in Figure 5.3. These magnitudes correspond to the maximum displacements applied to the bottom and top cylinder edges in mm. A schematic

of the procedure to apply these imperfections is shown in Figure 5.4 using the top edge as an example.

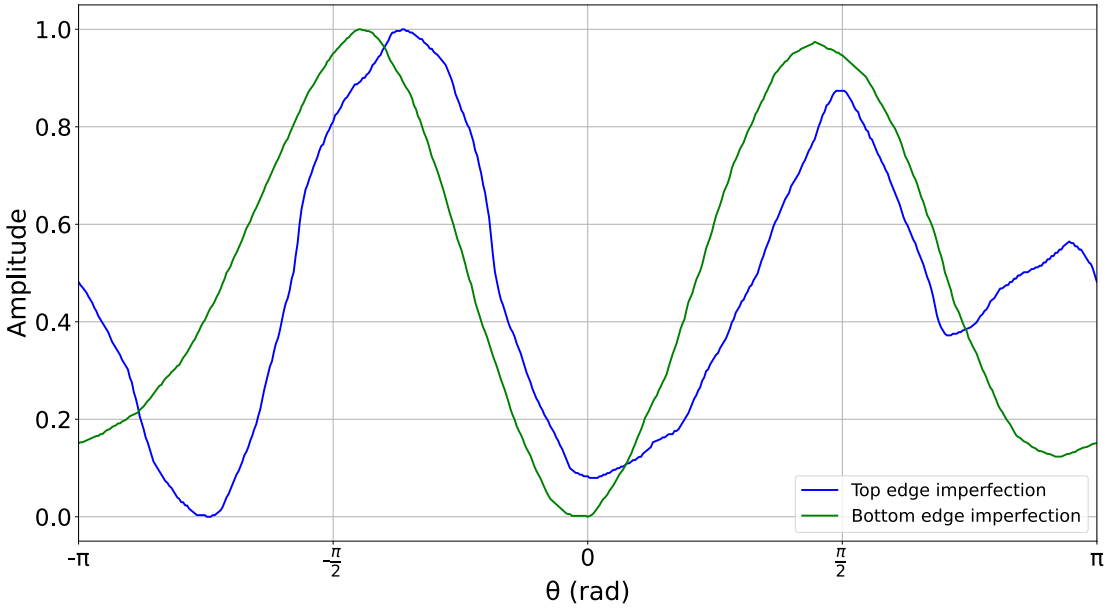

Figure 5.3 – IP imperfection patterns of the top and bottom edges [6]

Starting from the nominal coordinates of the nodes at the very top of the cylinder's mesh, in a first step, the axial coordinates were modified in the input file by extending the cylinder according to the top edge imperfection pattern, over which a multiplication factor according to the aforementioned magnitudes was applied. For example, for the lowest magnitude used of 0.01, the first node from Figure 5.4 a) had its axial coordinate modified by $dz1$. When looking at the magnitude of the top imperfection at 0 radians from Figure 5.3, and applying the aforementioned multiplier, it translates roughly to a value of 0.001mm. A similar process was performed for the nodes

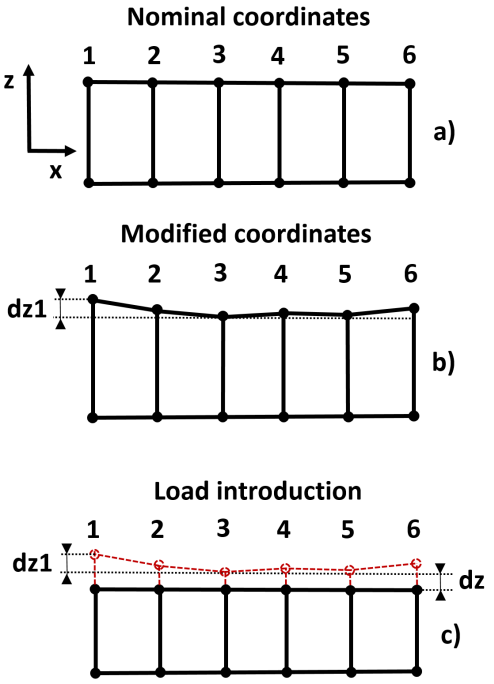

Figure 5.4 – Load imperfection introduction

at the bottom of the cylinder's mesh, the only difference being in the opposite sign of the amount by which the axial coordinate of the nodes was modified, such that the length of the cylinder at any circumferential position always increased.

Then, in a first non-linear analysis step, displacements were applied to the nodes at the top and bottom ends of the cylinder, such that at the end of this analysis step these nodes were perfectly flat again, introducing thus an uneven loading. While for the bottom nodes the magnitudes of the displacements applied were to bring back the nodes at their nominal axial coordinates, the displacement magnitudes applied at the top nodes also included a small uniform displacement dz, as shown in Figure 5.4 c). This uniform displacement was applied on the top nodes to simulate the way the uneven top and bottom surfaces of the cylinder flatten as the load applied increases. Then, a further uniform displacement was applied on the top nodes in a second non-linear step to increase the compressive load until buckling was reached. This approach to introduce loading imperfections is fairly common, with numerous studies focusing on the influence of loading imperfections and uneven settlement on the buckling response of shells using similar approaches [68–73].

Although not very common, and mostly when the compressive load introduction is displacement-based, local buckling can occur, and shape and loading imperfections are known to promote this effect [65, 71, 73, 74]. Given the various magnitudes of shape and loading imperfections applied in the FE model of the cylinder and the displacement-based load introduction, this behaviour was also encountered here. For VCT, the vibration modes need to be monitored across the load steps defined. However, due to the likelihood of vibration modes completely changing between consecutive load steps before and after local buckling, the VCT load step definition procedure described in Chapter 4, Section 4.1 for the numerical investigation is no longer applicable. Considering the frequent occurrence of local buckling for the higher magnitudes of the shape and loading imperfections applied and that local buckling occurred at relatively low load ratios with respect to the global buckling load, VCT load steps were also defined at load levels beyond the ones at which local buckling was seen, provided that the load-displacement response remained relatively linear. These apparent

linear regions in which VCT load steps were defined are further referred to here as VCT regions for an easier differentiation between the obtained VCT predictions.

Figure 5.5 shows the procedure used in this numerical study to define the VCT load steps. Once the non-linear analysis concluded, a script iterated through the load-displacement response to define the VCT load steps specific to that analysis. Initially, the non-linear global buckling load P_{nl} and its increment number inc_{max} were provided as inputs. The former was utilised in defining the VCT load step criteria, while the latter determined the loop's termination. Additionally, the number of VCT regions was set to one, with the corresponding starting load, F_{start}, set at zero. The initial apparent stiffness S_{ini} was determined based on the first two increments, as the ratio between the change in axial load and the one in axial displacement, and the loop commenced from the second increment (i=1). Subsequently, the increment number increased until either a load drop occurred, associated here with local or global buckling, or the maximum increment number was reached.

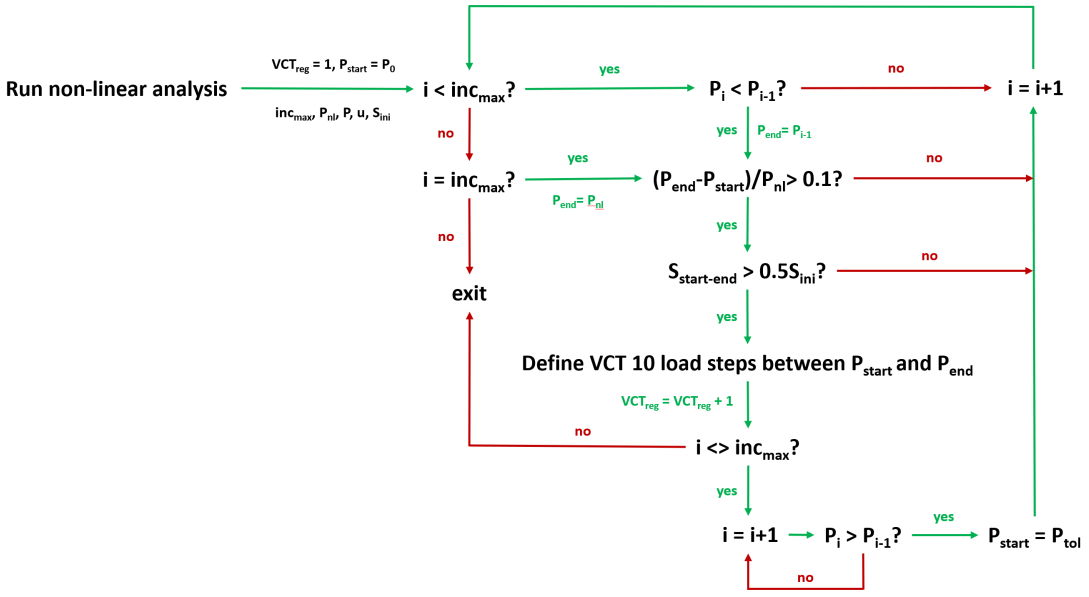

Figure 5.5 – VCT load steps definition procedure

Upon detecting a load drop, or reaching the maximum increment number, the maximum load in that region F_{end} was retrieved, and a first VCT load step definition criterion was applied. This criterion assessed whether the difference between the

minimum and maximum load of the region exceeded 10% of the global non-linear buckling load P_{nl}. While seemingly inconsequential for defining VCT load steps in the initial VCT region, this criterion prevented the definition of numerous irrelevant load steps when multiple load drops were observed within a negligible load ratio difference. This behaviour was typically observed immediately after local buckling, or near the global buckling load. If the first criterion was met, the average apparent stiffness in that region S_{start_end} was computed based on load and displacement values between consecutive time increments across the entire region. This average apparent stiffness was then used in a second VCT load step definition criterion, which evaluated whether the average stiffness in the region exceeded half of the initial stiffness S_{ini}. While also seemingly insignificant for defining VCT load steps in the initial region, this criterion was valuable in preventing the definition of load steps where the compressive response of the model was highly non-linear due to significant bending effects. These regions typically occurred after multiple changes in the localised buckling patterns and at relatively high load ratios, demonstrating a severe and constant decrease in apparent stiffness with negligible changes in the additional load carried. If the second criterion was also met, the VCT load steps were defined, and the VCT region number was updated. Subsequently, if the increment number reached inc_{max} the loop was terminated, and if not, the increment number was further increased until an increase in the load carried was observed. In the latter case, the minimum load level of the VCT region F_{start} was updated. Notably, F_{start} was updated by a value including a tolerance F_{tol}, instead of solely updating it with F_{i-1}, increment i corresponding to an increase in the carried load. This tolerance was needed here to prevent the definition of a VCT load step in potentially highly non-linear regions immediately following an increase in the load carried. The definition of F_{tol} was displacement-based, set as the load corresponding to $1.01u_{i-1}$, which effectively avoided the aforementioned highly non-linear regions. After updating F_{start}, the entire process repeated until the maximum increment of interest inc_{max} was reached, signalling the completion of the VCT load step definition procedure.

The vibration mode frequencies in unloaded state $F_{0,k}$ cease to be applicable when

load steps beyond local buckling are used to perform VCT, due to the discontinuity of the vibration modes across the VCT regions. Instead, the vibration mode frequency of the first load step in each specific VCT region served as the reference. Furthermore, when multiple VCT regions were identified, an investigation was conducted to determine whether VCT was more likely to predict the local, or the global buckling load. Additionally, two sets of critical buckling loads P_{cr} values were utilised, with and without out-of-plane imperfections introduced, to determine the most suitable option for robust VCT buckling load predictions. Finally, the new empirical VCT procedure, which involves plotting $(1\text{-}p)^2$ against $(1\text{-}f)$, was compared with the established analytical relation.

5.2 Results

In this section, the results of the numerical investigation on the sensitivity of the VCT predictions to shape and loading imperfections are shown. Subsection 5.2.1 addresses the buckling results obtained when shape and loading imperfections are applied in various magnitudes, while Subsection 5.2.2 addresses the numerical VCT results.

5.2.1 Buckling

Table 5.2 shows the reference buckling loads obtained numerically and experimentally for this cylinder, the latter being taken from [3]. Here, it can be seen that both P_{nl}, obtained from the FE model where the OoP imperfection pattern shown in Figure 5.2 has been introduced as is, and P_{exp} are significantly lower than the P_{cr} value obtained based on the pristine shape, reflecting the cylinder's high sensitivity to imperfections.

Furthermore, there is also a significant difference between the buckling load obtained from the non-linear analysis P_{nl} and the experimental result P_{exp}, these differences being most likely due to imperfections other than shape being present in the tested article and/or equipment, highlighting further the cylinder's high sensitivity to imperfections. Nevertheless, the excellent prediction provided by VCT shows that the

influence of various imperfection types on a structure's buckling load can also be reflected in their vibration response and thus in the VCT prediction.

P_{cr}	P_{nl}	P_{exp}	P_{VCT}
182.6kN	100.4kN	70.2kN	70.2kN (at 86%P_{exp})

Table 5.2 – SST1 reference buckling loads

Figure 5.6 displays the knockdown factors relative to the value derived from the model lacking shape imperfections (P_{cr}=182.6kN), across different out-of-plane (OoP) imperfection amplitudes. While minor OoP amplitudes have negligible effects on P_{cr}, the impact of OoP imperfections becomes notable when amplitudes surpass a value of 0.25. Upon surpassing this threshold, substantial variations arise, likely leading to significant alterations in the VCT predictions. Hence, their influence was investigated.

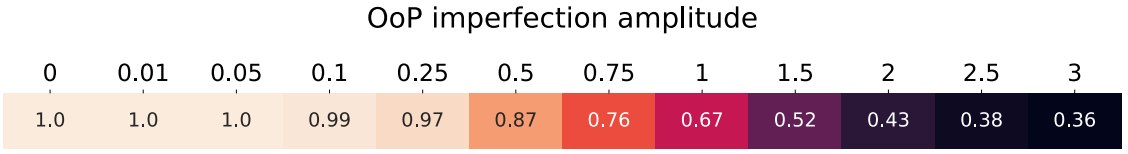

Figure 5.6 – Heatmap with the knockdown factors based on linear buckling analyses

Figure 5.7 depicts the knockdown factors derived from the non-linear analyses of FE models featuring varying amplitudes of out-of-plane (OoP) and in-plane (IP) imperfections, relative to the buckling load of the FE model without any imperfections, where P_{nl}=182.8kN. An essential observation regarding the amplitude of the IP imperfection employed (0.25 - corresponding to a maximum displacement of 0.25mm locally applied to the top and bottom cylinder edges) needs to be made. The buckling load for the FE model devoid of imperfections was reached at a displacement of 0.677mm. This indicates that, for the highest IP amplitude introduced, the cylinder's edges locally shorten by a substantial margin, roughly 0.5mm, thus qualifying as a severe loading imperfection.

Upon scrutinising this figure, several notable points emerge. Initially, even minor imperfections have a considerable influence over the buckling load, while further increasing the amplitudes yields relatively minor effects until reaching a certain threshold.

For the imperfection patterns utilised herein, this threshold for the OoP imperfection amplitude appears to be around 0.1, while for the IP imperfection is around 0.175, the knockdown factors surpassing a value of 0.9 beyond these thresholds. Moreover, upon exceeding a particular OoP imperfection amplitude threshold, the impact of the loading imperfections escalates, leading to a marked decrease in the buckling load. Additionally, for any given OoP imperfection amplitude, an IP imperfection amplitude threshold exists beyond which the buckling load decrease tends to stabilise, and vice versa. These imperfection amplitude thresholds observed align with findings from other studies in which the imperfection amplitudes were varied. An example is the case where the lateral load/displacement is increased in the single load perturbation approach [7, 65, 75], where the buckling load experiences a severe decline within a specific range of applied load/displacement, whereas beyond this range, the decrease is relatively minor by comparison.

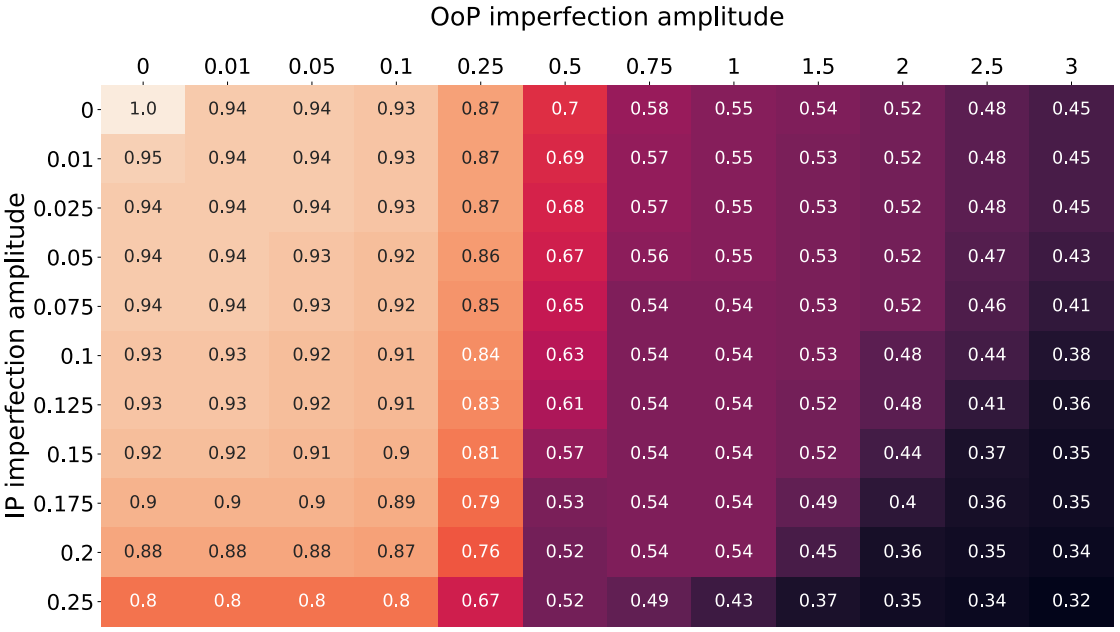

Figure 5.7 – Heatmap with the knockdown factors based on non-linear FE analyses

Heightened imperfection amplitudes triggered local buckling, resulting in discernible alterations in the load-displacement curves. The initial occurrences of local buckling were associated with a dimple-like pattern evident in the model's out-of-plane displacement field, typically positioned near the cylinder's mid-height. Subsequent

local buckling events either entailed modifications to the existing localised buckling patterns or the emergence of similar patterns on the opposite side. When a shift in the localised buckling pattern occurred, it signalled the appearance of additional adjacent dimple-like patterns alongside the existing one(s), or a slight migration of the existing pattern along the cylinder's circumference. The frequency of these occurrences generally rose with increasing imperfection amplitudes, as depicted in Figure 5.8.

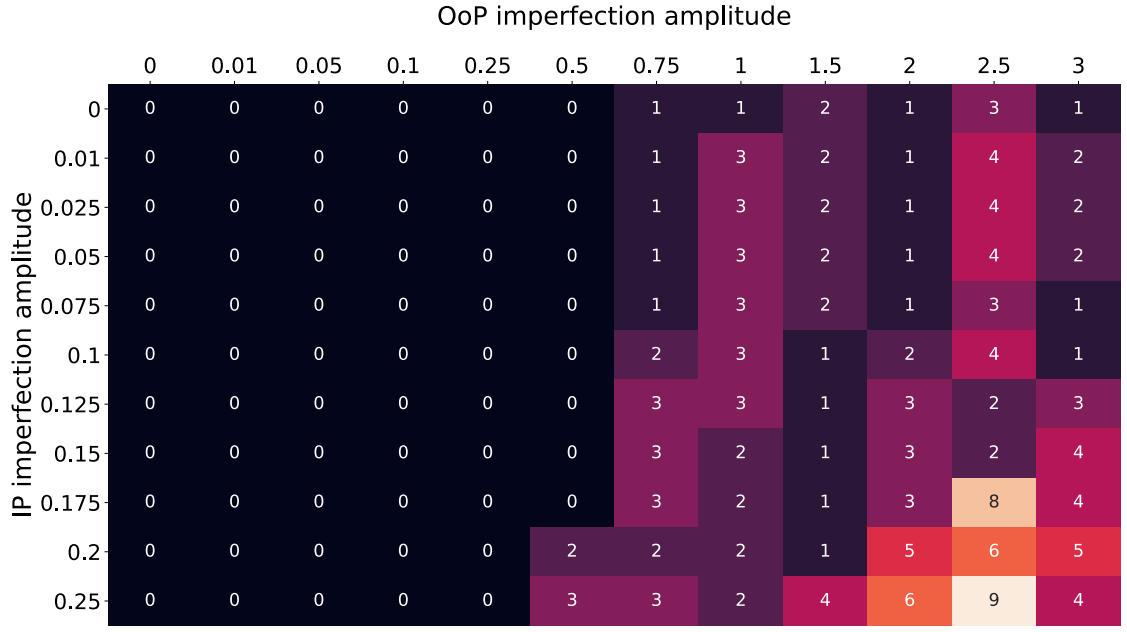

Figure 5.8 – Heatmap with the number of load-drops recorded

Notably, increasing the amplitude of OoP imperfections appeared to have a more pronounced effect on precipitating local buckling. However, once the threshold imperfection amplitudes leading to local buckling were surpassed, a distinct trend was not observed in the evolution of the number of local buckling events relative to the applied IP and OoP imperfection amplitudes. When looking at the model best representing the tested structure, with no loading imperfections and a shape imperfection amplitude corresponding to the measurement (OoP=1), it can be seen that this model also experienced a local buckling event, which occurred around 82.9kN. While during tests where the load introduction is displacement-based the structures can often take additional load beyond local buckling, it is not unreasonable to consider that local

events might still trigger a global buckling of the structure. Although the value at which this occurred in the numerical simulation with (OoP=1) is still not quite close to the experimental one at 70.2kN, the values at which local buckling occurred were smaller than the experimental value for IP imperfection amplitudes larger than 0.075. This, along with the cylinder's high sensitivity to imperfections, out of which only two types were included in these numerical simulations, increases the likelihood that the difference in the buckling loads obtained by experiment and by numerical simulations is due to local buckling triggering global buckling in the experiment.

Figure 5.9 illustrates the compressive behaviour of the finite element model with multiple local buckling events (IP=0.125 and OoP=1.5), showcasing the load-displacement response, apparent stiffness, OoP displacement, and the defined VCT load steps. Here, the load and stiffness values are normalised relative to the non-linear buckling load and initial stiffness, respectively, and shown in percentages. To account for loading imperfections stemming from uneven displacements at the top and bottom edge nodes, an average shortening was calculated based on the axial displacements of these nodes.

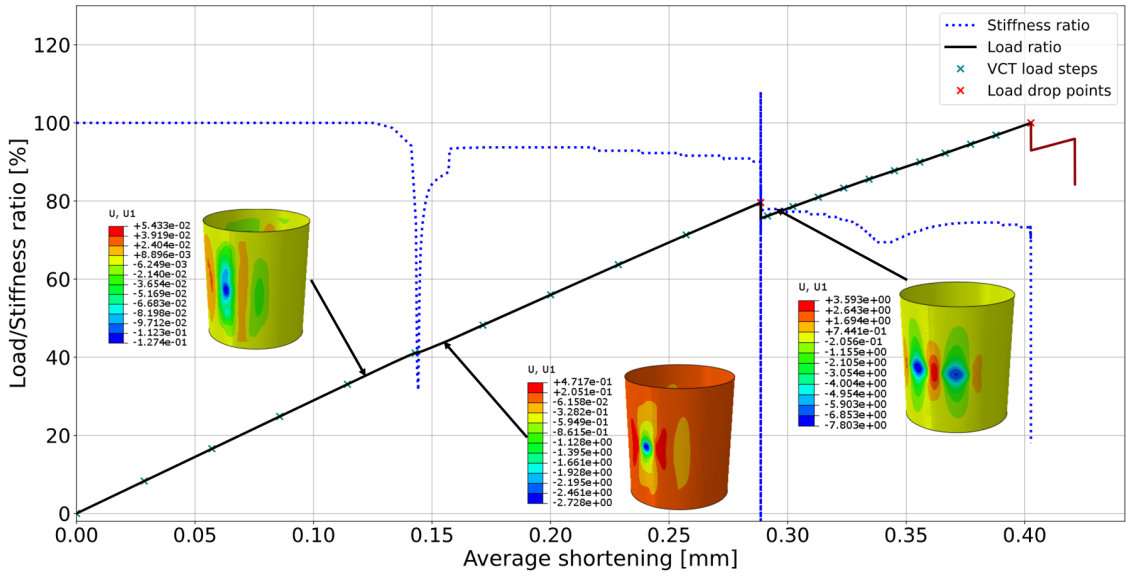

Figure 5.9 – Load ratio-displacement and stiffness ratio-displacement curves for IP=0.125 and OoP=1.5

The figure highlights that the introduced shape and loading imperfections led to

significant localised OoP displacements, particularly at the cylinder's mid-height. As the applied load increased, a distinct dimple-like local buckling pattern emerged in the region with large localised OoP displacements, occurring approximately at 40% of P_{nl} in the depicted example. Subsequently, around 80% of Pnl, a second local buckling event occurred, accompanied by an additional dimple adjacent to the initial one. At P_{nl}, yet another dimple manifested in the localised buckling pattern, beyond which increasing the applied axial displacement did not result in a higher reaction force.

This figure also highlights instances where the VCT load steps were exclusively defined at high load ratios. It is reasonable to consider that load ratios as elevated as those defined in this study may pose an excessive risk during experimental testing. Nevertheless, these VCT load steps at high load ratios were retained to explore the predictive capabilities of VCT when extending its use beyond the local buckling event. Additionally, multiple such local events may not be encountered during experimental tests, particularly if the load introduction is force-based, as local buckling may precipitate the global buckling of the cylinder. However, albeit uncommon, this behaviour may arise when the load introduction is displacement-based, as reported in [7, 50, 64, 73, 76].

Although the primary purpose of monitoring the apparent stiffness was to determine whether VCT load steps should be defined in the subsequent VCT regions in the event of local buckling occurring, there was also an additional objective. This was to detect any sudden stiffness variations in the VCT regions unrelated to load drops. Recognising these areas, akin to those depicted in the preceding figure, was crucial for elucidating scenarios where none of the monitored vibration modes were observed between consecutive load steps. In such instances, preference was given to the results obtained from the VCT steps at higher load ratios.

5.2.2 VCT results

Due to the varying evolution of vibration modes with the load applied and the occurrence of local buckling at different load ratios depending on the applied imperfection amplitudes, a direct comparison of the obtained results was not feasible. The diverse evolution of vibration modes with applied load meant that, in certain cases, there were insufficient frequency entries for the monitored vibration mode. Additionally, the occurrence of local buckling at different load ratios for different imperfection amplitudes would have required comparisons at load ratios as low as 30%, which are not recommended for reliable VCT buckling load predictions. Hence, the averaged VCT buckling prediction errors for up to 15 vibration modes were compared, instead of individual prediction errors for each mode. Furthermore, supplementary information such as the variance of the averaged errors, the averaged maximum load ratios, the number of vibration modes utilised, and the number of VCT regions defined for each case was provided. This additional information was considered valuable for a better comprehension of the results and identification of discrepancies. The results were compiled in heatmaps for all imperfection amplitudes, with heatmap cells coloured based on the averaged errors.

Figure 5.10a displays the averaged errors of the VCT predictions relative to the global buckling load using load steps in the first VCT region, analytical VCT procedure, P_{cr} for the perfect structure, and a maximum load ratio around 70%. To aid in understanding this figure, an example of the information contained in each cell is illustrated in Figure 5.10b. In the latter figure, the number in the red rectangle denotes the averaged errors of the utilised vibration modes, determining the colour of the heatmap cell. The blue rectangle provides information on the VCT regions defined for that model in the format x/y, where x represents the VCT region number for which the averaged errors are displayed and y represents the total number of VCT regions defined for that model. This information is valuable in discerning deviations among models, particularly when multiple local buckling events occur. Additionally, the green rectangle indicates the averaged maximum load ratios of the utilised vibration modes, aiding

in identifying potential deviations due to the desired load ratio not being reached. If the number of predictions within a load ratio tolerance of ±10% is less than 4, the cell information is underscored to emphasise this aspect. Finally, the purple rectangle presents information about the averaged errors in the format $\sigma : x/y$, where x represents the variance of the averaged errors shown, and y represents the number of vibration modes used. This was implemented to provide context for the averaged prediction errors and the variance itself, mitigating the risk of misinterpretation of the results.

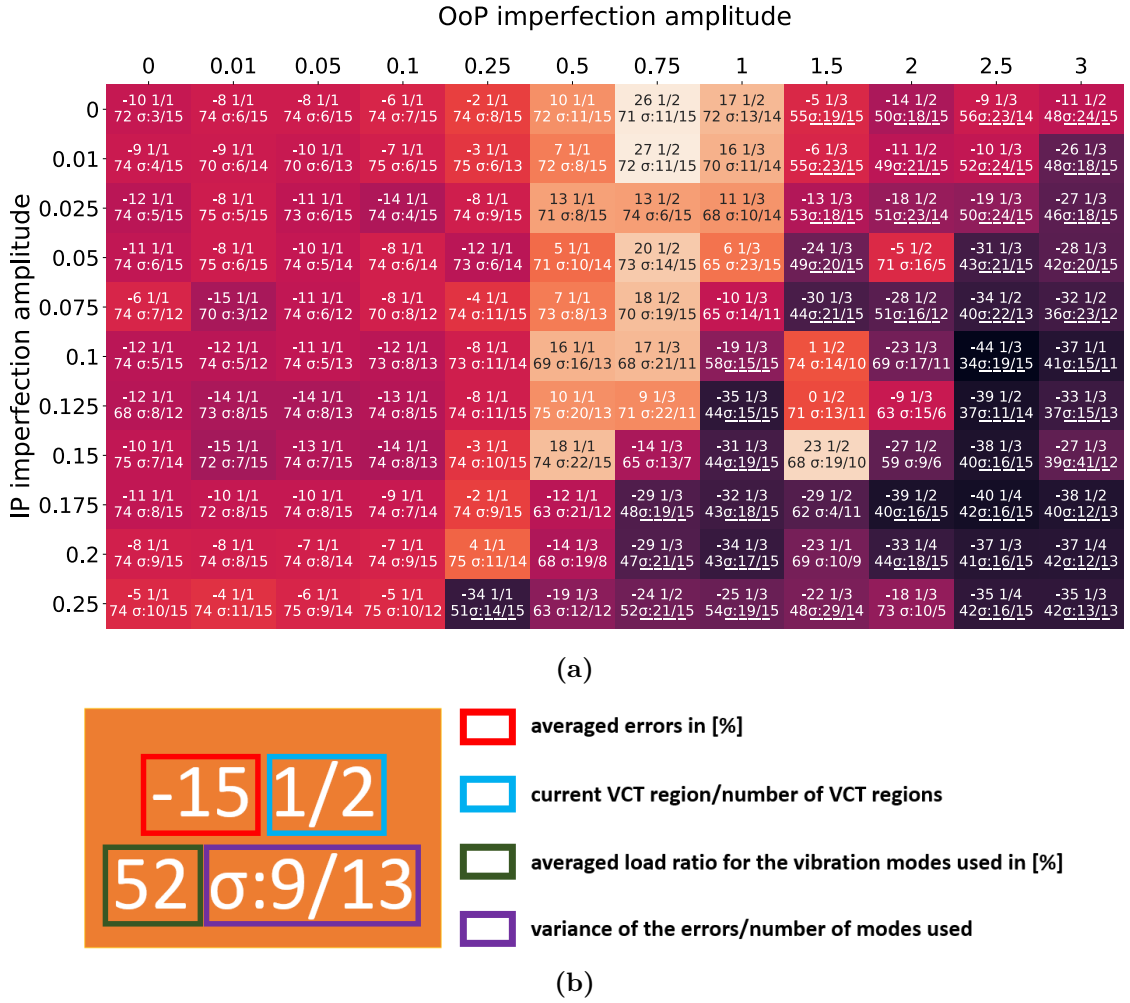

Figure 5.10 – Averaged errors heatmap for the initial VCT region for a load ratio around 70%, using the analytical VCT formulation and P_{cr} of the pristine structure (a) and heatmap cell information example (b)

Upon examining Figure 5.10a, it becomes apparent that VCT tends to provide re-

liable buckling load predictions for any given OoP and IP imperfection amplitude when the averaged maximum load ratio closely aligns with the targeted maximum load ratio. The lack of correlation between the averaged errors and the applied imperfection amplitudes suggests that VCT is generally insensitive to shape and loading imperfections, a notion also supported by VCT tests on nominally identical cylinders [50]. Even in cases where the averaged load ratio deviates from the target, primarily due to the occurrence of local buckling, as indicated by the underlined cell content, some VCT predictions remain reliable. However, when the maximum load ratio falls outside the target range, the VCT predictions tend to be generally over-conservative, especially at larger OoP and IP imperfection amplitudes.

Another noteworthy observation is that for certain OoP imperfection amplitudes, particularly between 0.5 and 1, the VCT predictions consistently tend to be unconservative. Although increasing the IP imperfection amplitude in these cases appears to mitigate the issue once a certain threshold is surpassed, it remains evident that certain OoP imperfection patterns may lead to unconservative VCT predictions. A double-check of this aspect was also performed for OoP=1, in which the mesh density was increased, and over-conservative VCT estimations were consistently found. Additionally, this behaviour was also found in VCT tests on nominally identical cylinders, in which there were instances where VCT significantly overestimated the buckling load [50], the numerical results provided here showing that shape imperfections alone can be one of the causes of this behaviour and that loading imperfections can have an influence on this aspect as well.

Upon surpassing a certain threshold of imperfection amplitudes, the variance of the averaged errors increased significantly, except for cases where only a few vibration modes could be used. This increase in variance implied that for some vibration modes, the VCT predictions were far more accurate. When selecting the best prediction for each case, only 29 out of the total 132 (22%) cases yielded an error larger than 10%, most of which being for the largest OoP and IP imperfection amplitudes.

Unfortunately, selecting the appropriate vibration mode beforehand during the experimental test can be challenging when different vibration modes yield significantly

different buckling load predictions. In this context, the quality of the second-order fit was assessed by averaging the distances between the points in the VCT characteristic chart and the fitted curve (residuals). The averaged residuals for the heatmap of averaged errors shown in Figure 5.10a are depicted in Figure 5.11, with a factor of 1E4 applied to enhance its visualisation. Moreover, the number of predictions used in computing the average residuals is presented below for a better understanding of the results and the possible differences between different imperfection amplitudes.

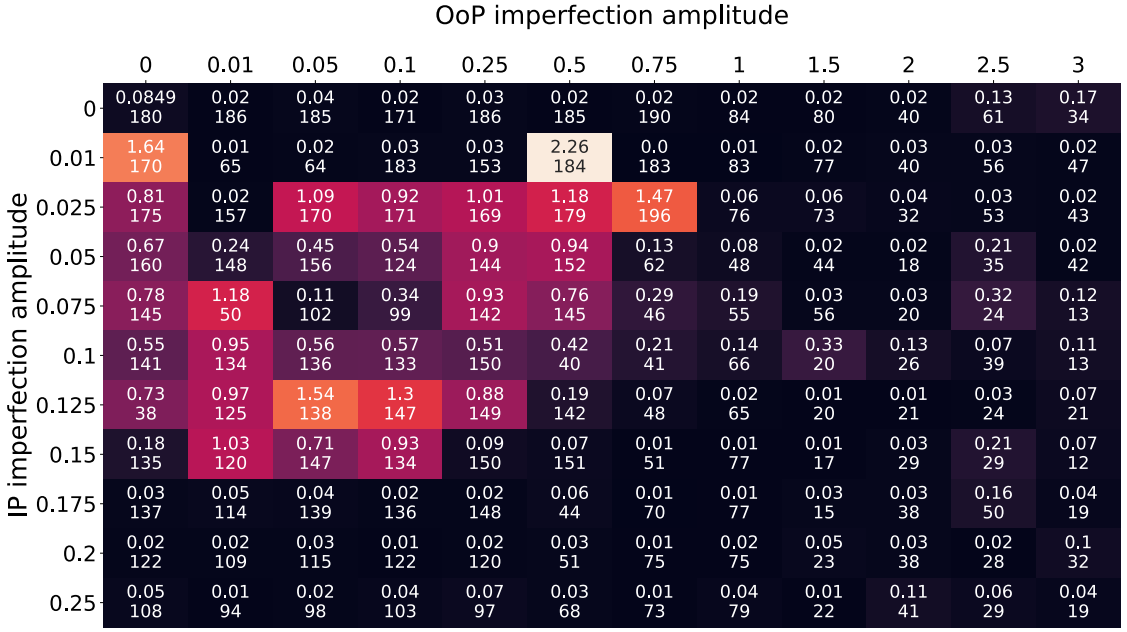

Figure 5.11 – Averaged residuals heatmap for the first VCT region, using the analytical VCT formulation and P_{cr} of the pristine structure

A comparison between the two aforementioned figures reveals that such a criterion for selecting vibration modes is not advisable, given the lack of correlation between a robust VCT prediction and the residuals of the fitted curve. Furthermore, a noticeable decrease in the number of residuals used to compute the average can be observed with increasing imperfection amplitudes, particularly with increasing the OoP one. This reduction occurs because increasing the imperfection amplitudes renders the structure more susceptible to vibration mode changes as the load increases, causing certain vibration modes to be successfully tracked across a lower number of load steps.

Figure 5.12 illustrates the averaged errors with respect to the global buckling load

utilising load steps in the second VCT region, employing the same methodology as described previously for Figure 5.10a. Unlike for the initial VCT region, no target maximum load ratio was imposed here, owing to the differing load ratios at the ends of each VCT region for the various imperfection amplitudes applied. Consequently, in this figure the underlined information now emphasises the cases where fewer than 5 vibration modes could be effectively utilised to provide a VCT prediction.

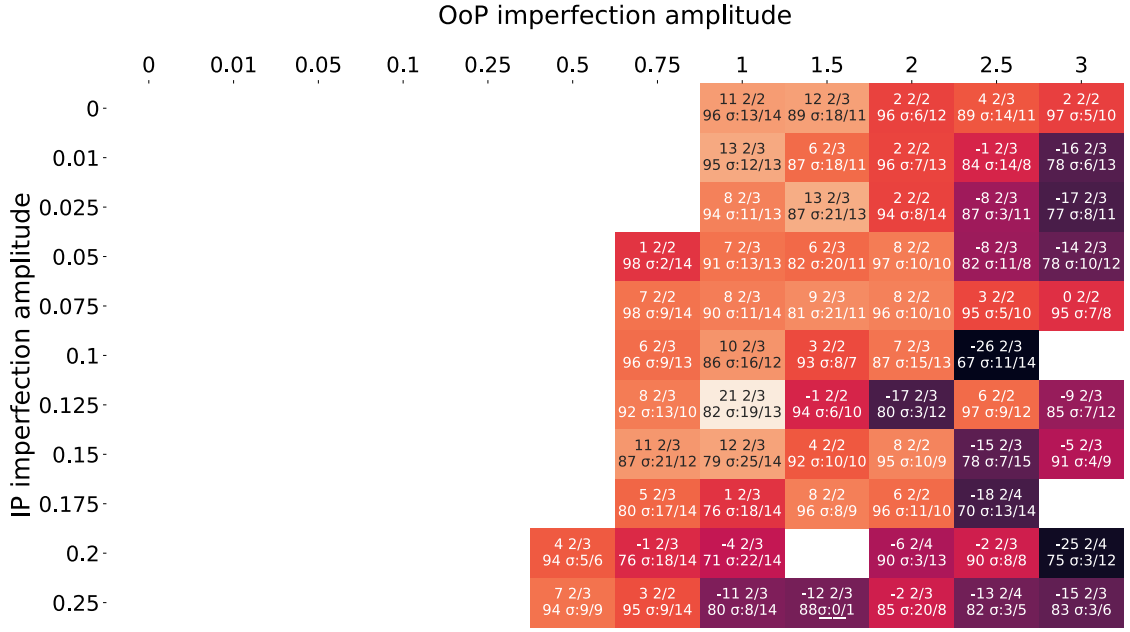

Figure 5.12 – Averaged errors heatmap for the second VCT region, using the analytical VCT formulation and P_{cr} of the pristine structure

In terms of VCT sensitivity to imperfections, the overall trends observed for the initial VCT region, along with their exceptions, also apply here. Unlike what was seen in Figure 5.10a, a distinct rise in the variance of the averaged errors with increasing imperfection amplitudes is not evident anymore. This is attributed to the more constrained ranges of load ratios used for these VCT predictions, resulting in a reduced variation in the predictions. Perhaps the most notable observation regarding these results is the inclination of the predictions to be unconservative.

Despite this, there are instances where vibration modes yield accurate VCT predictions, with only 2 out of the 62 (3%) cases displaying an error exceeding 10% when employing the vibration mode providing the best prediction. However, similar

to the results with load steps from the initial VCT region, low quadratic curve fit residuals do not necessarily indicate better predictions. Furthermore, caution is warranted when interpreting these results, given that all load levels used are at relatively high load ratios, thereby increasing the likelihood of the prediction being closer to the global buckling load. While some vibration modes exhibited a frequency response post local buckling aligning with expected behaviour when applying VCT, predictions using load steps in VCT regions beyond the initial one tended to be unconservative, rendering them generally unreliable for the VCT procedure employed here.

Another notable observation is the irregular behaviour observed in certain cases, where the frequencies of particular vibration modes increased rather than decreased as the applied load increased. This phenomenon appeared to be highly sporadic, as the load at which this behaviour occurred seemed to depend on the vibration mode and often did not correspond to a change in the model's apparent stiffness. Additionally, there were instances where, for a given vibration mode, the frequency initially increased and then decreased after reaching a certain load level, while for other vibration modes, the opposite trend was observed. Given that a decrease in vibration mode frequency is necessary to apply VCT, the load steps where an increase in frequency was observed were omitted from the prediction using that specific mode.

VCT parameter study

This study examined the impact of P_{cr} and the VCT method on prediction accuracy, as well as whether the predictions for cases with multiple VCT regions were more aligned with the local or global buckling loads. To achieve this, the averaged errors for each imperfection amplitude were compared while varying only the desired comparison parameter, and the instances where one case outperformed the other were counted. To ensure significant differences were considered, a tolerance of 5% was applied to differentiate between the compared averaged errors. The investigation also explored other variables to identify consistent combinations of VCT procedure, P_{cr}, and error type that consistently yielded robust predictions across all VCT regions. This resulted in eight comparison cases for each parameter studied and, given the

extensive analysis conducted, only an overview of the prominent trends observed is provided here, along with a discussion of these findings:

- The analytical approach works best in the initial VCT region when accuracy is desired.
- The empirical VCT procedure tends to be more conservative than the analytical one.
- P_{cr} obtained for the perfect structure generally provides the best accuracy.
- The empirical VCT procedure might be used in VCT regions beyond the initial one, when P_{cr} is obtained taking into account OoP imperfections.

This provides valuable novel insight regarding the use of VCT to predict the in-situ buckling loads of cylindrical shells, since it gives a better understanding of its predictive capabilities. When trying to predict the global buckling load using load steps in the initial VCT region, the analytical VCT method consistently gave the most accurate predictions, regardless of the P_{cr} values used, with the one for the perfect structure giving the best results. Similarly, P_{cr} for the perfect structure also seemed to provide the best results when predicting the global buckling load using the analytical procedure and load steps beyond the initial VCT region. When trying to predict the local buckling load using this method, it was noticed that these predictions were generally unconservative. Since using the P_{cr} with OoP imperfections taken into account generally lowers the predictions, using this value alleviated this issue somewhat, but the predictions became over-conservative after a certain OoP imperfection amplitude was exceeded.

It was also noticed that the empirical VCT procedure was more conservative than the analytical one, aspect also reported in [50]. This represents the main reason why this method generally gave better local buckling predictions, particularly when OoP imperfections were taken into account in the linear buckling analysis. This procedure was also found to be better than the analytical method in predicting the global buckling load when using load steps beyond the initial local buckling. This was regardless of the P_{cr} used and the differences between this method and the analytical

one were only marginal, most likely due to the restricted load ratio intervals of the load steps defined in these VCT regions. These predictions were considered better here than the ones obtained using the analytical method primarily because they were less unconservative, although not necessarily more accurate overall.

Figure 5.13 shows the averaged VCT prediction errors with respect to the global buckling load where the empirical VCT procedure was employed, using the P_{cr} that takes into account the OoP imperfections. When comparing this figure with its counterpart Figure 5.12, where P_{cr} for the perfect structure was used together with the analytical VCT procedure, a clear improvement regarding the unconservative predictions can be seen. Furthermore, the variance of the averaged errors is generally smaller, which can increase the confidence with regard to the obtained result. However, as previously mentioned, while using the P_{cr} that includes OoP imperfections can improve the unconservative predictions for some cases, it might also result in over-conservative predictions for others. While the overall accuracy is slightly lower than when the P_{cr} for the perfect structure was used, the more conservative nature of this approach is worth taking into account if predicting the global buckling load using load steps after local buckling has occurred is desired.

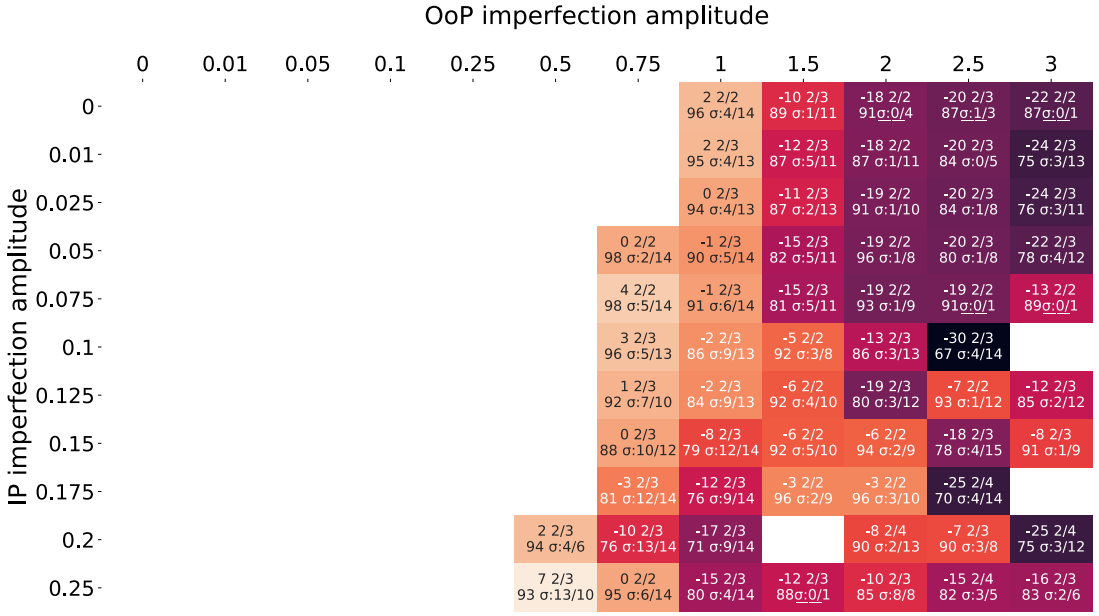

Figure 5.13 – Averaged errors heatmap for the second VCT region using the empirical VCT procedure and the P_{cr} taking into account OoP imperfections

Experimental validation

To add proper credibility to the possible use VCT with load steps defined beyond local buckling, as observed in the numerical investigation, experimental proof is needed. The particular change in the frequency response as observed in the numerical results upon local buckling occurring was found in the VCT results for multiple cylinders tested at the Technical University of Riga in an extensive experimental campaign focusing on the robustness of VCT for buckling load predictions for cylindrical shells under axial compression [51]. Two of these cylinders, labelled *D500H500L2N-02* and *D500H750L2N-01*, were therefore selected for an experimental validation.

Table 5.3 displays the dimensions, such as diameter, height, as well as the linear and experimental buckling loads of both cylinders. These cylinders were built using a Unipreg unidirectional prepreg material, with a lamina thickness of 1.044mm and the following layup [$\pm 24°/\pm 41°$]. The averaged material properties, measured via strain gauges, are shown in Table 5.4, where the subscripts T/C denote Tension/-Compression. The cylinder's manufacturing process involved manual lay-up on steel mandrels, followed by curing in vacuum bags for one hour at 80°C, and an additional three hours at 130°C [50].

D500H500L2N-02		D500H750L2N-01	
D=500 [mm]	L=500 [mm]	D=500 [mm]	L=750 [mm]
P_{cr}=16.54 [kN]	P_{exp}=10.47 [kN]	P_{cr}=17.02 [kN]	P_{exp}=9.65 [kN]

Table 5.3 – *D500H500L2N-02* and *D500H750L2N-01* cylinders' geometry, linear and experimental buckling loads

E_{1T}	E_{1C}	E_{2T}	E_{2C}	G_{12}	ν_{12}
116.44 [GPa]	91.65 [GPa]	6.73 [GPa]	6.39 [GPa]	3.63 [GPa]	0.34

Table 5.4 – Unipreg material properties [1]

The cylinders were tested using a Zwick Z100 quasi-static testing machine, where a displacement loading rate of 1mm per minute was applied. Parallel plates were used to introduce the load, with the testing machine's loading cell recording the load. The shortening of the cylinder was measured by averaging the measurements from three

LVDTs equally spaced across its circumference. The cylinder's vibration response was assessed using a Polytec laser vibrometer, with the frequencies of the measured modes and their corresponding loads shown in Table 5.5 [51].

D500H500L2N-02		D500H750L2N-01	
Load [kN]	Frequency [Hz]	Load [kN]	Frequency [Hz]
0	174.5	0	113.5
0.356	173.5	0.616	113
0.654	172	0.938	112
1.003	171	1.33	111
1.354	169.5	1.668	110.5
1.668	168.5	1.981	109.5
1.991	167	2.313	108.5
2.398	165.5	2.656	108
2.654	164.5	2.972	107
2.952	163	3.313	106
3.353	161.5	3.6	105
3.659	160	3.949	104
3.957	159	4.97	103.5
4.413	157	5.337	102.5
4.65	156	5.666	101.5
4.992	154.5	5.995	100.5
5.359	153	6.309	99.5
5.663	151.5	6.614	98.5
5.917	151.5	6.958	97
6.344	149.5	7.316	96
6.658	148	7.611	94.5
6.971	146.5	7.913	93.5
7.34	144.5	8.309	91.5
7.651	142.5	8.612	90
7.992	141		
8.347	139		
8.654	137		
8.963	135.5		

Table 5.5 – D500H500L2N-02 and D500H750L2N-01 cylinders' load-frequency response

In Figure 5.14, the characteristic VCT chart of the analytical VCT method is displayed for the *D500H750L2N-01* cylinder, where the initial load step was omitted due to inconsistent boundary conditions at insignificant load ratios.

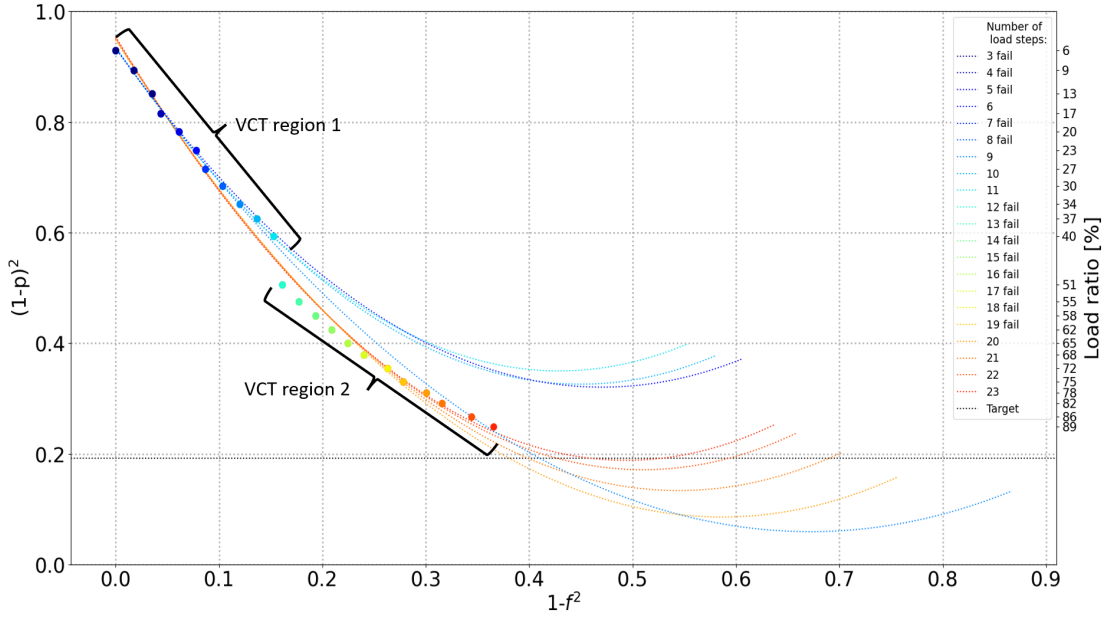

Figure 5.14 – D500H750L2N-01 VCT characteristic chart, analytical method

Using the data from Table 5.5, progressive quadratic fits were conducted by gradually increasing the load ratio. The targeted value, corresponding to the experimental buckling load, is shown as a black dotted horizontal line, while the load ratios are provided on the right vertical axis. A significant alteration in the frequency response of the cylinder is evident between the consecutive measurements at 40% and 51% load ratios, rendering the progressive predictions from the 12^{th} to the 19^{th} VCT load step unsuccessful. Upon the resumption of successful progressive predictions, it was observed that they decreased as the load ratio increased, deviating from the general trend. A similar behaviour was noted for the cylinder *D500H500L2N-02*, albeit with all progressive quadratic fits succeeding after the observed frequency response change, due to its smaller magnitude.

Given this significant change in the vibration response of the cylinder, the VCT load steps were divided into two distinct regions. Figures 5.15a and 5.15b illustrate the relative prediction errors with respect to the experimental buckling loads for

the *D500H500L2N-02* and *D500H750L2N-01* cylinders. The black curves represent progressive VCT predictions using all load steps, while the dark red curves represent predictions using only the load steps in the second VCT region. Solid lines depict VCT predictions using the analytical VCT method, whereas dashed lines represent predictions using the empirical VCT method.

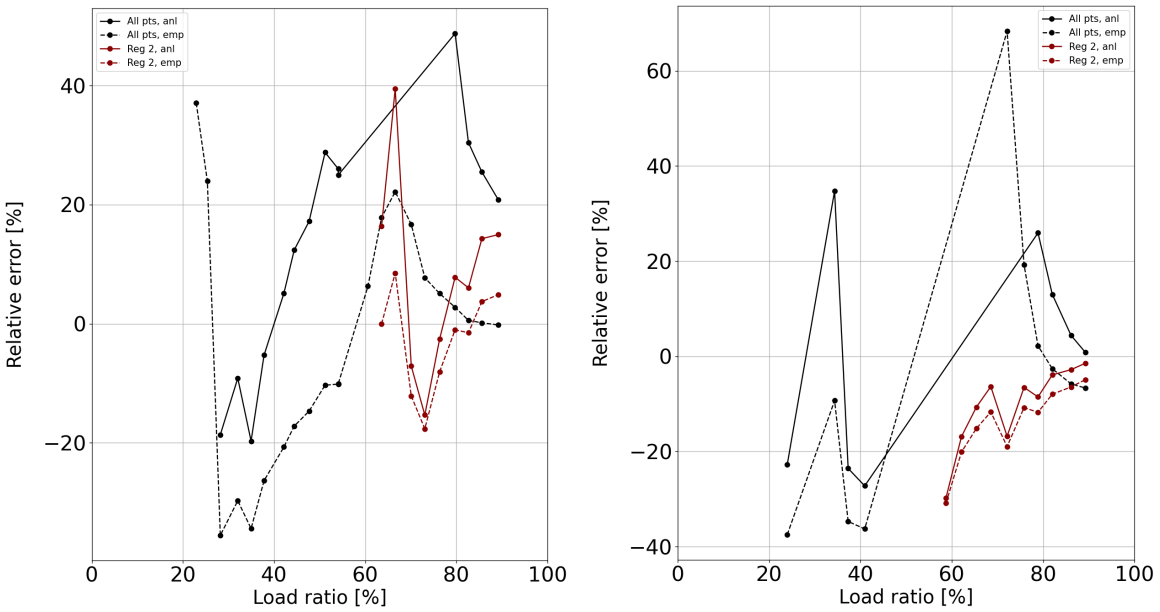

Figure 5.15 – Relative VCT buckling load prediction error with respect to the experimental buckling load of the analytical and the empirical VCT methods for D500H500L2N-02 a) and D500H750L2N-01 b) cylinders

Upon examining these figures, and comparing the solid lines with their dashed counterparts, it becomes evident that the latter are generally lower, indicating the empirically derived method's more conservative nature relative to the analytical approach. Additionally, a closer inspection reveals a higher likelihood of the empirical method to yield more successful predictions, as evidenced by the greater number of points along the dashed curves. Utilising load steps following a change in the cylinders' frequency response led to successful predictions for all available load steps, irrespective of the VCT method employed, and exhibited greater robustness compared to the analytical method in which all available load steps were utilised. However, while the empirical method utilising all load steps provided the best prediction for the *D500H500L2N-*

02 cylinder, for the *D500H750L2N-01* one, the best overall accuracy was attained by utilising all available load steps with the analytical method, albeit resulting in slightly less conservative predictions. Compared to the numerical results, a similar trend to that observed for the *D500H750L2N-01* cylinder emerged, with the utilization of load steps after the frequency response change generally yielding improved VCT buckling load estimations.

5.3 Conclusions

This chapter delved into the VCT's efficacy in predicting the buckling load of cylindrical shells under axial compression, considering various shape and loading imperfection amplitudes. The study also explores whether shape imperfections should be accounted for in the computation of P_{cr} or if, in cases of local buckling, VCT better predicts local, rather than global buckling loads for two VCT procedures.

The results indicate that VCT shows relative insensitivity to both shape and loading imperfections, as there is no discernible trend in the accuracy of averaged prediction errors depending on the applied imperfection amplitudes. This finding aligns with numerous experimental tests where VCT provided robust global buckling load predictions. However, specific shape imperfections may affect both the accuracy and conservatism of VCT buckling load predictions. Nevertheless, in such cases, VCT predictions typically decrease with increasing load ratio, simplifying the detection of this behaviour through a series of VCT predictions performed while incrementally raising the maximum load ratio.

In the cases where no local buckling occurred, the analytical method utilising P_{cr} for the perfect structure yielded optimal results consistently. While the global buckling load predictions using this method and load steps beyond initial local buckling were in general more accurate, but also more unconservative, than the empirical method's predictions, the disparity between the two VCT procedures was generally marginal in this regard. Similarly, for the subsequent VCT regions, employing P_{cr} for the perfect structure yielded the best accuracy overall.

Comparing the averaged predictions against local buckling loads revealed that using the analytical VCT method and P_{cr} for the perfect structure was often unconservative and inconsistent across multiple imperfection amplitudes. Incorporating shape imperfections into the linear buckling analysis and using the empirical VCT procedure improved the predictions for certain imperfection amplitudes, but led to overly conservative predictions for larger imperfection amplitudes. Therefore, using VCT to predict local buckling loads is not advisable.

Numerical findings suggest that predicting global buckling using load steps after local buckling occurs may be feasible. However, the established analytical VCT procedure and employing P_{cr} for the perfect structure often yield unconservative predictions. Including shape imperfections in the linear buckling analysis and utilising the empirical VCT procedure appears more reliable, resulting in more conservative averaged errors and reduced variance.

Furthermore, the trends observed in the numerical analyses were also found when using published experimental data. Notably, the measurements from two cylinders under axial compression, where a sudden change in frequency response was observed, confirmed the possibility of achieving robust VCT buckling load predictions using load steps after such frequency response changes.

Additionally, the empirical method's conservatism compared to the analytical one and the effect of frequency response changes on VCT predictions were also evident in the investigations based on experimental data. When all load steps were used, the frequency response changes triggered decreasing VCT buckling load predictions with increasing load ratios, rendering several predictions unsuccessful beyond this event. Conversely, using load steps exclusively after the frequency response change occurred yielded more robust VCT buckling load predictions compared to those using all load steps and the analytical VCT procedure, the predictions generally increasing with the maximum load ratio used as well.

6 VCT sensitivity towards combined loading

While compression buckling is a primary sizing criterion in the design of cylindrical shells, experimental campaigns aimed at validating these structures often consider combined load cases, where bending, transverse shear, torsion, or pressure loads are applied alongside axial compression. Among these combined load scenarios, the most extensively documented in the context of VCT is the combination of compression and pressure [4, 52, 66, 77], for which an analytical validation also exists. Additionally, the compression-torsion load case has been numerically validated in [52], where the torque level remained constant throughout the VCT load steps.

Given the general lack of studies on the robustness of VCT in predicting the compressive buckling loads of cylindrical shells under combined loading, this study numerically investigates the capability of VCT in this regard for bending, shear, and torsion loads applied in conjunction with the primary compression load, using the geometry and shape imperfections of six cylinders. Furthermore, the study examines the sensitivity of the analytical VCT procedure to varying magnitudes of additional loads applied alongside compression, the impact of including these additional loads in the linear buckling analysis used to determine the value of P_{cr}, and the effect of the load application sequence.

6.1 Methodology

Due to the limited prior research on using VCT to determine the compressive load at which cylindrical shells buckle under combined loading, six cylinders from existing literature were selected to evaluate the applicability of VCT for such load cases. The cylinder configurations chosen for this study include Z15 [2, 10], ZD27-29 [57], SST1 [3], and Z37 [3], all of which have been tested for buckling under axial compression. Except for Z15, VCT was also employed during the experimental tests of these cylinders, providing reliable buckling load estimates. Although experimental VCT was not performed in the buckling test of Z15, this cylinder was included in the study as a numerical benchmark, owing to the excellent accuracy of its numerical VCT buckling load estimation and its low sensitivity to the maximum load level used. Table 6.1 presents the nominal geometries of the investigated cylinders and their construction materials, while the material properties and layups are detailed in Table 6.2.

Cylinder	R [mm]	L_{free} [mm]	L_{tot} [mm]	t [mm]	Material
Z15	250	500	540	0.5	Hexcel IM7/8552
ZD27-29	250	560	600	0.5	Hexcel IM7/8552
SST1	250	500	550	0.5	AISI 304
Z37	400	800	840	0.75	Hexcel IM7/8552

Table 6.1 – Cylinder dimensions and materials

Cylinder	Layup	ρ [g/cm^3]	E_1 [GPa]	E_2 [GPa]	G_{12} [GPa]	ν_{12}
Z15	[±24°, ±41°]	1.58	142.5	8.7	5.1	0.28
ZD27-29	$[\pm 45°]_s$	1.58	142.5	8.7	5.1	0.28
SST1	-	7.8	193	-	77	0.29
Z37	[±34°, 0_2, ±53°]	1.58	142.5	8.7	5.1	0.28

Table 6.2 – Material properties of the Hexcel IM7/8552 UD CFRP ply and AISI 304 steel [2–4].

The robustness of VCT was examined in the presence of three additional load types applied alongside compression: bending, shear, and torsion. Since torsion loads in-

herently induce material shear in cylindrical shells, this study considers shear load in a more general sense, introducing it as an in-plane (lateral) displacement at the top edge of the cylinders, causing an axial misalignment between the top and bottom edges. The other two loads were introduced via rotations, with bending loads being applied to both the top and bottom ends of the cylinders, while torsion was applied only at the top end. To determine the magnitude of these displacements and rotations, non-linear analyses were conducted to establish reference values, corresponding to the points where the relationship between the applied displacements/rotations and the corresponding reaction forces/moments ceased to be linear.

For pure bending loads, this procedure was relatively straightforward due to the unstable buckling response of cylinders under bending, with reference rotations identified at the points of maximum reaction moments. However, for pure shear or torsion, clear drops in reaction forces/moments were not always observed across all cylinders. Thus, the reference displacements/rotations were determined at the points where the apparent stiffness, defined as the change in reaction force/moment relative to the applied displacement/rotation between consecutive analysis increments, decreased by more than 5% from the initial value. Once these reference displacements/rotations were determined, they were applied alongside compression, both individually in magnitudes of [10, 20, 30, 40, 50]% and together in magnitudes of [10, 20, 30]%, to assess the robustness of VCT under combined loading scenarios.

Regarding the applicability of VCT for combined load cases, an adjustment can be made to the load introduction sequence and definition of the VCT load steps to make the procedure more similar to the standard one for axial compression. This approach involves a sequential load introduction, where the additional loads are applied before compression, therefore the VCT load steps are defined at varying levels of compressive loading alone, while holding the additional loads constant. This ensures that the primary influence on the frequency response change comes from the compression load, with the additional loads acting as "imperfections", increasing thus the likelihood that the points on the VCT characteristic chart would follow a quadratic descent as compression load increases.

Conversely, when loads are introduced simultaneously, the additional loads directly influence the frequency response change, reducing the chances of a quadratic descent in the VCT characteristic chart as the compression load increases. Since this scenario is common in validation tests, the applicability of VCT for combined load cases was investigated for both a sequential and a simultaneous introduction of additional loads alongside compression.

When the points in the VCT characteristic chart display a quadratic decrease with increasing load levels, the accuracy of VCT largely depends on the value of P_{cr}. Typically, this value is calculated for the perfect structure, which generally yields reliable VCT predictions of buckling loads under axial compression. However, this reliability may diminish when additional loads are applied, as these loads are expected to both reduce the axial buckling load and alter the quadratic relation between the VCT load and frequency parameters. Moreover, the test article may differ significantly from its nominal configuration, with P_{cr} being highly sensitive to geometric and material imperfections. Hence, to evaluate the robustness of VCT under combined load conditions, the P_{cr} values used to obtain the VCT predictions were determined under 4 distinct scenarios:

- P_{cr_p} - perfect cylinder under pure compression
- P_{cr_i} - imperfect cylinder under pure compression
- P_{cr_cp} - perfect cylinder under combined loading
- P_{cr_ci} - imperfect cylinder under combined loading

The robustness of VCT for combined load cases was evaluated by monitoring both the prediction accuracy of the buckling loads compared to those obtained from non-linear analyses and the extent to which this accuracy differs from the pure compression load case. Since VCT is expected to produce reliable results even when using higher vibration modes, the first six vibration modes were used to make progressive buckling load estimations while gradually increasing the maximum load level. Utilising multiple vibration modes also provides better insight into the robustness of VCT for combined

load cases, as the accuracy of VCT predictions can vary depending on the cylinder, the type and magnitude of the additional loads applied, as well as on the vibration mode used.

The impact of additional loads on the VCT predictions was evaluated by assessing the averaged relative errors of the VCT estimates with respect to P_{nl}. In computing these averages, only the predictions for which the maximum load level was between 60% and 80% with respect to P_{nl} were used. This specific load ratio interval was selected based on practical considerations and on the investigation regarding the influence of this parameter over the VCT predictions shown in Chapter 4. The lower limit at 60% was chosen given the reliable predictions obtained at this load level using numerical data, as well as due to the low risk of buckling occurring during an experiment at this load level with respect to a best estimation resulting from the preliminary analysis. Conversely, the upper limit at 80% was chosen due to both the reliable predictions obtained based on experimental data at this load level (including the influence of measurement errors) shown in Chapter 4, and to the relatively low risk of buckling occurring during an experiment at this load level with respect to a best estimate resulting from a thorough preliminary analysis.

6.2 FE models

The numerical models of the cylinders were created using Abaqus FE software and were modelled with S8R shell elements. The number of elements varied between cylinders, depending on the mesh refinement required for convergence. Table 6.3 provides a summary of the mesh configurations for each cylinder, while Figure 6.1 gives an overview of the applied loads (highlighted in bold) and boundary conditions.

In Figure 6.1, the areas of the undeformed cylinder mesh highlighted in red represent the overhang regions, which correspond to the difference between L_{tot} and L_{free} in Table 6.1. These overhang areas were radially supported during the experimental tests of the cylinders, and in the numerical models were fully coupled to reference points at the top and bottom ends, centrally located with respect to the cylinder cross-sections.

These reference points were used to apply boundary conditions and introduce loads. The coupling ensured that the nodes in the overhang areas followed the rigid body motion of their corresponding reference points, maintaining their relative positions throughout the analysis. All degrees of freedom at these reference points, except those used to apply the loads, were constrained.

Cylinder	Elements across circumference	Elements across height	Total no. of elements
Z15	120	42	5040
ZD27	180	68	12240
ZD28	180	70	12600
ZD29	192	78	19776
SST1	200	70	14000
Z37	140	50	7000

Table 6.3 – Summary of the cylinder's mesh definitions

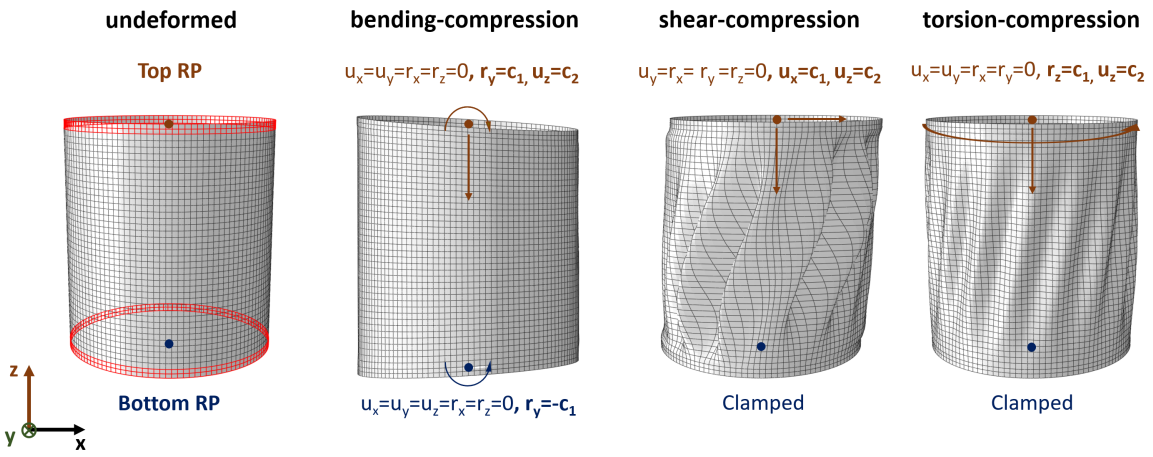

Figure 6.1 – FE models loads and boundary conditions

The boundary conditions described, and shown in Figure 6.1, were similar or identical to those used in previous studies on the buckling response of cylindrical shells under bending [78–88], transverse shear [89–96], or torsion [97–104] in conjunction with axial compression. These boundary conditions were applied for both the sequential and simultaneous load introduction procedures.

For a sequential load introduction, the additional loads (besides compression) were introduced in a separate analysis step, where a rotation/displacement c_1 was applied at the relevant reference points, the axial translation at the top being allowed at this point. The compression load c_2 was then introduced in a subsequent analysis step via

an axial displacement at the top reference point, while the initial rotation/displacement was held constant. When bending, shear, and torsion were applied together with axial compression, the same boundary conditions as for bending were specified at the bottom reference point, while at the top reference point, the conditions $u_y = r_y = 0$ were applied, as the other degrees of freedom were used to introduce the additional loads.

The shape imperfections of all cylinders were measured and incorporated into the FE models using the inverse averaging method described in [7], which adjusts the radial coordinates of the nodes. Additionally, thickness imperfections were measured and included for the Z15 and ZD27-29 cylinders, following the procedure outlined in [67], and briefly described in Chapter 4. In this approach, the material properties of the elements were modified using the rule of mixtures, assuming that any difference between the measured and nominal thickness is due solely to variations in resin quantity. On average, the influence of both shape and thickness imperfections was also accounted for in the models used to determine P_{cr} for the idealised cylinder configurations. These models employed the mean radius derived from the measured shape imperfections and material properties based on the average thickness.

Initial estimates of the P_{cr} values in the presence of the aforementioned additional loads were obtained by introducing these loads in a non-linear analysis step, followed by a linear buckling analysis step in which compression was applied. These initial P_{cr} estimates were then validated by performing linear buckling analyses in which the additional loads and their corresponding initial P_{cr} estimates were introduced simultaneously in a single analysis step. The eigenvalues obtained were checked to ensure they fell within a 1 ± 0.01 range. A similar procedure was used for non-linear analyses involving sequential introduction of additional loads, with the difference being that the second analysis step was also non-linear, and an axial displacement was applied to the top reference point.

6.3 Results

6.3.1 Buckling

Table 6.4 presents the buckling loads obtained from various analyses: linear buckling of pristine P_{cr_p} and imperfect P_{cr_i} cylinders, non-linear analyses with imperfections P_{nl}, and experimental results P_{exp}. Generally, the inclusion of detailed imperfections in the linear buckling analysis led to a reduction in P_{cr} values, with the exception of the ZD27 cylinder, where P_{cr_p} was smaller than P_{nl}. For ZD27, the increase in buckling load when accounting for imperfections was due to the inability to accurately represent the imperfection pattern using a perfect circular shape, even with the mean radius derived from measured shape imperfections and material properties corresponding to the mean thickness.

Cylinder	P_{cr_p} [kN]	P_{cr_i} [kN]	P_{nl} [kN]	P_{exp} [kN]
Z15	30.41	29.99	24.70	23.36
ZD27	23.27	29.57	25.89	20.47
ZD28	22.3	21.57	19.8	21.49
ZD29	25.01	21.66	19.14	21.86
SST1	182.56	112.25	101.6	70.2
Z37	89.43	87.31	73.84	59.0

Table 6.4 – Cylinder buckling loads summary

Significant discrepancies between model predictions and experimental results were observed for the ZD27, SST1, and Z37 cylinders, likely due to other imperfections related to loading, boundary conditions, or material properties that were not fully captured in the FE models. For reference, the study shown in [4] reported a difference of approximately 25% in the buckling loads of ZD27 measured at two different testing facilities, underscoring the high sensitivity of cylindrical shells to loading and boundary conditions imperfections. In the table above, the higher experimental buckling load P_{exp} for the ZD27 cylinder is shown, as the lower one measured at the second

facility was likely due to the loading and boundary conditions imperfections present in that test.

Figure 6.2 illustrates the ratios of P_{cr_cp}, P_{cr_ci}, and P_{nl} relative to P_{cr_p} for various magnitudes of bending loads applied alongside compression, the 0% amplitude representing the pure compression load case. To enhance clarity, vertical blue lines are drawn to separate the results for different cylinders. The figure shows that the inclusion of imperfections had varying effects on the buckling loads of the cylinders. In most cases, a reduction in buckling load was observed, with the SST1 cylinder exhibiting the most significant decrease. This high sensitivity to imperfections for SST1 was also confirmed experimentally [3], as shown in Table 6.4 and mentioned earlier in Chapter 5.

Figure 6.2 – P_{cr_cp}, P_{cr_ci} and P_{nl} ratios with respect to P_{cr_p} in presence of bending

For all cylinders, the buckling loads decreased as the magnitude of the applied bending load increased, with the rates of decrease being relatively consistent across the different cylinders, except for SST1 when shape imperfections were present. In the case of SST1, the rate at which P_{nl} decreased with increasing bending load differed from the others, primarily due to the occurrence of local buckling at a lower load level than the maximum one reached. This local buckling was influenced by the cylinder's imperfection pattern and was also the reason why a significant difference between P_{nl} and P_{cr} under pure compression was found. However, for the highest magnitude of bending load, where local buckling did not occur, the P_{nl}/P_{cr_p} ratio was similar

to that of the other cylinders. Additionally, for this cylinder also a slight initial increase of the P_{cr_ci} with the bending load magnitude was seen. This likely occurred due to the reduction of compression load in the cylinder area in which local buckling occurred due to the applied bending load. Nevertheless, the P_{cr_ci} decrease for the highest magnitude of bending applied was also in line with the ones for the other cylinders.

Figure 6.3 depicts the ratios of P_{cr_cp}, P_{cr_ci}, and P_{nl} relative to P_{cr_p} for various magnitudes of shear loads applied alongside compression. Unlike bending, the effect of shear on the compressive buckling loads varied significantly among the cylinders. Generally, P_{cr_cp} decreased for all cylinders, but at the lowest shear magnitude, this decrease was notable only for the Z15 and SST1 cylinders.

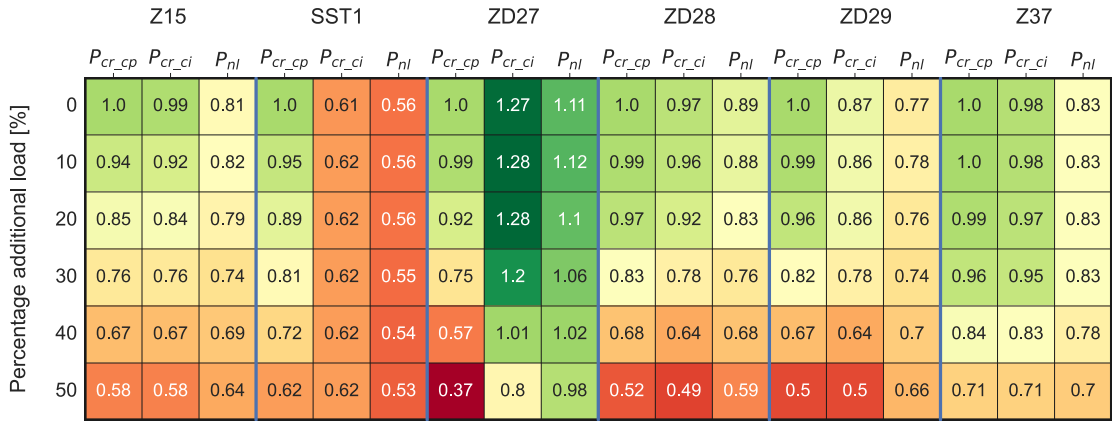

Figure 6.3 – P_{cr_cp}, P_{cr_ci} and P_{nl} ratios with respect to P_{cr_p} in presence of shear

For some cylinders, both P_{cr_ci} and P_{nl} initially increased with increasing the shear load. The rate of change in buckling load relative to shear magnitude also varied among the cylinders, with Z37 and ZD27 being at the extremes. Increasing shear load generally reduced the P_{cr_ci} values, except for SST1, where no significant changes were observed compared to the pure compression load case. Non-linear analyses also generally showed a decrease in buckling load with increasing shear, with the relative reduction in P_{nl} varying among cylinders. The smallest reduction was 0.7 for Z37, and the largest was 0.53 for SST1. For SST1, P_{nl} showed minimal variation with increasing shear load, due to local buckling occurring at all shear levels. Unlike bending, shear had a lesser effect on the maximum load reached for this cylinder,

primarily due to local buckling. Also, an important observation is that for certain shear magnitudes, P_{nl} exceeded both P_{cr_cp} and P_{cr_ci} for several cylinders. This represents an unrealistic behaviour in the context of VCT, where the ratios between P_{nl} and P_{cr} should be less than 1.

Figure 6.4 presents the ratios of P_{cr_cp}, P_{cr_ci}, and P_{nl} relative to P_{cr_p} for different magnitudes of torsion loads applied alongside compression. As with the previous cases, the influence of additional torsion load varied among cylinders. For the ZD cylinders, P_{cr_cp}, P_{cr_ci}, and P_{nl} generally increased with the magnitude of the torsion load. In contrast, other cylinders exhibited a decrease in these values as the torsion load magnitude increased.

Percentage additional load [%]	Z15			SST1			ZD27			ZD28			ZD29			Z37		
	P_{cr_cp}	P_{cr_ci}	P_{nl}	P_{cr_cp}	P_{cr_ci}	P_{nl}	P_{cr_cp}	P_{cr_ci}	P_{nl}	P_{cr_cp}	P_{cr_ci}	P_{nl}	P_{cr_cp}	P_{cr_ci}	P_{nl}	P_{cr_cp}	P_{cr_ci}	P_{nl}
0	1.0	0.99	0.81	1.0	0.61	0.56	1.0	1.27	1.11	1.0	0.97	0.89	1.0	0.87	0.77	1.0	0.98	0.83
10	0.93	0.91	0.79	0.94	0.61	0.55	1.02	1.3	1.15	1.02	0.98	0.91	1.02	0.89	0.8	1.0	0.98	0.82
20	0.85	0.83	0.76	0.87	0.6	0.53	1.04	1.32	1.17	1.03	1.0	0.93	1.04	0.91	0.82	1.0	0.98	0.81
30	0.76	0.75	0.72	0.79	0.59	0.52	1.06	1.34	1.2	1.05	1.01	0.94	1.05	0.93	0.83	1.0	0.97	0.79
40	0.68	0.67	0.67	0.7	0.57	0.51	1.07	1.36	1.21	1.06	1.02	0.95	1.07	0.94	0.84	0.88	0.86	0.75
50	0.59	0.58	0.62	0.6	0.53	0.5	1.06	1.38	1.21	1.08	1.03	0.93	1.08	0.94	0.84	0.75	0.73	0.69

Figure 6.4 – P_{cr_cp}, P_{cr_ci} and P_{nl} ratios with respect to P_{cr_p} in presence of torsion

Additionally, P_{nl} was only higher than P_{cr_cp} and P_{cr_ci} for the Z15 cylinder when subjected to 50% of the reference torsion load, namely the load level at which this cylinder buckled under pure torsion in the non-linear analysis.

Figure 6.5 displays the ratios of P_{cr_cp}, P_{cr_ci}, and P_{nl} relative to P_{cr_p} for various magnitudes of bending, shear, and torsion loads applied alongside compression. The figure reveals that the effect of these additional loads was similar to that of bending alone, as a general trend of decreasing buckling loads with increasing the additional loads is observed. The only exception to this trend is for the SST1 cylinder, which showed a slight initial increase in P_{cr_ci}.

An important point to highlight here is that the compressive buckling loads under

additional bending or shear can vary significantly depending on the direction of these loads when imperfections are present. This study focuses on evaluating whether VCT can reliably predict the axial load at which cylinders buckle in the presence of additional loads. For this purpose, the key factor was the consistency of the load application direction, rather than the specific load application direction itself. However, in practical scenarios, the alignment of bending or shear loads with respect to the cylinder's imperfections is crucial for achieving accurate correlations between experimental and numerical data.

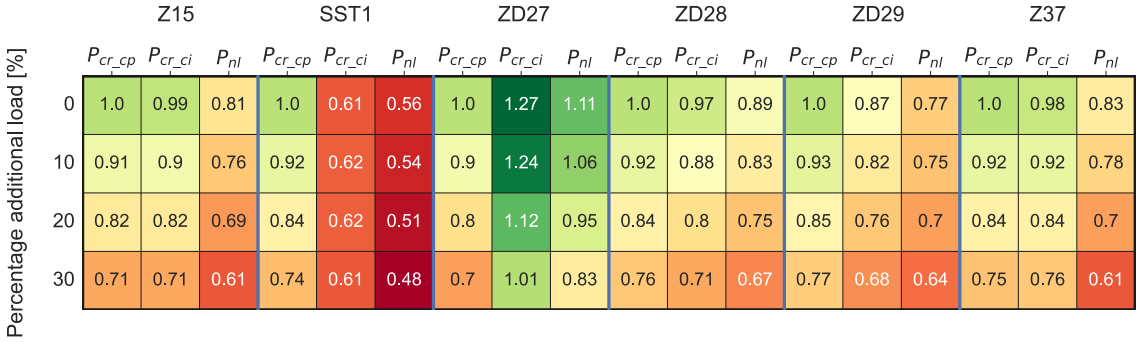

Figure 6.5 – P_{cr_cp}, P_{cr_ci} and P_{nl} ratios with respect to P_{cr_p} in presence of bending, shear and torsion

6.3.2 VCT results

This section examines the robustness of the VCT predictions on the axial load at which buckling occurs under the influence of additional bending, shear, and torsion loads, applied either individually or together alongside axial compression. In this investigation, the additional loads were applied either before or simultaneously with axial compression, and the robustness of the VCT predictions was evaluated using two metrics: the relative error compared to axial buckling loads obtained from non-linear analyses P_{nl}, and the change in relative error from the axial compression load case for which the VCT approach was initially developed. Additionally, the impact of incorporating shape imperfections and additional loads into the buckling analysis to determine the reference P_{cr} value was also explored.

VCT in presence of bending

Figure 6.6 illustrates the relative errors with respect to P_{nl} of the VCT predictions for the axial load at which buckling occurs under various magnitudes of additional bending applied before compression. Additionally, the differences in relative errors between the predictions for the combined load case and those for the pure compression load case are also shown. In this figure, besides the vertical blue lines drawn to differentiate the results for different cylinders, a horizontal blue line was also drawn to separate the relative errors of the VCT predictions from the differences between the errors for the bending-compression load case and those for the pure compression load case. The horizontal top axis labels indicate the type of P_{cr} used in the VCT predictions, while the right vertical axis shows the percentage of the reference bending load introduced.

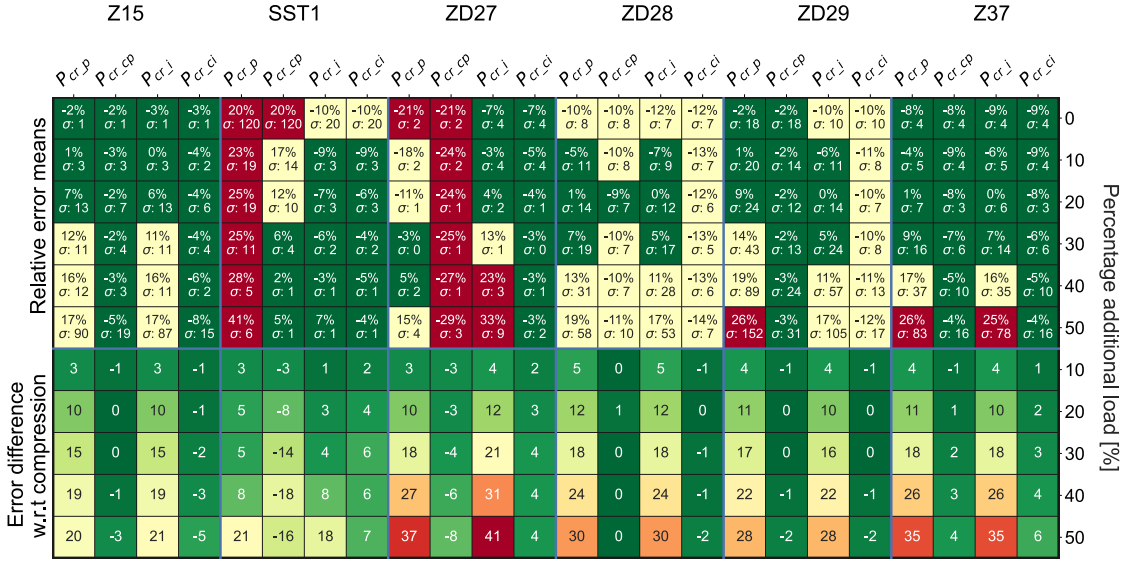

Figure 6.6 – VCT predictions in presence of bending, sequential load introduction

As previously mentioned, the shown averages are computed using the VCT predictions of the first 6 vibration modes, with maximum load ratios between 60% and 80% relative to P_{nl}. These averaged values are displayed in the upper half of the figure in percentages at the top of each cell. In addition, the variances corresponding to the VCT prediction errors are shown at the bottom of the corresponding cells to provide insight into the sensitivity of the predictions to maximum load levels and vibration

modes. The colour scheme in the upper half of the figure indicates the robustness of the predictions, with mean relative errors within 10% of P_{nl} being shown in green, those between 10% and 20% shown in beige, and the ones above 20% shown in red. Conversely, the colour scheme in the lower half of the figure, which shows the differences in mean relative errors with respect to the pure compression case, ranges from best in green, to worst in red.

Starting with the reference predictions for pure compression shown on the first line, it is evident that these were generally reliable, except for the SST1 and ZD27 cylinders when the P_{cr} values used were based on the models without imperfections. For SST1, this behaviour aligns with the findings shown in the previous Chapter 5 and is attributed to its specific shape imperfection. For ZD27, the large prediction error when using the P_{cr} of the perfect cylinder is due to the notably higher P_{nl} values compared to P_{cr_p} and P_{cr_cp}.

When using the P_{cr} values obtained for pure compression, whether for pristine or imperfect structures, the VCT predictions generally increase when increasing the bending load. This trend was not observed when incorporating bending loads into the P_{cr} calculations, as the behaviour in this regard differed between cylinders. In terms of reliability, including bending in the P_{cr} computation appears to yield better results. This is evidenced by the overall lower relative errors of the VCT predictions compared to P_{nl} and the more consistent mean error differences when compared to the pure compression load case. This trend is evident in the lower half of the figure, where it can be seen that using P_{cr_cp} or P_{cr_ci} results in significantly lower differences in relative errors compared to using P_{cr_p} or P_{cr_i}. Additionally, the variance within the errors is consistently lower when using P_{cr_cp} or P_{cr_ci}, regardless of the cylinder or bending magnitude applied.

Figure 6.7 serves as a counterpart to Figure 6.6, depicting the case where the bending loads are applied simultaneously with compression. In this scenario, the consistency and trend of the VCT prediction errors with increasing bending load are also generally more predictable when using P_{cr_cp} or P_{cr_ci}. However, predictions based on P_{cr} for pure compression typically proved to be more accurate than those based on

P_{cr_cp} or P_{cr_ci}, despite the less consistent evolution of these predictions with respect to bending magnitude. When P_{cr_cp} or P_{cr_ci} were used, the obtained predictions consistently decreased with increasing the magnitude of the bending load. On the other hand, when P_{cr_p} or P_{cr_i} were used, the predictions tended to increase, at least initially, with increasing the magnitude of bending applied. These aspects, together with the conservative predictions for the reference pure compression load case, implied that the accuracy of the predictions employing P_{cr_p} or P_{cr_i} could only decrease, while the ones employing P_{cr_p} or P_{cr_i} could also increase. Therefore, the P_{cr} for pure compression often yielded better overall prediction accuracy compared to those in which the additional bending load was taken into account.

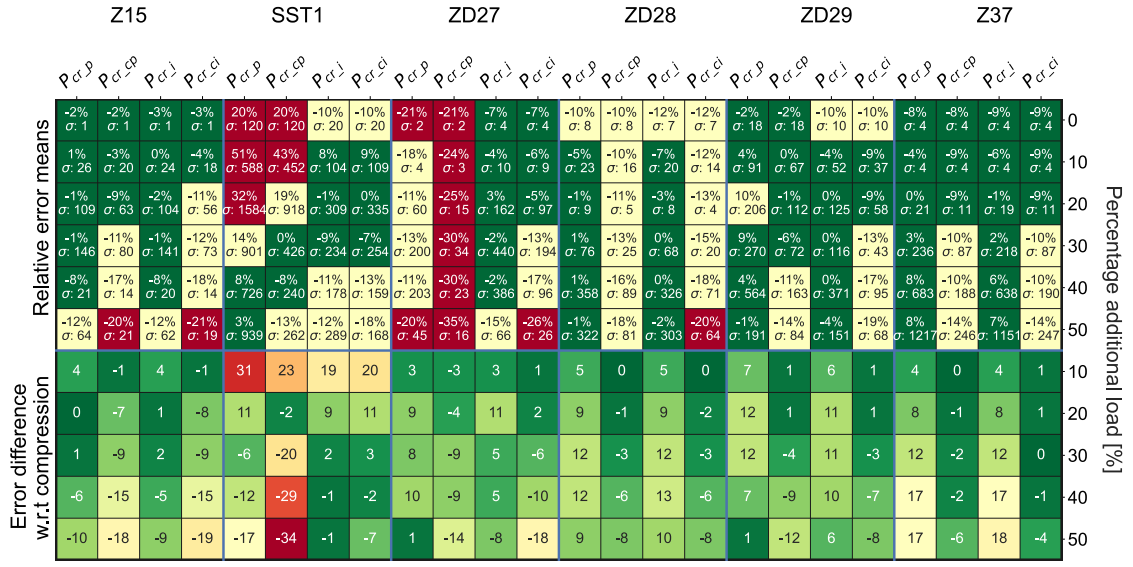

Figure 6.7 – VCT predictions in presence of bending, simultaneous load introduction

In terms of overall accuracy, VCT predictions for simultaneous bending and compression are comparable to those for sequential loading. However, a notable increase in the dependency of the VCT predictions on the maximum load level used was observed in this case. This is evident from the larger variance in the averaged errors as the bending load magnitude increases. Such behaviour is expected, given that, besides the changes in compression load, the ones in bending load magnitudes are also reflected in the vibration response. Additionally, it appears that there are specific threshold magnitudes of bending beyond which the VCT predictions become unreliable, these thresholds varying between the cylinders.

VCT in presence of shear

Figure 6.8 illustrates the relative errors of the VCT predictions on the axial load at which buckling occurs, with various magnitudes of shear introduced before compression, along with the differences in these relative errors compared to the predictions for the pure compression load case. The figure reveals that shear loads have a more pronounced effect on the VCT predictions than bending does, generally causing the predictions to decrease as the shear load magnitude increases. An exception to this trend was noted for the ZD28 and ZD29 cylinders, where the predictions increased with shear loads greater than 30% with respect to the reference one.

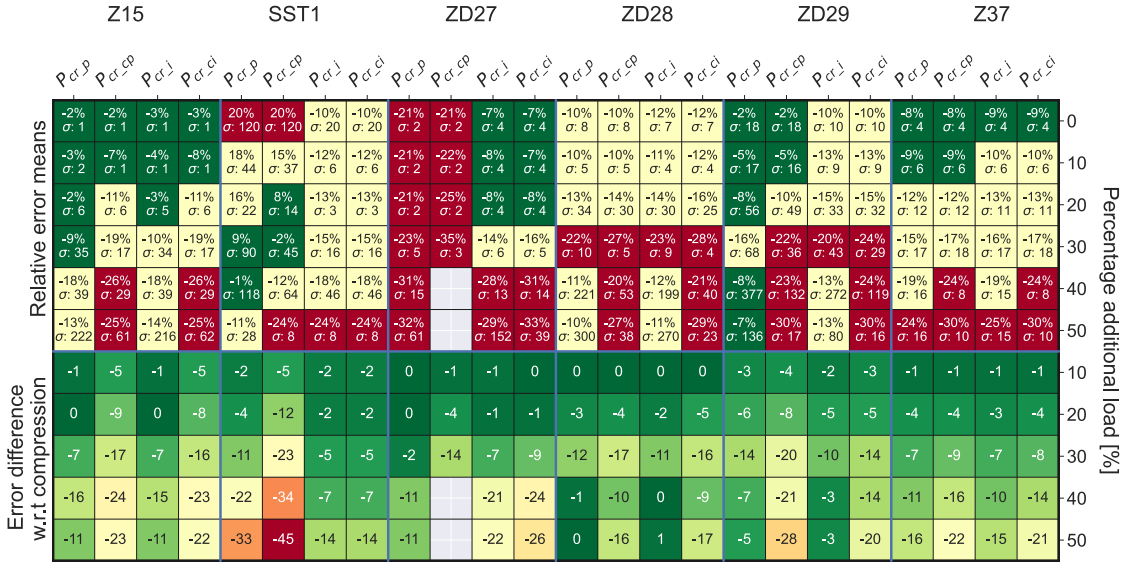

Figure 6.8 – VCT predictions in presence of shear, sequential load introduction

In contrast to the sequential introduction of bending and compression, using P_{cr_p} and P_{cr_i} for a pure compression load case tended to yield more accurate predictions in this case. Among these, P_{cr_p} generally provided slightly better results, except for SST1 and ZD27. Reliable predictions were typically obtained only for shear load magnitudes up to 20% or 30%, depending on the cylinder. Beyond these magnitudes, the relative errors and their variance became significantly larger.

For ZD27, no valid predictions were available using P_{cr_cp} for shear load magnitudes exceeding 30%, due to P_{cr_cp} being substantially lower than P_{nl} in these cases, as illustrated in Figure 6.3. Consequently, in the VCT characteristic chart, the value of

$(1\text{-}p)^2$ began to increase beyond a shear load ratio of 60%, therefore no valid VCT predictions were found between load ratios of 60% and 80%. Although other cases showed instances where the reference P_{cr} was greater than P_{nl}, the value of $(1\text{-}p)^2$ only started to increase from a load ratio higher than 60%, and the valid VCT predictions up to that threshold were maintained.

Figure 6.9 is the counterpart to Figure 6.8, showing results where the shear load was applied simultaneously with compression. In this scenario, the VCT predictions generally decreased with increasing shear load, except for the SST1 cylinder. As with bending, applying shear and compression simultaneously typically reduced the robustness of the VCT predictions. Overall, reliable VCT predictions were obtained for lower shear load magnitudes compared to the sequential introduction case. Nonetheless, the best results were still achieved using P_{cr} values from the pure compression load case, although reliable predictions were found at slightly lower shear magnitudes than in the sequential load introduction scenario.

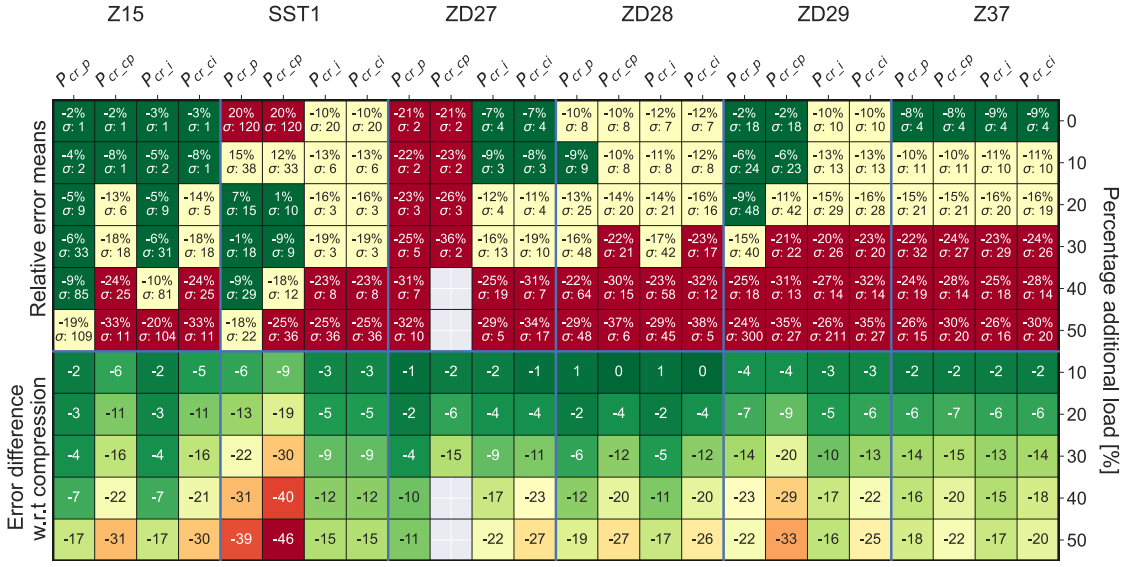

Figure 6.9 – VCT predictions in presence of shear, simultaneous load introduction

VCT in presence of torsion

Figure 6.10 illustrates the relative errors of the VCT predictions for the axial buckling load with various magnitudes of additional torsion applied before compression,

along with the differences in relative errors compared to the predictions for the pure compression load case. The effect of torsion on the VCT predictions is similar to that of shear, with predictions generally decreasing as the magnitude of torsion increases. However, whether torsion should be included when determining the reference P_{cr} value for VCT is less clear, due to the differences among cylinders regarding this aspect. Specifically, for cylinders Z15 and Z37, using the P_{cr} for pure compression provided the most accurate VCT predictions, while for the other cylinders, incorporating torsion into the P_{cr} calculation yielded slightly better results. The threshold magnitudes for reliable VCT predictions also vary among cylinders, generally ranging from 20% to 30% of the reference torsion load. Unlike shear, the thresholds for torsion where the error differences significantly exceeded 10% compared to the pure compression load case are typically observed at 40% or higher torsion loads, except for Z15 and SST1. This suggests that, for a sequential load introduction, VCT is slightly less sensitive to additional torsion compared to additional shear.

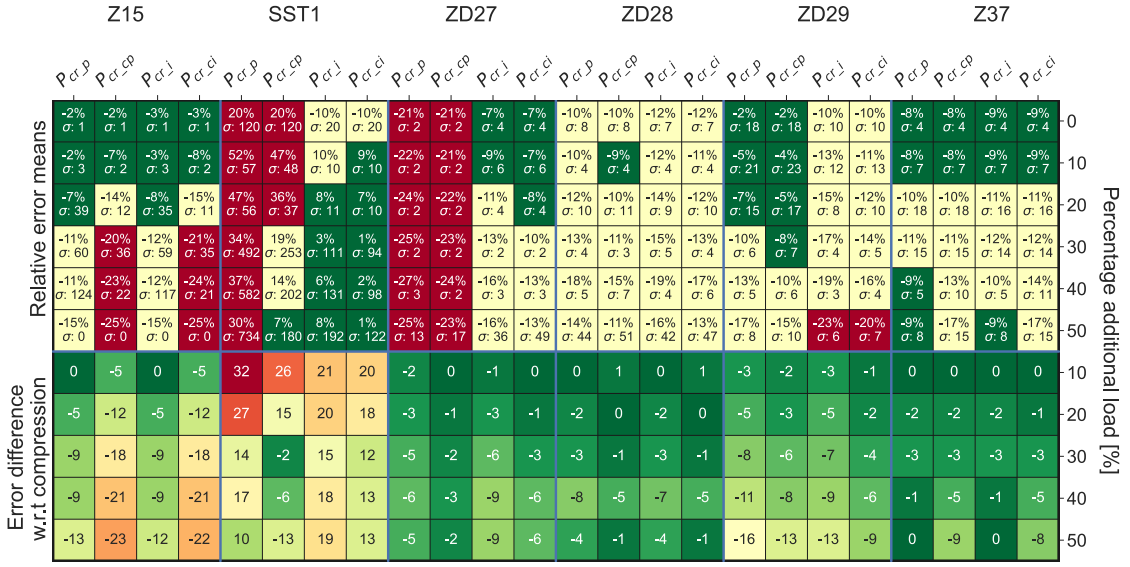

Figure 6.10 – VCT predictions in presence of torsion, sequential load introduction

Introducing torsion load simultaneously with compression had a similar impact as introducing shear load, as depicted in Figure 6.11. For all cylinders, the VCT predictions for torsion loads greater than 10% were unreliable, with predictions generally decreasing as the magnitude of the torsion load increased. As in the sequential load introduction case, using P_{cr} for pure compression yielded better results for cylinders

Z15 and Z37, while accounting for the additional torsion load in the P_{cr} calculations provided slightly better outcomes for the other cylinders. Furthermore, unlike the sequential case where VCT was less sensitive to torsion than to shear, when these loads were introduced simultaneously with compression, there were no distinct differences in the method's sensitivity to varying magnitudes of shear or torsion.

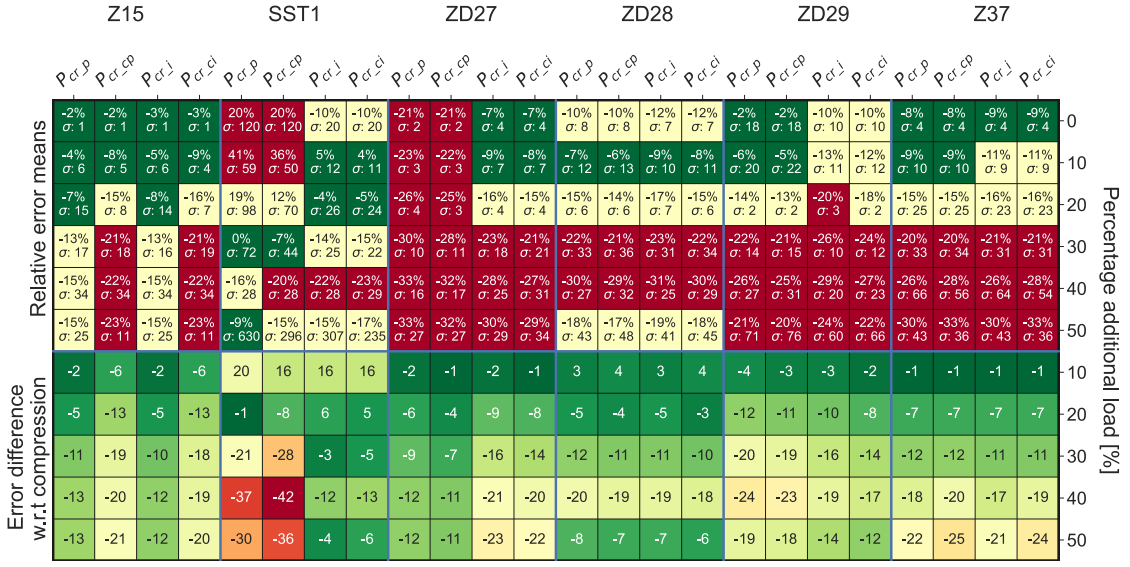

Figure 6.11 – VCT predictions in presence of torsion, simultaneous load introduction

VCT in presence of bending, shear and torsion

Figure 6.12 illustrates the relative errors in the VCT predictions for the axial load at which buckling occurs, with varying magnitudes of additional bending, shear, and torsion applied before compression, along with the differences compared to the predictions for the pure compression load case. The figure shows that VCT could still deliver reliable predictions when bending, shear, and torsion are applied before compression. However, robust VCT predictions were not consistently achieved for a single type of P_{cr}. Specifically, predictions using P_{cr} for pure compression yielded better results for Z15 and Z37, while P_{cr} for combined loading generally provided better results for the other cylinders. This trend aligns with previous observations: the best VCT predictions for bending-compression obtained by incorporating the bending load into P_{cr} calculations, for shear-compression using P_{cr} from a pure compression case, while for torsion-compression the optimum P_{cr} was cylinder-specific, thus unclear.

While the choice of P_{cr} did not consistently affect the accuracy of the VCT predictions, it did have a notable impact on the variance of the relative errors, with lower variances observed when the additional loads were considered in the P_{cr} calculations. This effect varied between cylinders and became more pronounced as the magnitude of the additional loads increased.

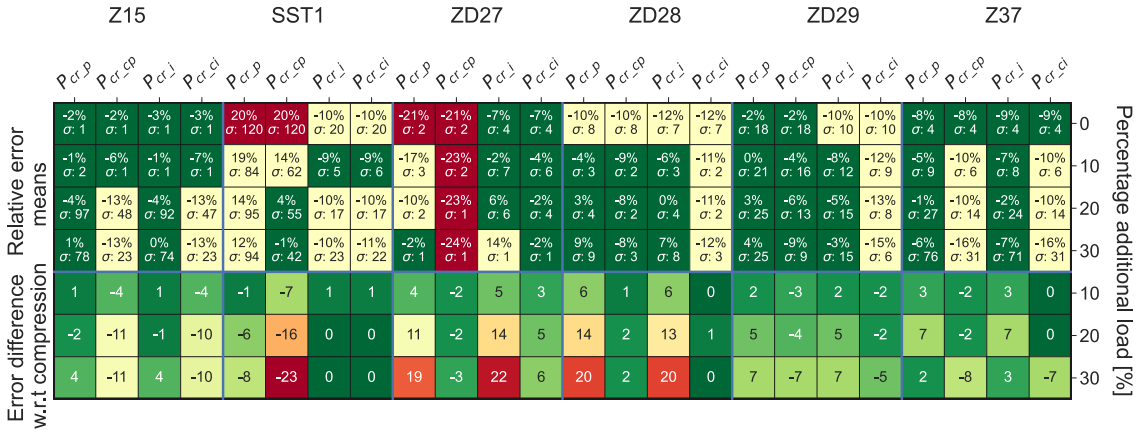

Figure 6.12 – VCT predictions in presence of bending, shear and torsion, sequential load introduction

The simultaneous application of bending, shear, and torsion along with compression also adversely affected the robustness of the VCT predictions, as depicted in Figure 6.13.

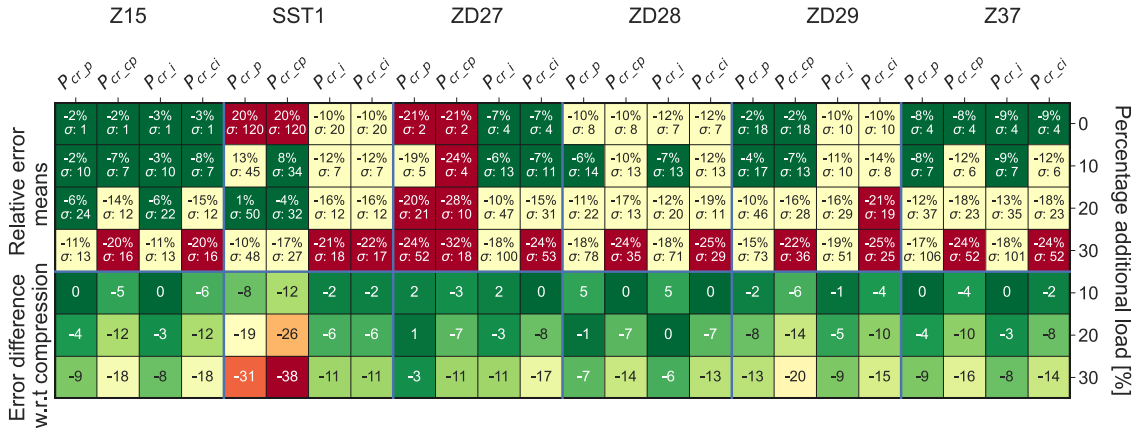

Figure 6.13 – VCT predictions in presence of bending, shear and torsion, simultaneous load introduction

For additional load magnitudes exceeding 10%, the prediction accuracy was generally poor for some cylinders and showed considerable variation with the level of additional

load applied. When these loads were applied simultaneously, the most reliable VCT predictions were consistently achieved using the P_{cr} values under pure compression. In contrast, when these loads were introduced sequentially, the P_{cr} giving the best accuracy varied between cylinders. This differs from the case where either bending, shear, or torsion was applied in addition to compression, where the same type of P_{cr} generally provided the best results for a specific cylinder, regardless of whether the loads were applied sequentially or simultaneously.

6.4 Discussion

The numerical analysis presented here indicates that VCT is likely to deliver reliable predictions of the axial load at which cylindrical shells buckle when subjected to compression combined with bending, shear, or torsion, regardless of whether these loads are applied individually or in combination, as well as if applied before or simultaneously with compression. Generally, the VCT predictions are more robust when additional loads are applied before compression, as the vibration response is assessed at various compression levels while keeping the additional loads constant. In contrast, when loads are applied simultaneously, the variation of the vibration response is also due to the additional loads and introduces additional complexity, thus negatively impacting the robustness of the VCT predictions. This effect is particularly pronounced with shear or torsion, likely due to a significant material tension being introduced. Bending, on the other hand, has a less severe impact, as the tension induced on one side of the cylinder is counterbalanced by the compression introduced on the opposite side. This difference is reflected in the generally higher magnitudes of reference bending loads at which VCT provided reliable buckling load estimates when compared to additional shear or torsion loads applied alongside compression.

It is also crucial to note that the sensitivity of the VCT predictions to the maximum load level increases with the amount of additional load applied, making the threshold magnitudes beyond which VCT is unreliable highly dependent on the maximum compression load level. For instance, with maximum compression levels in a 70%-80%

range relative to P_{nl}, the VCT predictions remained robust beyond the threshold values mentioned in the previous section and determined based on the predictions within a 60%-80% range relative to P_{nl}.

To better illustrate these aspects, the VCT charts for the ZD29 cylinder under simultaneously applied bending and compression (P_{cr}=P_{cr_cp}, r_x=30%r_{x_ref}) are presented in Figures 6.14 and 6.15, corresponding to the second and fourth vibration modes, respectively. In these figures, quadratic fits were progressively made by increasing the number of load steps/maximum load level considered, emphasising the sensitivity of the VCT predictions to the maximum compression load level used. The load levels for each measurement are expressed as ratios relative to P_{nl} on the right vertical axis, with the target value ξ^2 corresponding to P_{VCT}=P_{nl} (0% VCT prediction error) highlighted in magenta. The second and fourth vibration modes were tracked over differing numbers of load steps, as well as varying minimum and maximum load levels, which accounts for the differences between the two figures regarding these aspects.

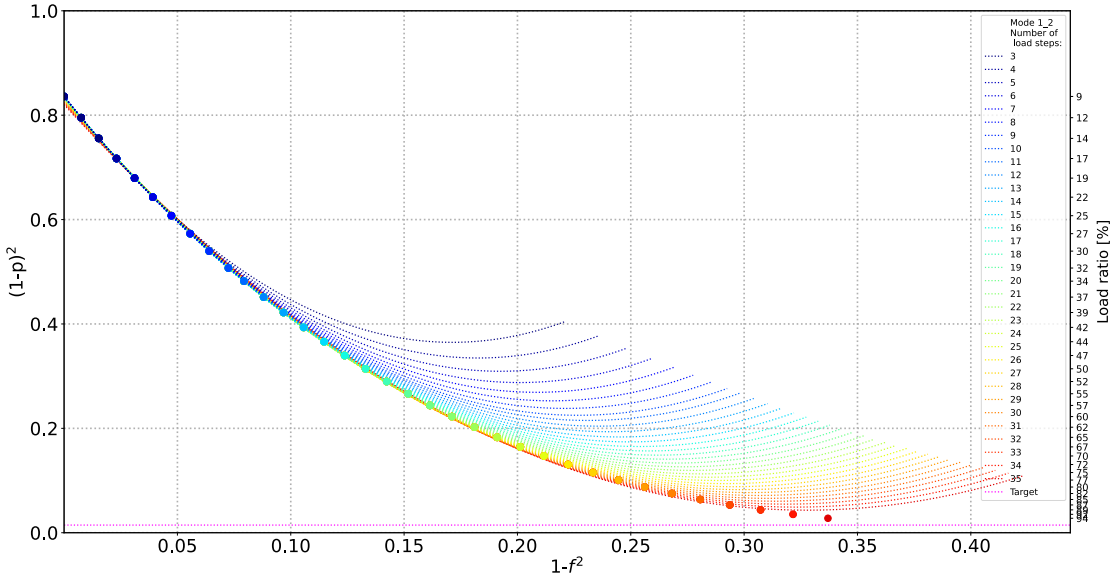

Figure 6.14 – Progressive VCT predictions for the ZD29 cylinder under bending-compression simultaneously introduced, P_{cr}=P_{cr_cp}, r_x=30%r_{x_ref}, for the 2^{nd} vibration mode

In Figure 6.14, the influence of simultaneously applied loads on the VCT predictions is evident from the points in the VCT characteristic chart for the second vibration mode. Specifically, there is a significant variation in the quadratic fits performed as a function

of the maximum load level. This variation arises because the points in the VCT characteristic chart no longer follow a consistent quadratic behaviour, with deviations increasing as the applied load level rises. However, this phenomenon was not observed for all vibration modes. For instance, the VCT characteristic chart for the same load case using the fourth vibration mode, shown in Figure 6.15, exhibits a clear quadratic response. A similar behaviour was noted when compression was sequentially introduced alongside torsion or shear in particular, although at magnitudes beyond which VCT yielded poor predictions. Additionally, frequent changes in the vibration response as the applied load increased, where previously monitored vibration modes were no longer detectable, contributed to the poor performance of VCT at high levels of torsion and shear.

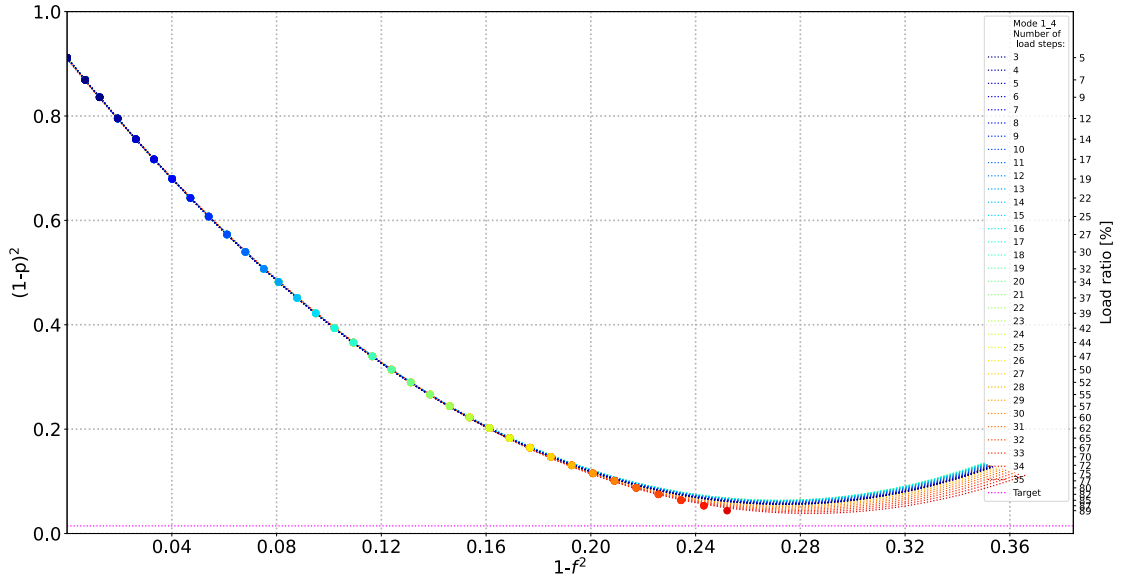

Figure 6.15 – Progressive VCT predictions for the ZD29 cylinder under bending-compression simultaneously introduced, P_{cr}=P_{cr_cp}, r_x=30%r_{x_ref}, for the 4^{th} vibration mode

Determining whether to account for additional loads when calculating P_{cr} for robust VCT predictions depended on the type of load and the manner in which it was applied. For additional bending loads, it was crucial to incorporate them into the P_{cr} calculation. For additional shear loads, the P_{cr} value from the pure compression load case was generally more appropriate. In the case of torsion, the need to consider additional loads was specific to each cylinder, making it less straightforward. When

bending, shear, and torsion were applied together with compression, the necessity of including these loads in the P_{cr} calculation varied depending on whether the loads were applied sequentially or simultaneously. For a sequential loading, this aspect varied among cylinders, whereas for a simultaneous loading, the best results were obtained when using P_{cr} under pure compression.

Except for SST1 and ZD27 cylinders, including imperfections in the P_{cr} calculation was generally not crucial, as the most reliable VCT predictions were typically obtained using the nominal cylinder configuration. For SST1, as discussed in Chapter 5, its shape imperfection signature, which led to local buckling at much lower loads than global buckling, meant that P_{cr} for the nominal configuration did not provide robust predictions. However, the local buckling observed could not be directly linked to poor VCT predictions when using P_{cr} for the perfect structure. Adjusting the amplitude of the shape imperfection pattern in the non-linear analysis often resulted in reliable VCT predictions with P_{cr} for the nominal configuration, regardless of whether local buckling occurred. Conversely, poor VCT predictions with P_{cr} for the perfect structure were noted within a range of shape imperfection magnitudes below the threshold at which local buckling occurred.

A cross-check involving applying SST1's shape imperfection pattern to other cylinders, and vice versa, showed that SST1's poor VCT predictions were not only due to its shape imperfection, but also to its geometry and material properties. When SST1's shape imperfection was applied to the other cylinders, reliable predictions were generally obtained using P_{cr} for the perfect structure, except for Z15. When other cylinders' shape imperfections were applied to SST1, the VCT predictions were mostly poor, except for that of the Z37 cylinder. For the cases where the VCT predictions were largely unconservative, accounting for SST1's shape imperfection when determining P_{cr} resulted in reliable predictions, albeit making some predictions overly conservative for other cylinders. This behaviour underscores the sensitivity of VCT predictions for SST1 to various factors, its FE model being used in this study despite its poor numerical VCT predictions for a better assessment of VCT's capabilities of predicting axial buckling loads under combined loading scenarios.

Conversely, for ZD27 the VCT predictions using its nominal configuration to compute P_{cr} were unreliable due to a different reason. Namely, the influence of its imperfection pattern was not adequately captured by the mean radius determined from its shape imperfection pattern and the recalculated material properties based on the average thickness measured. Specifically, the thickness imperfection had a strengthening effect (higher thickness than its nominal one), raising its buckling load such that P_{nl} from the non-linear analysis of the imperfect structure exceeded the P_{cr} obtained from the linear buckling analysis of the perfect structure. This discrepancy created an inherent inconsistency with the VCT formulation used here, as accurate predictions would have required a negative value of $\sqrt{\xi_k^2}$ from Equation 2.3, and the quantity $(1\text{-}p)^2$ on the y-axis of the VCT characteristic chart would have also increased between P_{cr} and P_{nl}.

While the shapes of the vibration modes are generally irrelevant in numerical VCT applications, they become crucial in practical settings where the frequencies and shapes of the vibration modes are usually monitored over a limited area, rather than the entire surface of the cylinder. Under pure compression, cylindrical shells typically exhibit vibration modes with multiple waves around their circumference, as the material experiences a uniform load distribution before buckling. However, when additional loads are applied alongside compression, certain areas of the cylinder may experience significant components of these additional loads, potentially leading to localised vibration modes. Detecting these modes experimentally can be challenging, so the numerical models were inspected to determine their potential presence. It was found that indeed such localised vibration modes appeared for several cylinders at high magnitudes of additional loads, usually within the first four. However, their occurrence was limited, and other vibration modes retained multiple waves around the circumference, offering flexibility in selecting the area to monitor during tests.

Additionally, there was a higher tendency for vibration mode changes at large magnitudes of shear and torsion loads. Although mode changes were predominantly observed at the largest shear and torsion magnitudes, where the VCT predictions were already unreliable, this issue may become significant in practical scenarios in which structures with more sensitive frequency responses are tested. While in this

numerical investigation the detrimental influence of this aspect was alleviated by the large number of load steps defined, in real tests the same number of measurements could be impractical due to time constraints, and frequent mode changes could render the vibration mode frequencies unusable.

Since the additional loads were applied through displacements or rotations, the resulting reaction forces and moments slightly varied with respect to the ones observed in the analyses run to determine these reference values, due to the interaction between the additional and compressive loads applied. This variation became particularly significant at high load ratios, where the magnitudes of the reaction forces/moments were below those corresponding to the reference ones. Therefore, the investigation was repeated using FE analyses where bending, shear, or torsion were applied as forces/-moments to double-check the results obtained when the introduction of the additional loads was displacement/rotation-based. The differences between the results obtained from displacement/rotation-based load applications and those from force/moment-based applications were minimal. The largest discrepancies in both P_{nl} values and the relative errors of the VCT predictions with respect to it were within a few percentage points. Furthermore, these only occurred at the highest additional load magnitudes that generally exceeded the identified threshold values beyond which VCT became unreliable. Within the range of bending, shear, or torsion magnitudes for which VCT provided reliable predictions, the relative errors between the displacement/rotation and force/moment-based load introduction analyses were below 1%.

6.5 Conclusions

This chapter presents a numerical investigation into the feasibility of using the Vibration-Correlation Technique (VCT) to estimate the axial load at which cylinders buckle under combined loading conditions. The study involved applying, bending, shear, and torsion loads, in addition to compression, via displacements or rotations, either individually or all together, and either sequentially (additional loads applied before compression) or simultaneously. The vibration responses of multiple cylinders were

determined across various axial load levels to perform VCT predictions, and the robustness of the obtained VCT predictions was evaluated based on two criteria. First, the accuracy of the VCT predictions was compared to the axial buckling loads P_{nl} obtained from non-linear analyses, and second, the deviation in accuracy relative to the predictions for the pure compression load case was assessed. Additionally, the VCT predictions were made using two cylinder configurations (perfect and imperfect) and considering or ignoring the additional loads when determining P_{cr}, resulting thus in four different reference values.

The investigation's outcome was that VCT can reliably predict the axial buckling loads of cylinders under combined loading, if the additional loads are within specific thresholds. These thresholds varied significantly depending on the type of additional load, on whether compression was applied sequentially or simultaneously, as well as across the different cylinders. Generally, the VCT predictions were more reliable when the additional loads were applied sequentially, as the changes in the frequency response mainly reflected variations in the compression load level. Although the accuracy of the VCT predictions was typically reduced by the presence of additional loads, bending had a lesser impact compared to shear and torsion. This difference was attributed to the fact that the tensile stress caused by shear and torsion loads is not counterbalanced as effectively as the tensile stress from bending, which is offset by compression on the opposite side of the cylinder.

For combined bending and compression loading, accounting for the bending load when calculating P_{cr} was crucial for the robustness of VCT predictions when these loads were introduced sequentially. However, when bending and compression were applied simultaneously, the same behaviour was not observed across all cylinders. Although the predictions in the aforementioned case were more consistent with the expected behaviour when increasing the magnitude of bending, an overall better prediction accuracy was reached when using the P_{cr} values in which bending was not taken into account.

In contrast, when bending, shear, and torsion were applied together with compression the opposite was seen. The importance of considering these additional loads

when determining P_{cr} for reliable VCT predictions varied between cylinders when compression was introduced after the additional loads, while the most reliable VCT predictions were consistently obtained using P_{cr} for a pure compression load case when these loads were simultaneously applied. When additional shear was introduced, P_{cr} for pure compression generally provided the most reliable predictions, regardless of whether compression was applied sequentially or simultaneously. On the other hand, for the torsion-compression combined load case, it was unclear whether the additional torsion should be considered when calculating P_{cr}, as the results varied between cylinders.

Overall, the differences between incorporating or excluding additional loads when computing P_{cr} became significant primarily at higher magnitudes of additional loads. Furthermore, the magnitude of additional loads applied had no influence over which type of P_{cr} provides the best VCT estimates in the cases where this aspect was cylinder-specific. These observations hold true for both sequential and simultaneous load introductions, indicating that VCT can reliably predict the axial load at which cylindrical shells buckle under combined loading, provided that the additional loads are relatively low, using the same approach as for pure compression and irrespective of the loading sequence, or the P_{cr} type used.

7 Experimental validation of VCT for compression-bending load cases

In this chapter, the experimental test results of a cylindrical shell representative to a real-scale launcher structure tested under two bending-compression load cases are presented. Given the confidentiality restrictions associated with these types of tests, the results treated here are predominantly from a VCT perspective.

7.1 Tested structure

The tested cylindrical structure was manufactured by welding four curved aluminium panels, out of which three had embossments, the nominal diameter and height being 5410mm and 3109.25mm, respectively. The thickness of the panel bays was constant, apart from the edges that had a higher thickness due to welding constraints. The load cases for which VCT was applied had different levels of non-uniform compression, introduced by four hydraulic actuators equidistantly placed across the barrel's circumference and connected to the test rig. Figure 7.1a shows an overview of the tested barrel together with the panel labels, while Figure 7.1b shows the position of the actuators and the area of interest, for which the displacement field was measured using digital image correlation (DIC) equipment.

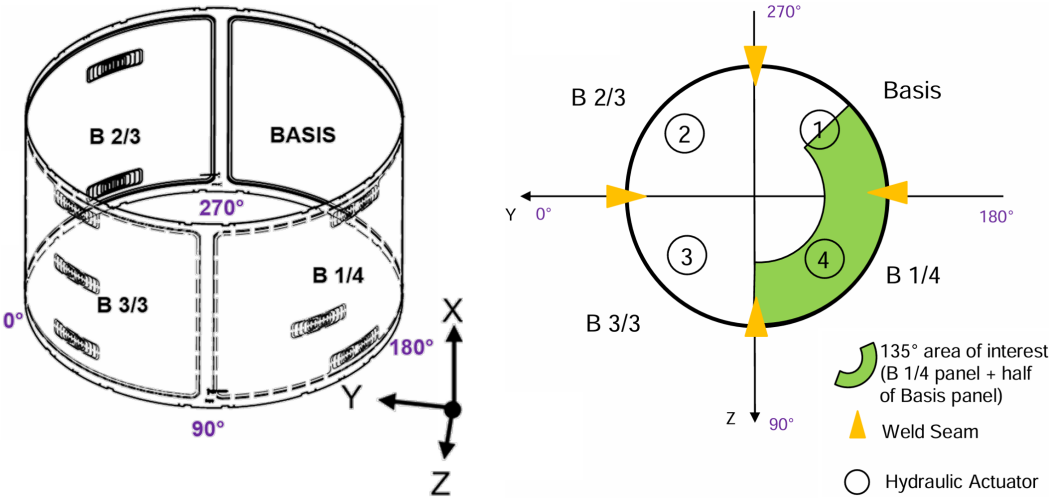

(a) **(b)**

Figure 7.1 – Barrel's overview (a); actuator positions and area of interest (b)

The actuator loads applied in the two load cases are shown in Table 7.1, in normalised form. Given the actuator positions and loads introduced, load case 1 (LC1) was defined such that buckling was initiated on the B 1/4 panel, while load case 2 (LC2) was defined such that buckling initiated on the welding seam between B 1/4 and B 1/1 (Basis) panels.

Actuator	1	2	3	4
Load case 1	0.898	0	0.898	1
Load case 2	1	0	0	1

Table 7.1 – Actuator normalised load ratios for load case 1 and load case 2

Figure 7.2 shows a CAD section cut of the barrel mounted in the test rig and the boundary conditions at the top and bottom edges. As it can be seen from this figure, the edges had simply supported boundary conditions via contact, with any existing gaps between the barrel edges and the test rig being closed with aluminium shims. Additionally, radial support at their inner side was provided by adjustable guiding plates. Inside the test rig, four columns equally distributed along the barrel's circumference can also be seen besides the hydraulic actuators, their role being to prevent the upper part of the test rig from coming off in the event that an actuator malfunction or a control loop anomaly occurs.

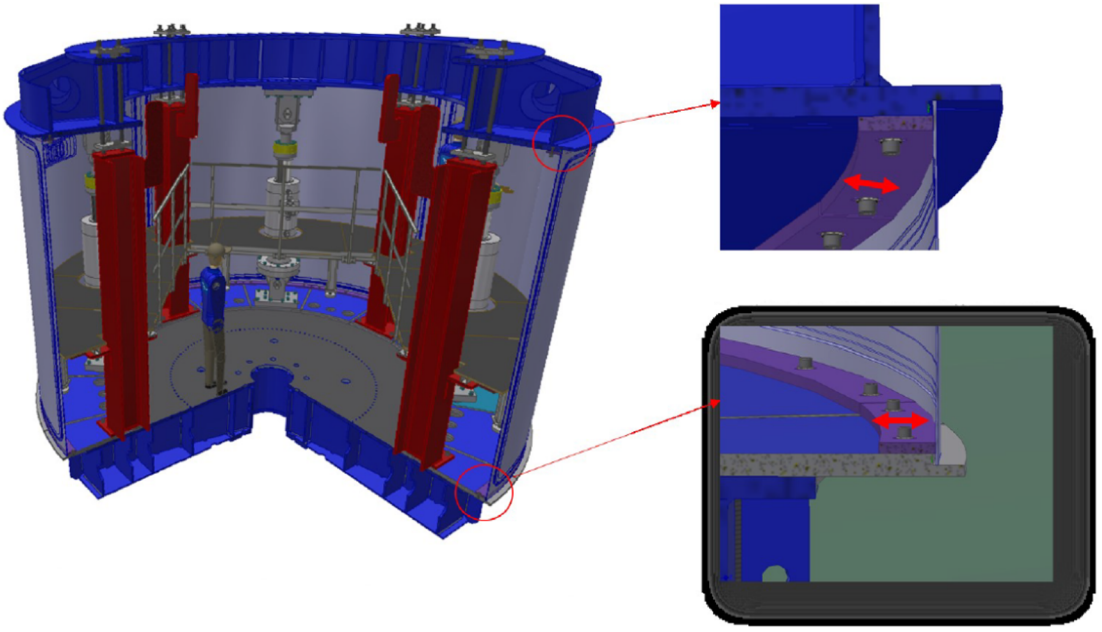

Figure 7.2 – Barrel test rig and boundary conditions

7.2 Numerical analysis

Prior to the experimental test, a series of numerical analyses were performed to determine the P_{cr} values for LC1 and LC2, assess the feasibility of VCT to predict the buckling load for these cases, as well as to provide valuable information in defining the experimental VCT setup.

Given that the test rig can have an important influence on the buckling response of the barrel, its CAD model was used to build the mesh of its bottom and top loading structures. Table 7.2 shows an overview on the number of nodes, elements, and element types used, while Figure 7.3 shows the FE model used in the numerical analyses.

Part	Number of nodes	Number of elements
Bottom test rig	335 782	343 079 (S4R/S3)
Barrel	264 870	263 818 (S4R/S3R
Bottom test rig	102 333	101 810 (S4R/S3)

Table 7.2 – Number of nodes, elements and element types

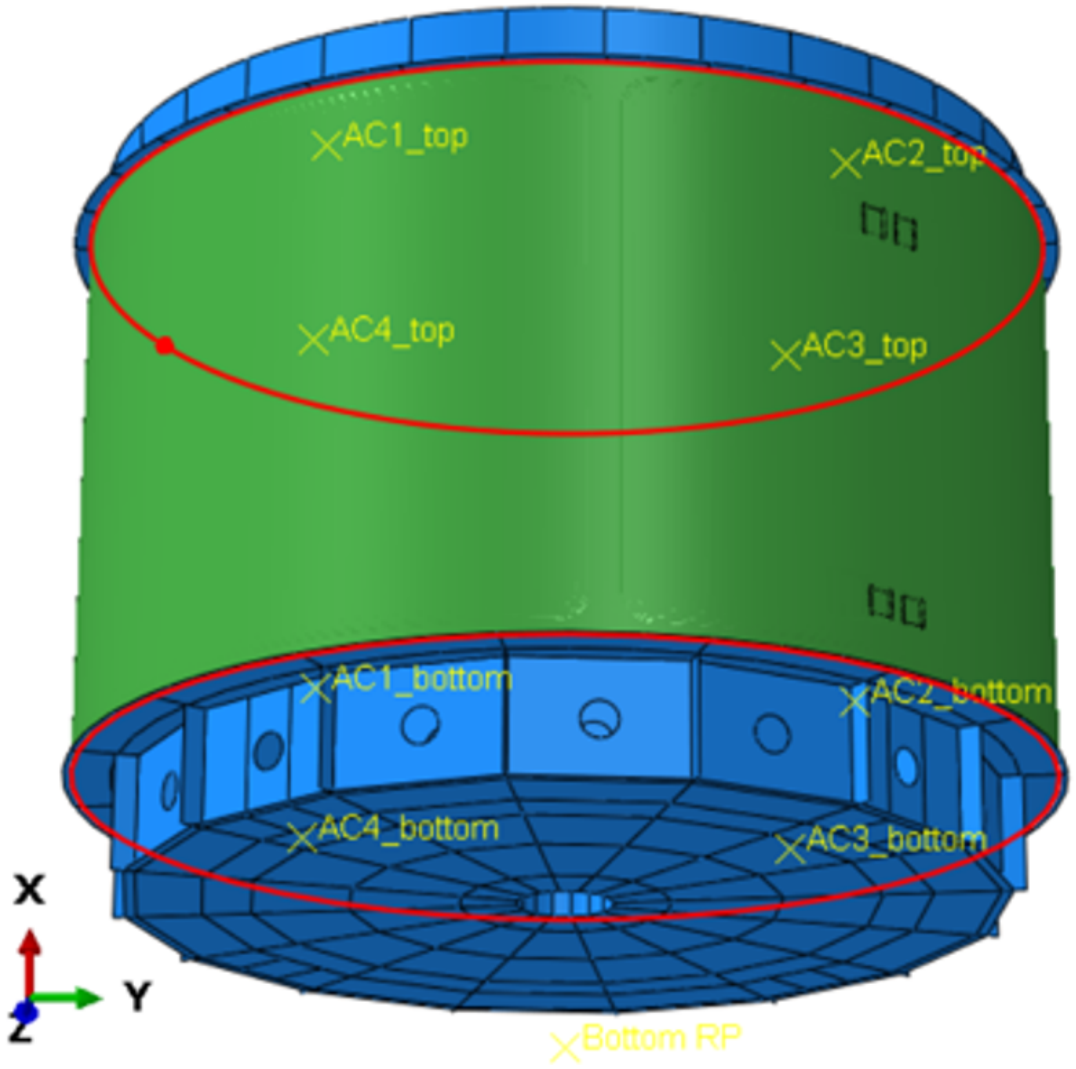

Figure 7.3 – Barrel FE model

Starting from the bottom up, the nodes in the areas in contact with the rig legs were fully coupled with a bottom reference point, for which all its degrees of freedom were restrained. Next, the nodes corresponding to the contact patch between the bottom test rig and the actuators were also fully coupled with bottom reference points, restraining thus these nodes from moving with respect to the test rig during the analysis. A similar approach was also used for the top test rig, the difference being that the top reference points had only the translations in the horizontal plane restrained and force-based loads were introduced according to the ratios shown in Table 7.1. The complex boundary conditions at the barrel rig interfaces were simplified with

tie constraints, since under load, the barrel edges were considered to follow closely the movement of the test rig, and modelling in detail the contacts at these interfaces would have increased significantly the computational effort, with little benefit in studying the feasibility of VCT for the load cases tested.

Considering that cylindrical structures with large radius/thickness ratios are particularly sensitive to imperfections, to increase the relevance of the numerical investigations a linear buckling analysis was performed to obtain buckling modes that were further used to introduce shape imperfections. The buckling analysis performed was for a uniform compression load case, as obtaining buckling modes more evenly distributed across the barrel's circumference was desired, given that using the loads of LC1 or LC2 induced highly localised buckling modes. The buckling mode imperfections applied are shown in Figure 7.4, these modes being chosen given their position on the barrel, namely on the panels seeing larger loads. The magnitude of the introduced imperfections was such that the largest out-of-plane deviation was 50% with respect to the panel bay thickness.

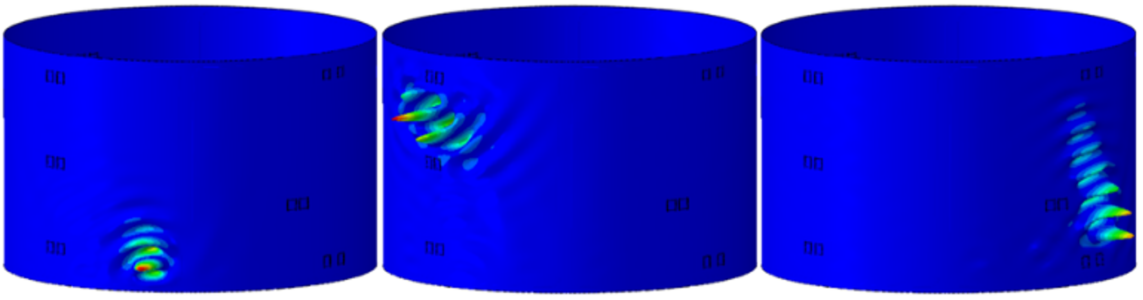

Figure 7.4 – Barrel shape imperfections applied

7.2.1 VCT results

For the numerical VCT analysis, the frequency response was requested in steps of 5% with respect to the buckling load obtained from the non-linear analyses P_{nl}. Figure 7.5 shows the relative errors of the VCT predictions using the first 10 vibration modes for LC1 with respect to P_{nl}. In this plot, the load ratio between the maximum load level used in the VCT prediction and P_{nl} is shown on the horizontal axis, while

on the vertical axis the relative error of the VCT prediction with respect to P_{nl} is shown. As it can be seen from this plot, VCT was able to provide reliable buckling load predictions, provided that the load ratio used was high enough. For this load case, the predictions tend to be within 20% when the maximum load used was at least 75% with respect to P_{nl} and within 10% for maximum load ratios higher than 90%. As expected based on the outcome of the study on the feasibility for combined load cases shown in Chapter 6, there is a significant sensitivity towards the load ratio of the VCT predictions, given that the load cases applied here are similar to bending-compression simultaneously introduced. Additionally, a behaviour discussed in more detail in Chapter 4 regarding the evolution of the prediction with the load level applied is also present. Namely, decreasing VCT predictions with increasing the maximum load level used were observed for each vibration mode displayed, either at lower load ratios, or throughout the entire range, reason why the initial predictions for the majority of the vibration modes shown here were unconservative.

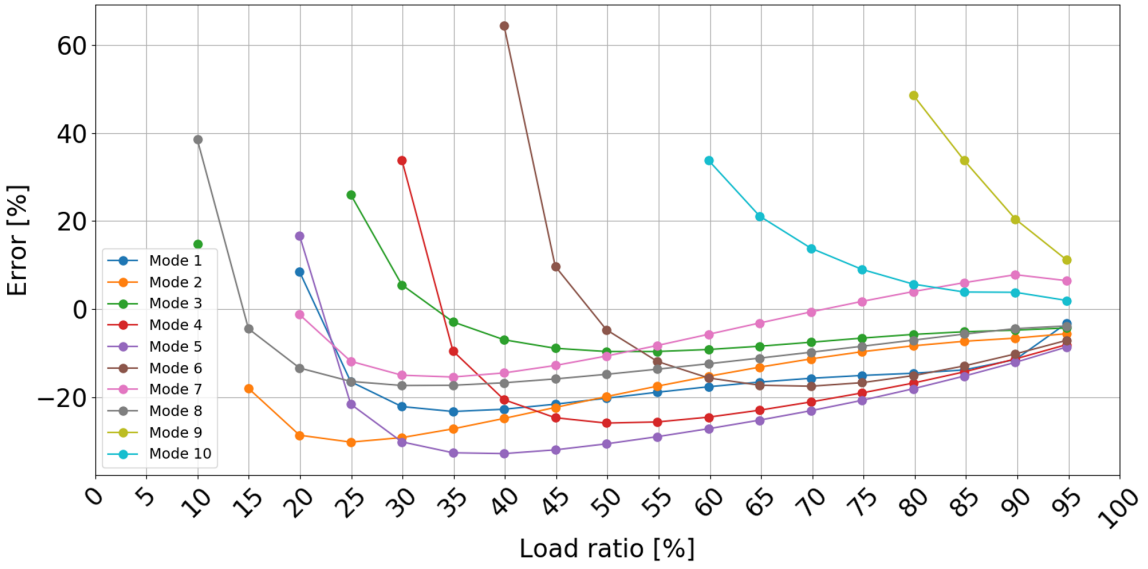

Figure 7.5 – VCT relative error with respect to P_{nl} for LC1

When looking at the load levels of the initial predictions for each vibration mode shown, it can be seen that there is a relatively large variation between them. This occurred given that the number of load steps over which each vibration mode could be tracked varied, reason why for the 9^{th} vibration mode, for example, the first

prediction could only be made at a load ratio of 80%. While this load ratio may be already above the one at which one may take the risk to hold the load level constant for the vibration measurement, these cases in which initial predictions are possible only at relatively high load ratios represent exceptions. Furthermore, given that the inherent imperfections present in each test and structure favour consistent vibration modes as the load increases, while also decreasing the likelihood of vibration mode changes, these behaviours were not expected during the experimental tests.

Figure 7.6 shows the relative errors of the VCT predictions with respect to P_{nl} using the first 10 vibration modes for LC2. When compared to the results for LC1, two important differences can be seen. First, the VCT predictions were unsuccessful for some vibration modes between certain load ratios, as the vibration modes initially tracked could no longer be found beyond a given load level specific to each of the modes where this behaviour was observed. Second, the predictions also have a higher sensitivity towards the maximum load ratio used than for LC1. For this load case, the predictions tend to be within 20% when the maximum load used was at least 85% with respect to P_{nl}, while the majority of the predictions were within 10% only for the highest load ratio used of 95%.

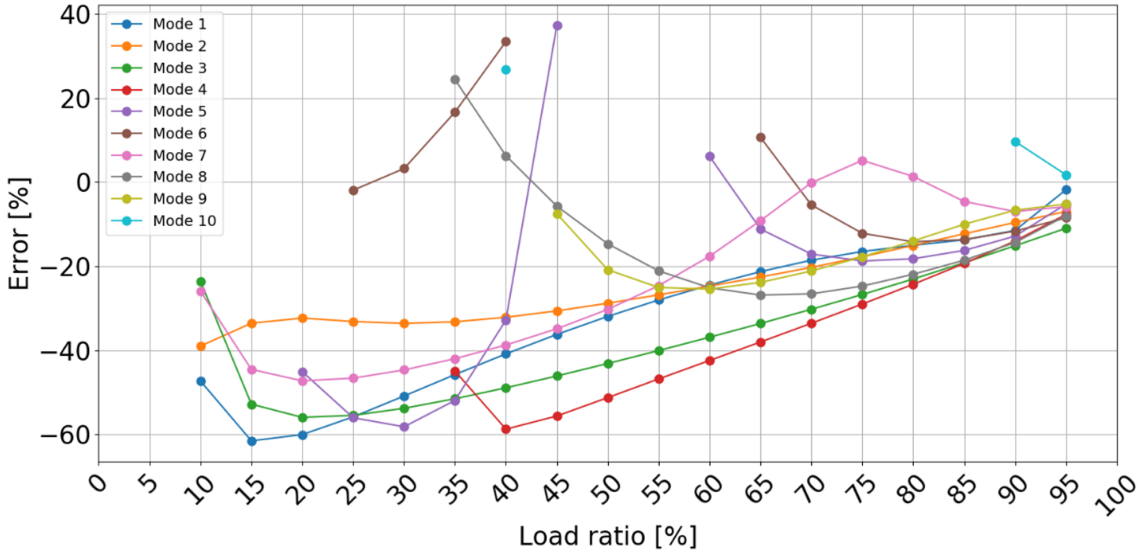

Figure 7.6 – VCT relative error with respect to P_{nl} for LC2

The numerical results for LC1 and LC2 were also used in defining the experimental

setup for VCT. In this regard, the same procedure as the one shown in Chapter 4 was used to determine an optimum number of load steps and a minimum load level desired for reliable predictions. The outcome of this preliminary investigation was that, similarly to the study shown in Chapter 4, 8 to 9 load steps were found to be adequate for these load cases as well. On the other hand, the recommended load ratio was around 90%, or higher, given the high sensitivity of the VCT predictions for this case towards both the load ratio and the vibration mode used. Furthermore, given the compression-bending combined load case, it was also verified that the shapes of the vibration modes are not localised and could therefore be accurately identified considering the fixed position of the laser vibrometer. The lower bound for the measurement window and the minimum resolution were also defined based on the numerical results. The lower bound of the measurement window was given by the first vibration mode in unloaded state, found at a frequency around 24Hz. Conversely, the minimum measurement resolution required was defined at 0.16Hz, given that between the consecutive load steps at load ratios of 0% and 5% the frequency drops were around this value.

7.3 Experimental VCT tests

The barrel's vibration response was measured using a loudspeaker to excite the structure and a Polytech PSV400 2D laser vibrometer scanner to measure its vibration modes and frequencies. Given the low curvature of the barrel, a 2D measurement system, instead of a 3D one, was considered enough to capture the barrel's vibration response. Figure 7.7 shows an aerial view of the barrel and its experimental setup. In the bottom left part of the figure the loudspeaker used to excite the structure can also be seen, this being positioned in the proximity of the area monitored by both the DIC system and the laser vibrometer.

Due to spacing constraints, the area monitored by the laser vibrometer was the same as the one monitored by the DIC equipment, for which a speckled pattern was applied. This, together with the uneven surface of the barrel, due to the dimples resulting from

a shot peening process, raised difficulties in the vibration response measurement, since surfaces with high reflectivity are better suited for the laser scanning system.

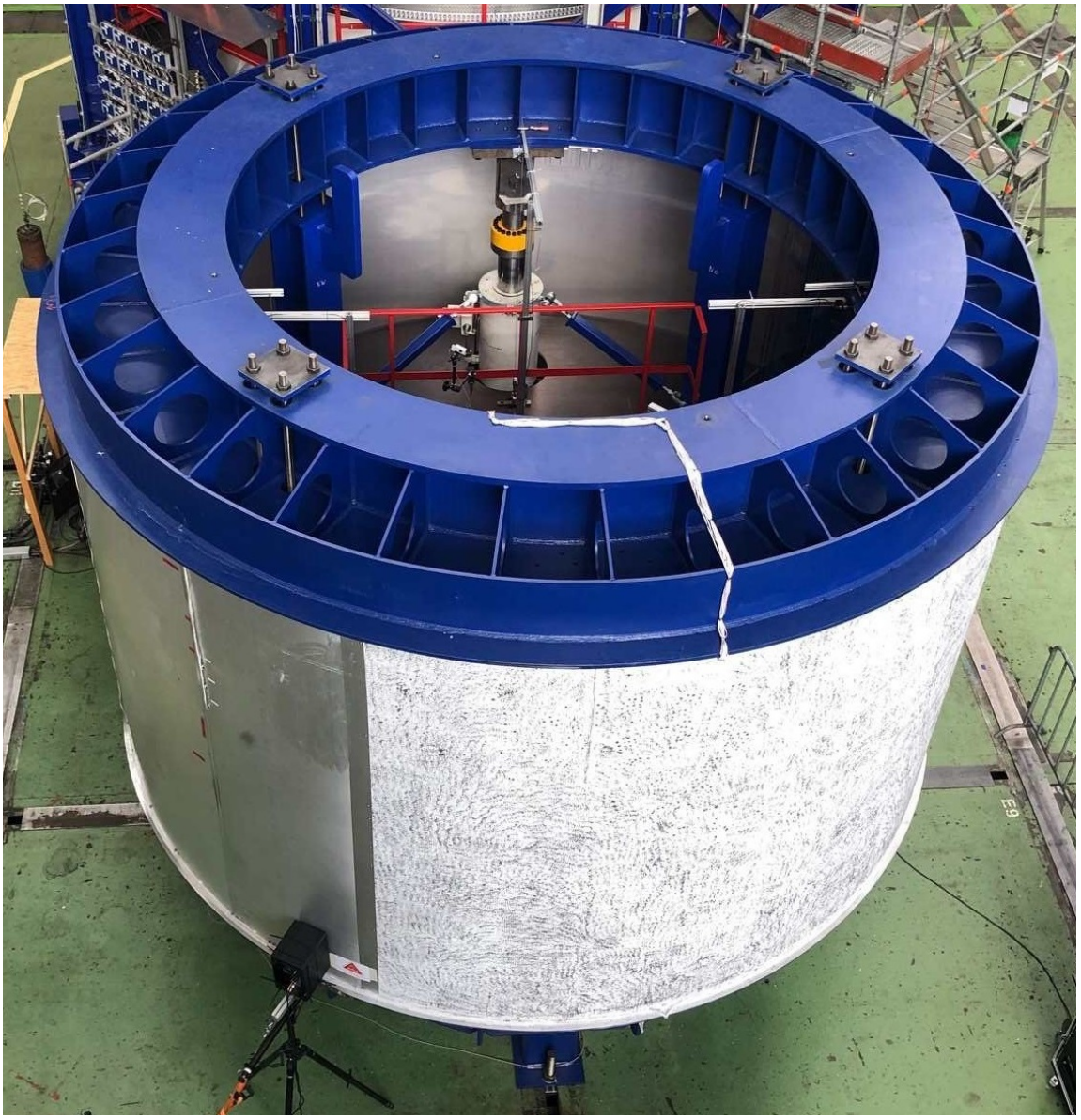

Figure 7.7 – Experimental setup of the barrel structure

Given the novelty of applying VCT during the buckling test of a cylindrical shell representative to a real-scale launcher structure, a conservative approach was taken regarding the structure's loading sequence. This presumed loading the structure before the last 3 VCT load steps at a load ratio higher than the one of the subsequent load steps. In doing so, it was verified that the structure would be able to sustain

the load defined for the next VCT load steps over the time needed to perform the vibration measurement. Additionally, a more conservative maximum load level to be measured than the one recommended based on the numerical analyses was chosen as well, given the relatively high risk of buckling occurring during the last vibration response measurement.

Figure 7.8 shows the VCT load steps and loading sequence for LC1, with the test time in minutes being shown on the horizontal axis, while on the vertical axis the normalised load with respect to the buckling load is shown. As it can be seen from this figure, the initial/reference load was not in an unloaded state, but at a small load ratio needed to initialise the 'closed' control loop. This initial load feedback was important in initialising the loop, as in the lack of it, in the worst-case scenario the control loop could have dictated actuator extension, which would have continued until either the actuators reached their maximum extension or the mechanical end stops. At this load level, needed to initialise the loop, any potential minor remaining gaps between the structure and loading rig would also be closed, thus providing consistent boundary conditions for the remaining load steps. Furthermore, for this load case a single pre-load was applied before the last 3 VCT load steps, during which a local bending was observed around a load ratio of 81%.

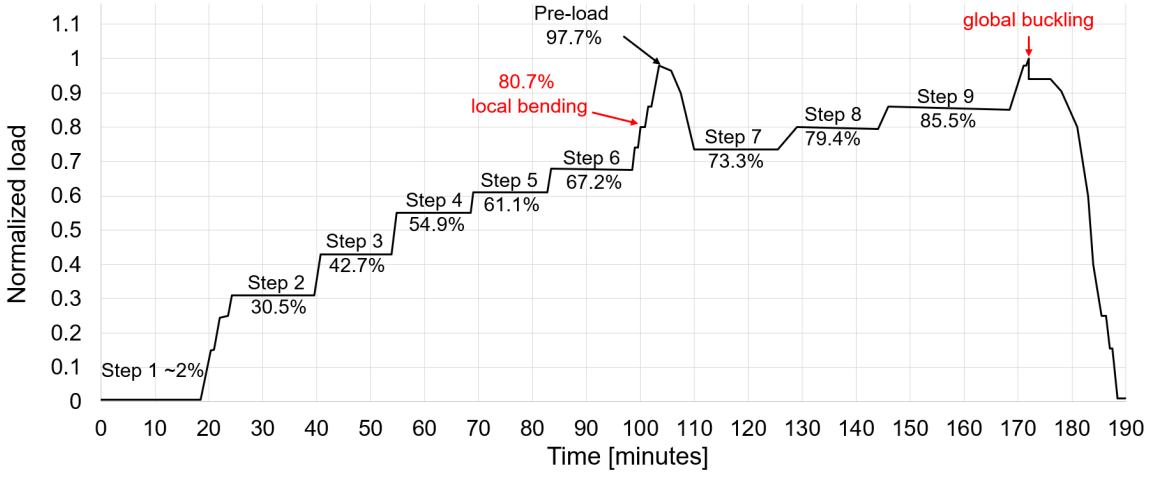

Figure 7.8 – VCT load steps and loading sequence for LC1

Figure 7.9 shows the frequency response for the first two load steps, together with the frequency response in unloaded state, in which the frequency is shown on the

horizontal axis and the magnitude is shown on the vertical axis. While a vibration measurement of the structure in unloaded state was not initially planned, this vibration measurement was taken to ensure that the VCT-related measuring equipment performed as intended, during the time the final checks prior to the main buckling test were made.

In this figure, two specific regions are highlighted to show an unexpected behaviour in the barrel's frequency response as the load applied increased. In the first highlighted region in red, it can be seen that either a vibration mode disappeared between load steps 1 and 2, or that a vibration mode significantly changed its frequency, which renders this specific vibration mode unusable for VCT. Furthermore, in the second highlighted region (in green) it can be seen that even when the frequencies of a vibration mode between the first 2 load steps were close to each other, the frequency of some modes increased with increasing the applied load, which also renders these vibration modes unusable for VCT. This implies that the first step did not ensure a load high enough to provide consistent boundary conditions with respect to the subsequent load steps, an aspect also stressed by the high similarity between the frequency response in the first load step and that in unloaded state. Due to this reason, the measurements at this load step could not be used for VCT.

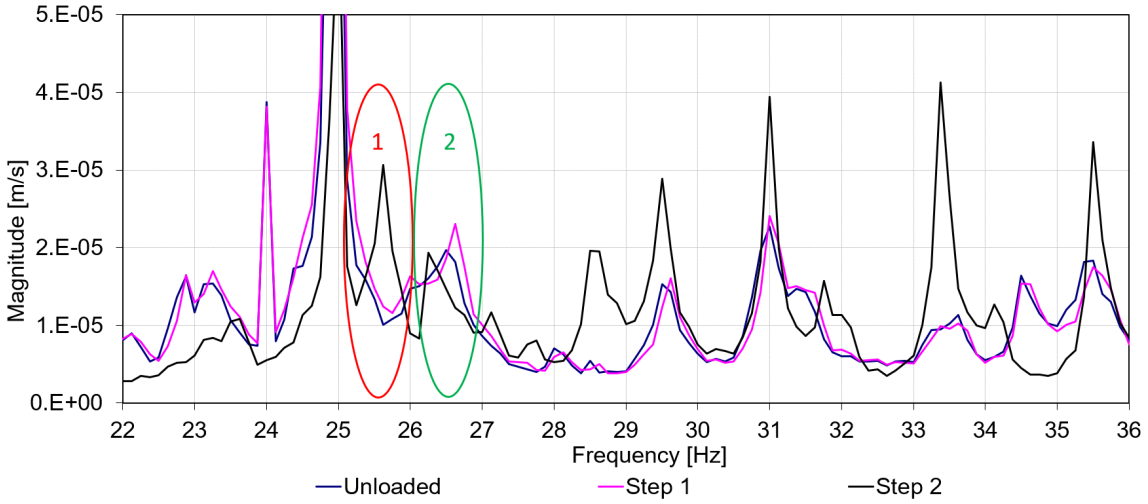

Figure 7.9 – Vibration response for the first 2 load steps of LC1

Figure 7.10 shows the frequency response for the usable load steps for LC1, in which

the in-situ monitored vibration modes are highlighted. Upon inspecting this figure, another unexpected behaviour can be noticed, which is best seen when comparing the evolution of the peaks, depicting vibration mode frequencies as the load applied increased, for the vibration modes 4, 5, and 6. The expected behaviour for the frequency evolution with increasing the applied compression load is displayed by mode 5, as the frequency of this vibration mode decreases as the applied load increases. On the other hand, after the 6^{th} load step the vibration mode 4 was no longer found, while the frequency of vibration mode 6 remained constant for the last 3 load steps. This meant that a change in the general frequency response occurred between load steps 6 and 7, which influenced almost all vibration modes. This change was given by the local bending occurring during the pre-loading stage before the last 3 load steps, local bending that did not disappear as the load was decreased for the 7^{th} vibration measurement.

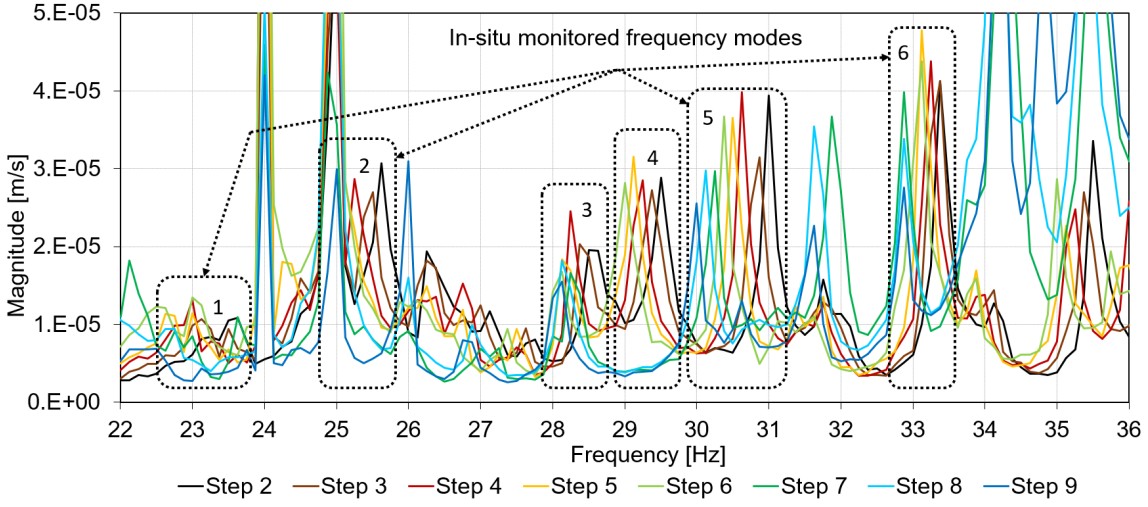

Figure 7.10 – Vibration response for the usable load steps and in-situ monitored vibration modes for LC1

The change in the frequency response between load steps 6 and 7 can also be seen in the vibration modes monitored in situ and deemed most reliable/likely to provide a robust VCT prediction, namely modes 1 and 5. The shape of these vibration modes is shown in Figure 7.11, where it can be seen that, while there is still a resemblance between the mode shapes at load steps before and after the 6^{th} load step, the consistency of these vibration modes is significantly higher either before, or

after the 6^{th} load step.

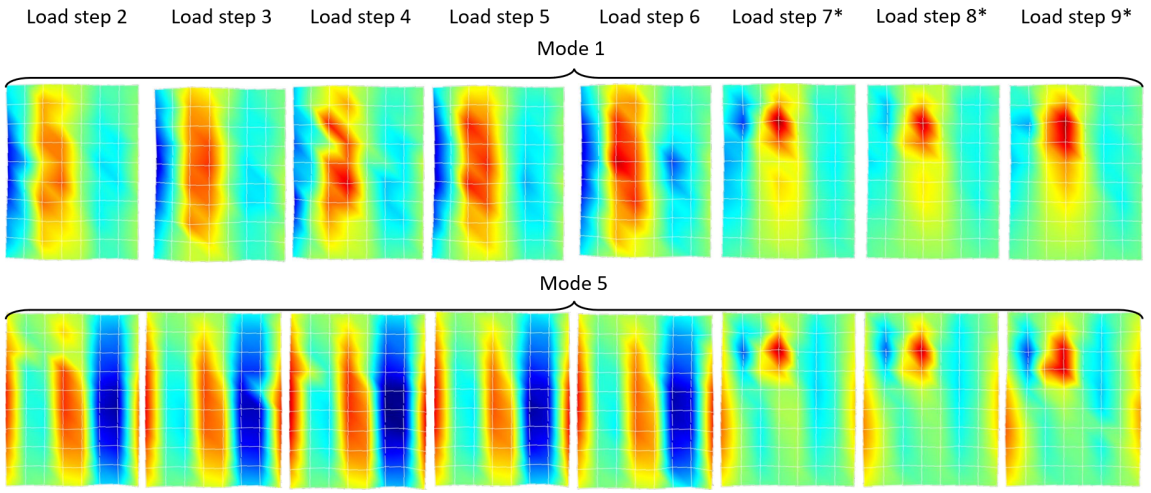

Figure 7.11 – Vibration modes of the modes 1 and 5 monitored in-situ for LC1

Figure 7.12 shows the relative errors of the VCT predictions based on modes 1 and 5 monitored in-situ. As it can be seen from this figure, vibration mode 5, as anticipated during the test, gave the most accurate prediction, with a relative error around 5%, while the best prediction given by mode 1 was around 21%. When comparing these results with the ones from the numerical analysis for this case, shown in Figure 7.5, it can be seen that for the highest load ratio tested, the prediction error was within the expected interval. Nevertheless, the sensitivity towards the maximum load ratio of the predictions based on experimental data was higher than anticipated based on the numerical analyses. In the numerical analysis, the lowest relative error was within 35%, regardless of the load ratio, and within 30% for a load ratio of 60%, which was the lowest load ratio for a valid prediction based on experimental results. On the other hand, in the predictions based on experimental results, at a maximum load ratio of 60% the error was between 40% and 45%.

After the test, an in-depth analysis of the experimental data was performed, and VCT predictions were performed using all the other vibration modes identified. Nevertheless, although vibration modes providing better accuracy were identified, these were not deemed representative due to their unusual behaviour. The aforementioned behaviour was primarily characterised by a lack of valid progressive predictions as the

load applied increased, aspect also favoured by the change in the vibration response of the structure between the load steps 6 and 7.

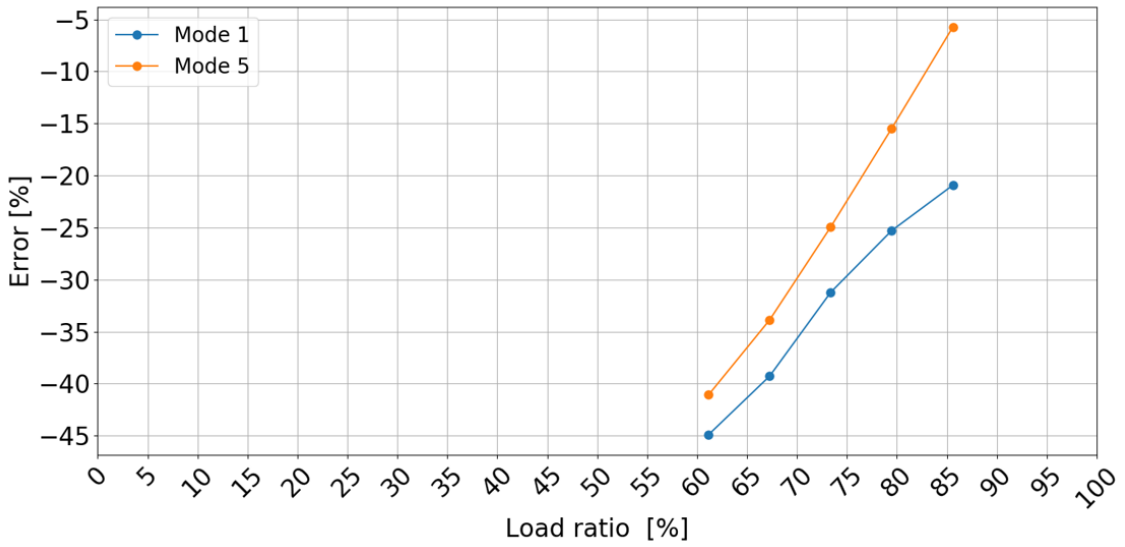

Figure 7.12 – LC1 VCT prediction error based on modes 1 and 5 monitored in-situ

Figure 7.13 shows the VCT load steps and loading sequence for LC2. Given the local bending observed for LC1 when a single, high pre-load was applied before the last 3 VCT load steps, the pre-loading approach was changed for LC2. In this approach, before each of the last 3 load steps, the load was increased by roughly 6% with respect to the buckling load, this load level being above the one at which the vibration response of the barrel was measured in the subsequent VCT load step.

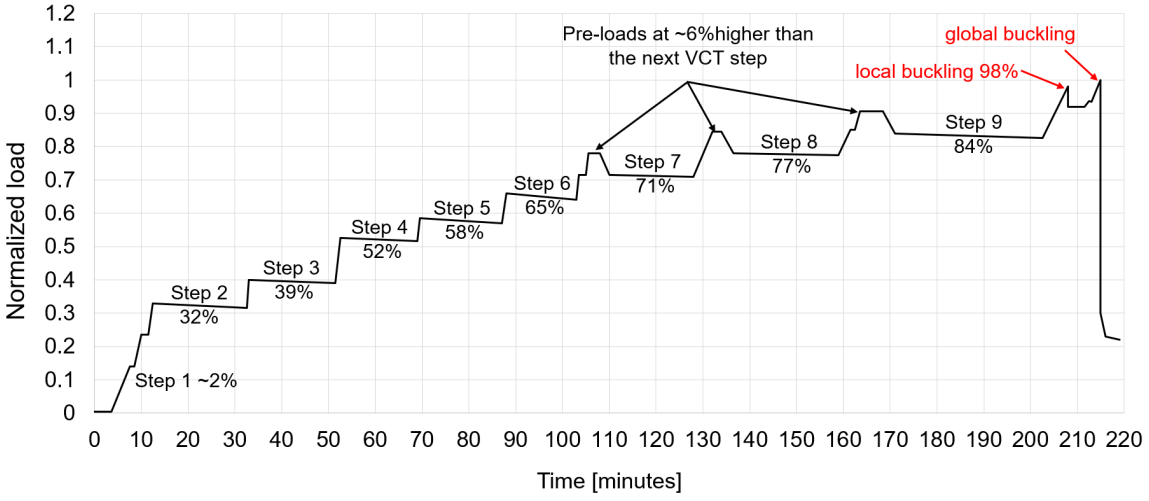

Figure 7.13 – VCT load steps and loading sequence for LC2

As it can also be seen in this figure, the load during the vibration response measurement was not kept perfectly constant, reason why the load used in the VCT prediction was the average load over the duration of the vibration measurement.

Similarly to LC1, a lack of consistency between the vibration modes of the first two load steps was also observed for LC2, as it can be seen from Figure 7.14. For this purpose, an area in which this behaviour is clearly seen was highlighted. In this area, it can be seen that the curve in black corresponding to the vibration response of the barrel for the first load step has 4 well-defined peaks, associated with vibration modes, while for the subsequent load steps in this region there are only 3.

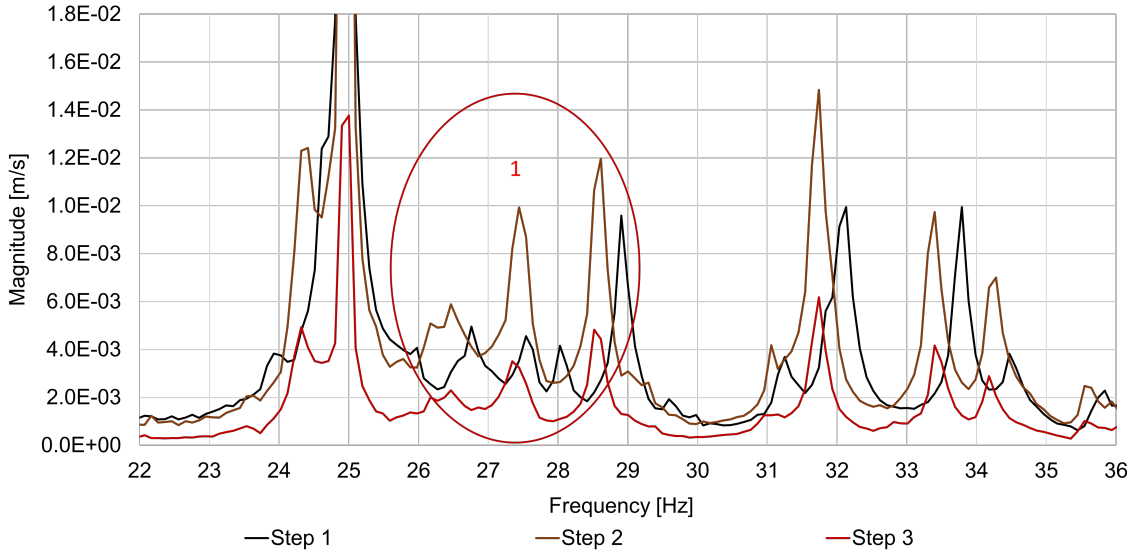

Figure 7.14 – Vibration response for the first 3 load steps of LC2

Nevertheless, for LC2 the correlation between the vibration response for the first load step and the ones that followed was significantly better than for LC1, as it can be seen when comparing figures 7.9 and 7.14, meaning that some of the vibration modes could be used in the VCT procedure.

Figure 7.15 shows the frequency response for the VCT load steps for the LC2 load case, in which the modes monitored in situ deemed most likely to provide a reliable prediction are highlighted, while the shapes of these modes are shown in Figure 7.16. In these figures, the vibration response and mode shapes for the first step were left out. This was chosen due to the uncertainty that this low load was enough to provide

consistent boundary conditions with respect to the subsequent load levels, therefore the initial measurement was not used in the VCT buckling load estimations provided in situ. Furthermore, the frequency response at the last load step was also left out due to the lack of consistency with the ones at lower load levels. This behaviour was similar to the one shown for LC1 in Figures 7.9 and 7.10 between the first two load steps and between the load steps before and after the 6^{th} one, respectively. Given the limited time to query the other measurements taken and the limited access to other measurement data, the reason for this behaviour cannot be given with a large degree of confidence. Nevertheless, given its occurrence at a relatively high load ratio, it was likely caused by a local effect, be it local bending as for LC1, or a local buckling.

An interesting observation is that in this figure, as well as in all the previously shown frequency response charts, an apparent vibration mode that does not change its frequency as the load increases can be seen at 25Hz. Given the consistency with which it appeared for both load cases, its constant frequency at 25Hz (regardless of the load case and level), as well as that this is exactly half of the power supply frequency, it was considered that this response was due to some interference between the laser vibrometer and the rest of the power equipment in its proximity and not an actual vibration mode.

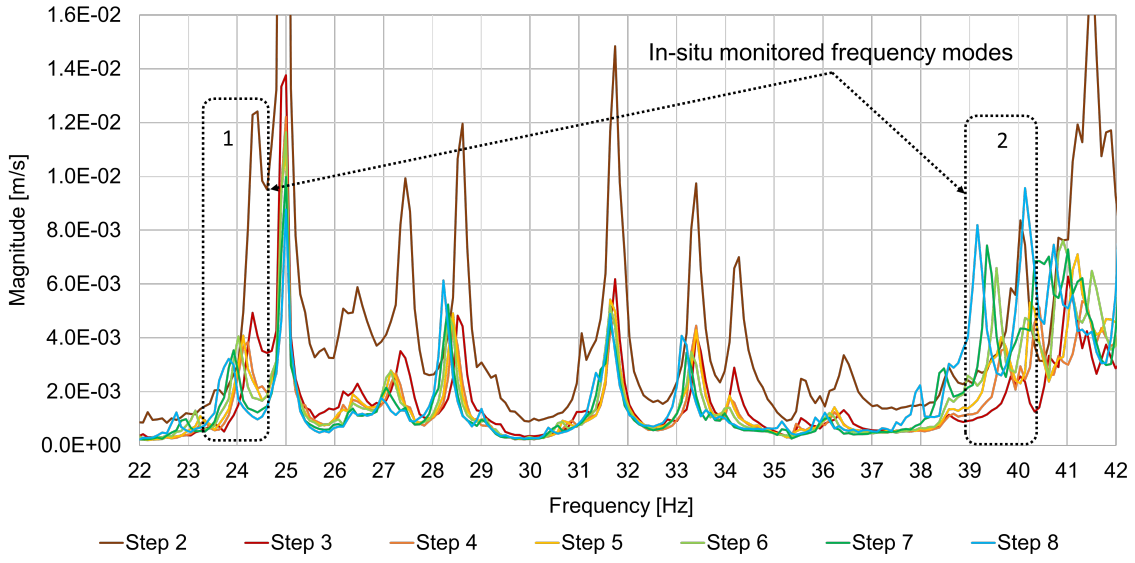

Figure 7.15 – Vibration response for the usable load steps and in-situ monitored vibration modes for LC2

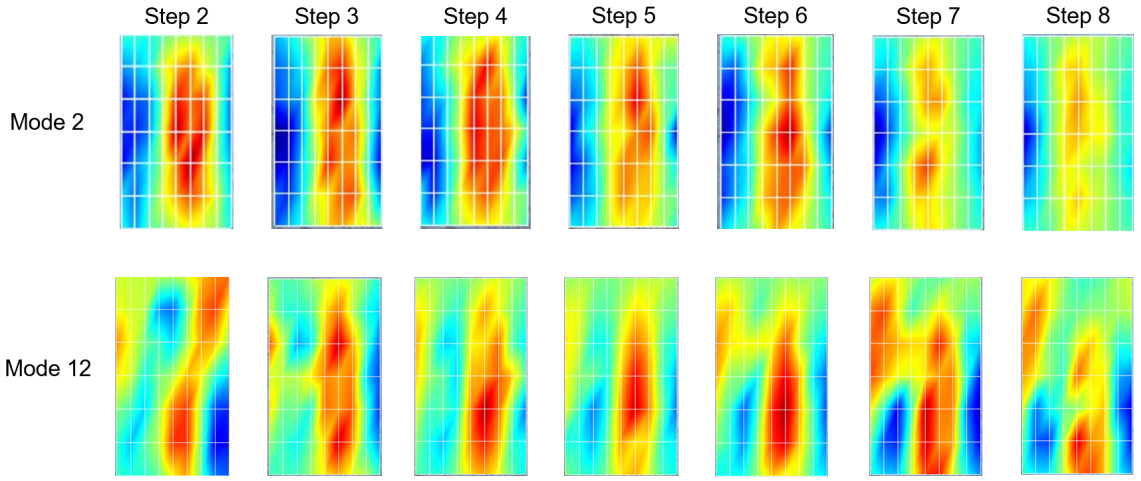

Figure 7.16 – Vibration modes of the modes 2 and 12 monitored in-situ for LC2

Figure 7.17 shows the relative errors of the VCT predictions for LC2, based on the vibration modes 2 and 12 monitored in situ. The best predictions, as expected, were obtained for the maximum load ratio available at 77%, with a 15% error for mode 2 and a 24% error for mode 12. Similarly to LC1, these predictions also fall within the expected error interval based on the numerical analysis, in which the prediction error for the majority of the vibration modes used at this load ratio was between 15% and 27%. Furthermore, for LC2 the expected relative error as a function of the maximum load ratio used in the VCT prediction was in a better agreement with the numerical analysis than for LC1. For LC2 the prediction errors at lower load ratios, including the one for the lowest load ratio of 57%, were also in line with the numerical results. While the in-situ VCT predictions for LC2 were slightly poorer than the ones for LC1, this fact is primarily due to the unusable last measurement. However, given the general approximately linear progression of the prediction with the maximum load ratio, extrapolating the predictions for modes 2 and 12 for the same maximum load ratio as for LC1, at 86%, would yield relative errors of 6% and 16.5%, which are comparable with the relative errors obtained for LC1 and also in line with the expected error interval for this load ratio based on the numerical analysis. When analysing the measurement data after the test, similarly as for LC1, other vibration modes did not yield a significantly better prediction than the one obtained using mode 2, with one exception in a mode for which the relative error of the prediction was 1%.

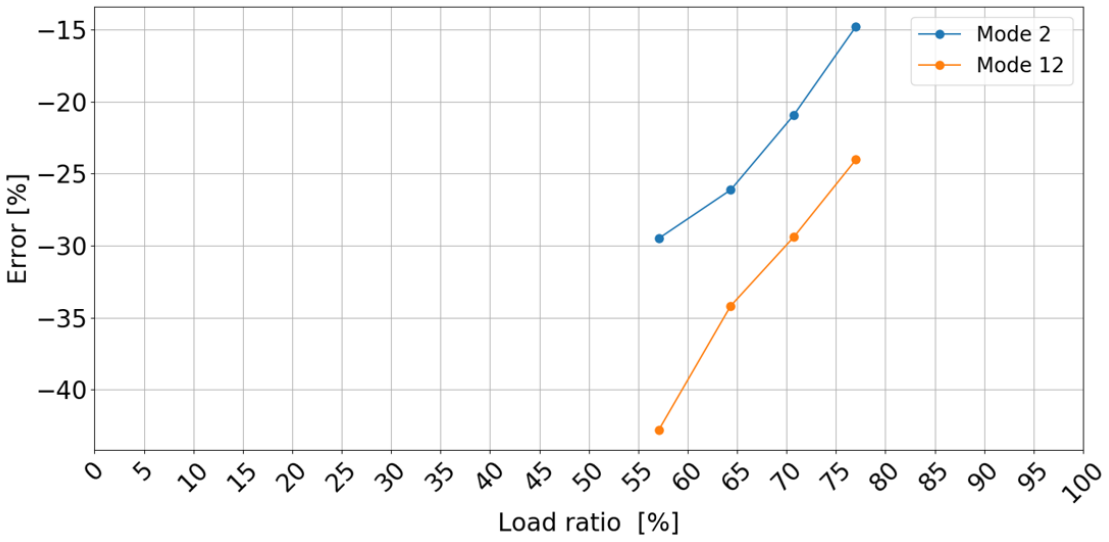

Figure 7.17 – LC2 VCT prediction error based on modes 2 and 12 monitored in-situ

7.4 Discussion

The VCT experiment for these load cases represented a novelty, considering that, to the author's best knowledge, it was the first time when VCT was applied for a cylinder representative to a real-scale launcher structure and also the first time when VCT was used to predict the load at which a cylindrical shell would buckle under uneven compression loads designed to induce significant bending components. Therefore, although the experiment in itself was a great success, the learning curve of using VCT for real-scale structures for load cases other than uniform axial compression remains steep, with plenty of room left for optimisation.

During this experimental campaign, two of the most restraining factors were that the VCT experiment was more of an add-on and not fully integrated into the overall experiment, while the other was time. Not having a fully integrated VCT test in the overall experiment meant that there were also some limitations on the fidelity of the FE model used in the numerical analysis and in obtaining the P_{cr} needed to obtain buckling load estimations via VCT. While the latter was previously shown in Chapter 5 to generally provide better VCT estimates when the geometry of the perfect structure is considered, in Chapter 6 it was also shown that for a bending-compression

load case this may no longer be valid and that slightly different average thickness and radius can have a significant impact on the value of P_{cr}. If such imperfections were present and the value of P_{cr} would have significantly changed when taking these into account, the P_{cr} values used here might not have been the best in the context of VCT, as for the ZD27 cylinder discussed in Chapter 6. Furthermore, the measured imperfections might have also helped to improve the correlation between the expected VCT error as a function of the maximum load ratio taken into account between the numerical and experimental VCT results.

While the first factor's influence was primarily on the robustness of the preliminary numerical analysis and on the outcome itself in a direct manner, time limitations had a less direct detrimental influence. The time constraints present restrained the robustness of the measurements, which indirectly also influenced the outcome of the experiment. Given that the allocated time was between 3 and 4 hours, compromises had to be made regarding the number of load steps, monitored area, density of the measurement grid, and measurement resolution.

While the number of load levels for which vibration measurements were taken was chosen according to the procedure described in Chapter 4 as a bare minimum to avoid the influences of possible measurement deviations, the actual number of load steps that could be used during the experiment was significantly lower due to unforeseen events. First, given that the load was not large enough to provide consistent boundary conditions with those at the following load levels, the measurement at the lowest load level was discarded entirely for LC1, while for LC2, it was only usable for a limited number of vibration modes. Furthermore, the high, single, pre-load before the last 3 measured load steps for LC1 induced a local bending that remained present throughout the rest of the test. This local bending caused a change in the vibration response of the structure, which in turn led to losing track of the majority of the monitored vibration modes before the pre-load was applied. This implied that for the vast majority of vibration modes identified, only 5 out of the initially planned 9 measurements could be used to perform buckling load estimations via VCT.

Following the first test for LC1, some changes were made for the test of LC2. One of

these changes was to further reduce the number of load steps, from 9 to 8, due to time constraints. While this aspect is not obvious from the measurement data, given that 9 load steps were quoted for both load cases, it can be seen in Figure 7.13 that the time corresponding to the first measurement was less than 4 minutes, which is significantly lower than the time needed to perform the measurements for the other load levels. Nevertheless, given the unique opportunity to perform VCT on a real-scale structure and to gain further insight, this vibration measurement was taken during the time needed to double-check all running equipment for the buckling test, even though the measurement at this load level proved unusable for LC1. The other significant change was in the pre-loading procedure before the last 3 load levels measured, which changed from a high, single, pre-load to lower pre-loads applied before each of the last 3 load steps measured. This change proved to be an inspired one, given that a change in the vibration response occurred for LC2 as well, this time between the last 2 load steps. In hindsight, had this change not been implemented, most likely it would have meant that the majority of the vibration modes from the last 3 measurements could not have been used as for LC1. Support for this affirmation is given by the change in the structure's equilibrium state that occurred between the last two load steps, leading to a vibration response change. Based on the experience gained from LC1, this change would have likely also occurred during a single, high pre-load and remained there for the rest of the test. Regardless of whether the unplanned load step around 2% for LC2 is taken into account or not, the number of generally usable measurements for LC2 was 7, which represents a significant improvement when compared to LC1, although still not completely satisfactory for research purposes.

Next, the area measured and the density of the measurement grid were also influenced by time constraints. While these have a somewhat lesser influence on the outcome, given that vibration modes can also be identified on frequency response charts, increasing the measured area can help with a better identification and tracking of vibration modes throughout the load levels measured. That said, increasing the area measured can only be done while ensuring that the pitch between the points is sufficiently small relative to the expected span of the circumferential waves and height

of the longitudinal waves of the vibration modes. Failing to do so can result in a poor identification and tracking of vibration modes, therefore lowering the confidence that the monitored vibration modes are accurately tracked across the measured load levels. However, increasing the density of the measurement grid has a direct influence on the measuring time when using a laser vibrometer, given that the measurement is taken for each grid point sequentially. On the other hand, using a high number of accelerometers mounted on the structure would highly increase both the complexity and the costs of the test setup, while also potentially influencing the buckling response of an imperfection-sensitive structure.

Lastly, the vibration measurement resolution was also affected by the imposed time constraints, as increasing it comes at a time penalty as well. The measurement resolution for LC1 was 0.125Hz, this being increased for LC2 to 0.1Hz. The initial resolution was chosen based on the numerical analysis, where at lower load levels the expected frequency drop of a vibration mode between consecutive load steps with a load ratio difference of 5% was between 0.1Hz and 0.16Hz for the vibration modes between 24Hz and 26Hz. Additionally, in the numerical analysis the vibration modes were tightly packed, with 8 modes being found between 24Hz and 26Hz. However, during the experimental test it was found that the frequency drops between the same load levels were slightly lower, therefore, ideally the measurement resolution should have been higher. Furthermore, the density of vibration modes found experimentally was significantly lower than expected based on numerical results, given that within the same interval only 2 vibration modes were found, instead of 8 as in the numerical analysis. While the number of vibration modes found within the aforementioned frequency window could have changed when including measured thickness and shape imperfections in the FE analyses, the chosen measurement resolution was also not sufficiently high to accurately identify low-energy vibration modes. The room for improvement left regarding the vibration measurement resolution can be seen in all previously shown frequency response charts, including for LC2 for which the measurement resolution was increased. In all these aforementioned figures, some of the peaks corresponding to vibration modes are not well-defined, especially the lower-

energy ones, which made the identification of their vibration frequency ambiguous, thus adversely impacting their use in the context of VCT.

7.5 Conclusions

In this chapter, the experimental validation of VCT for predicting the buckling load of a cylindrical shell representative to a real-scale structure under combined loading was shown. Given that the applied loads for the two load cases tested were uneven compression loads designed to induce significant bending within the structure, these load cases fall somewhere in between the ones applied in the investigation of the robustness of VCT in presence of in-plane imperfections, shown in Chapter 5 and the ones applied in the investigation on the robustness of VCT when applied to combined loads in which compression and bending were simultaneously applied, shown in Chapter 6.

The preliminary numerical investigation proved reliable in estimating the expected prediction error with respect to the maximum load ratio used, as well as the frequency window in which the first vibration modes would be found. A fair estimation was also provided regarding the expected frequency drop of the vibration modes as a function of the load applied, with the experimental investigation revealing that the aforementioned drop was slightly lower than expected.

Overall, VCT was able to provide reliable in-situ buckling load predictions for the load cases tested, despite the multiple shortcomings in applying this method which came primarily due to time constraints. For the first load case tested, the relative error of the in-situ VCT estimation using the vibration mode thought at the time most likely to yield a reliable prediction was around 5%, which was also in line with the numerical results. A more reliable prediction was not identified in the post-test analysis either, primarily due to a change in the structure's equilibrium state during the single, high, pre-load before the last 3 load levels measured, which induced a change in the structure's vibration response that remained present throughout the rest of the test. This meant that the majority of the vibration modes identified prior to

the pre-load could not be found in the subsequent load steps. On top of that, the load level of the initial measurement taken was not enough to provide consistent boundary conditions with the remainder of the load steps. Hence, the vibration response at this load level was inconsistent with those of the following load steps. This, together with the vibration response change beyond the 6^{th} load step, meant that for this load case, the majority of the vibration modes found could be used to perform VCT using only 5 out of the initially planned 9 load steps.

The experience gained from the first test was used to bring improvements to the second test, two of them being particularly relevant. Firstly, the pre-loading procedure was changed from a single, high, pre-load before the last 3 measurements, to pre-loads of a lower relative magnitude, but applied before each of the last 3 measurements taken. Secondly, the measurement resolution was increased from 0.125Hz to 0.1Hz. Owing to the change in the pre-load procedure, the number of load steps from which the majority of vibration measurements could be used for VCT increased from 5 for LC1, to 7 for LC2.

For LC2, the vibration mode monitored in situ, and thought to yield the most reliable estimation, provided a prediction within 15% with respect to the buckling load. Although this error was larger than the one obtained for LC1, it was attributed to the lower maximum load ratio that could be used in this prediction, at around 77%, with respect to the one for LC1 at roughly 86%. Given the approximately linear relationship between the maximum load ratio and the VCT estimation, extrapolating the error obtained for LC2 for the same maximum load ratio as measured for LC1 gave a prediction error of 6%, an accuracy similar to the one obtained for LC1.

The two experiments in which uneven compression loads, defined to induce significant bending components, were applied to a cylindrical shell representative to a real-scale launcher structure confirmed the versatility and robustness of the VCT method to predict in situ the buckling loads of such structures, where loads other than uniform compression are present. This, given the room left for improvement regarding the preparation for the experimental VCT procedure and the procedure itself, shows that VCT is a reliable non-destructive method to predict the axial loads at which these

structures buckle under combined loading, regardless of their size.

8 Practical guidelines

In the research conducted, there were several recurrent observations which can be useful in increasing the likelihood of a positive outcome of an experimental VCT test. In this chapter, a set of guidelines meant to support the preparation and conduct of the experimental test, as well as its outcome, is given as follows:

- The frequency window in which the first vibration modes are expected to appear can be determined beforehand, and measuring the vibration response of the structure in this particular frequency range can reduce the experiment time.
- The frequency measurement resolution can be defined based on the changes in the frequency of the vibration modes observed in a preliminary numerical analysis between the first two load steps.
- The desired number of load steps, maximum load level, and sensitivity to frequency deviations of the VCT predictions can be determined using the approach described in Section 4.1 of Chapter 4.
- Performing successive VCT estimations is useful in determining whether the obtained predictions might have a conservative or unconservative nature.
- The P_{cr} obtained for the perfect structure tends to provide the best VCT estimations, provided that its value is higher than the P_{nl} for the imperfect structure.

- In the event that local buckling occurs at a significantly lower load level than the one expected for global buckling, the frequency response beyond the local event may be used to obtain reliable VCT predictions, case in which using the

empirical VCT approach and the P_{cr} of the imperfect structure is recommended, due to the more conservative estimations obtained.

- When VCT is applied to combined load cases, performing the vibration measurements at different levels of compression alone is preferred, case in which the first measurement should be at 0 compression load.
- For combined load cases in which bending, shear, and/or torsion are applied next to compression, threshold values of these additional loads beyond which the VCT estimations cease to be reliable exist. Given that the threshold magnitudes of these loads varied slightly between the cylinders investigated in this study and significantly with the maximum load level used in the VCT procedure, prior to an experimental test, the applicability of the method for that specific structure, magnitude of additional loads applied, and desired maximum load level measured should be investigated.
- For bending-compression load cases, taking into account the bending load when determining the value of P_{cr} is essential for large magnitudes of bending applied.

- For shear-compression load cases, the P_{cr} obtained for the pure compression load case tends to provide the best VCT estimations

- When torsion, or multiple loads, are applied next to compression, whether the additional load(s) besides compression should be taken into account when determining the value of P_{cr} appeared to be cylinder specific, therefore this aspect should be clarified through numerical analyses before testing.
- If pre-loads are desired to ensure buckling would not occur during the time needed to perform vibration measurements, a sequential approach in which pre-loads are applied at load levels slightly higher than those of the subsequent vibration measurements is preferred instead of a single pre-load meant to cover the load levels of the subsequent measurements. In doing so, the risk of a local event occurring during a single, high, preload and remaining there throughout the rest of the measurements is reduced, promoting thus having a higher number of measurements that can be used in estimating the buckling load via VCT.

9 Final remarks

In this chapter, the key findings of the research conducted are shown in Section 9.1. Section 9.2 addresses the study's limitations, while in Section 9.3 several future research topics, aimed at adding further support to the study's conclusions and overall capabilities and limitations of VCT, are proposed.

9.1 Summary

The research conducted was aimed at showing that VCT can be a reliable non-destructive method to predict the axial load level at which cylindrical shells buckle, by addressing key aspects that may limit its application within the industry. In Chapter 4, focus was given to the VCT experiment design, by investigating the significance of the number of measurements taken and the maximum load level measured, including the influence of possible frequency measurement deviations. In the absence of frequency measurement errors, a clear variation in the buckling load estimations provided by VCT was only observed when varying the maximum load level taken into account. In this case, a strong positive monotonic relation between the predictions obtained and the maximum load level was observed in the results from numerical models. On the other hand, while varying the number of measurements taken a similar relation was not observed, taking into account more measurements did narrow the amplitude of the VCT predictions.

Regarding both the number of measurements and the maximum load level taken into account, threshold values beyond which significant changes were not observed

with respect to the baseline VCT predictions (employing all available load steps) were identified, these values being useful in preparing an experimental test. However, these threshold values were significantly influenced when frequency deviations were included, increasing proportionally with the magnitude of the frequency deviations introduced. This aspect was observed both in the analysis performed on numerical data, as well as in the one performed on experimental data. For the largest magnitude of random frequency deviations included, the recommended number of load steps based on the analysed data was at least 9, and with a maximum load level of at least 70%. These recommendations were made given that the differences between both the numerical and experimental VCT predictions when these conditions were satisfied lay predominantly within 10% with respect to the baseline predictions. Nevertheless, it was acknowledged that the identified threshold parameters may be different for other structures, therefore applying the procedure used in this investigation is recommended when these values need to be determined for an experimental test.

The investigation shown in Chapter 5 revealed that the method is generally insensitive to shape and loading imperfections, as in the absence of other detrimental factors, the VCT predictions showed little variation as a function of the applied magnitudes of these imperfections. The aforementioned detrimental factors consist of a low maximum load level, local buckling occurring, or a combination of cylinder configuration and imperfection signature that may render unreliable VCT predictions. In the numerical model of the cylinder used for this investigation, local buckling was observed when the magnitude of its shape imperfection introduced exceeded a certain value. Furthermore, the VCT predictions were also severely unconservative within a specific amplitude range of the shape imperfection introduced, even for amplitudes that did not induce local buckling. Thus, suggesting that this behaviour was given by the combination of the magnitude of its shape imperfection applied and/or cylinder configuration. For the cases where local buckling was seen, VCT proved unable to predict the load level at which it occurred. Nevertheless, given that the frequencies of some vibration modes in the load steps exclusively beyond this local buckling event still displayed the expected quadratic decrease in the VCT characteristic chart, VCT

predictions were also performed using these. While the analytical VCT procedure yielded overall unconservative predictions, the empirical VCT procedure proposed in [50], in which the P_{cr} for the imperfect structure was used, seemed to ameliorate the unconservative predictions and provide more reliable estimations on the global buckling load than the analytical procedure.

The method's applicability for combined load cases was addressed in Chapter 6, where the robustness of the VCT predictions on the axial load level at which buckling occurs when subjected to additional bending, transverse shear, and/or torsion was shown. In this investigation, it was found that VCT was able to provide reliable predictions of the buckling axial load, regardless of the type of additional load applied, load introduction method, and type of P_{cr} used, provided that the magnitude of the additional loads applied was low enough. Regardless of the type of additional loads, the best predictions were obtained when these loads were kept constant and the load steps were defined at different levels of compression load alone. Furthermore, while increasing the magnitude of the additional load applied lowered the robustness of the VCT predictions, regardless of the type of additional load introduced, a significantly lower influence for the bending-compression load case, when compared to the transverse shear-compression or torsion-compression load cases, was observed. In the former case, taking bending into account when determining the value of P_{cr} rendered reliable VCT predictions for significantly larger magnitudes of bending applied than when using the P_{cr} obtained for pure compression. Conversely, for the transverse shear-compression the opposite was observed, while for torsion-compression this aspect appeared to be cylinder-specific, as it did for the case when these additional loads were applied together next to compression in a sequential manner. On the other hand, when bending, transverse shear, and torsion were simultaneously introduced together with compression, the P_{cr} for the pure compression load case provided the most reliable predictions.

The majority of the key findings from the aforementioned investigations were validated on a VCT test of a cylindrical shell representative to a real-scale launcher structure, subjected to uneven compression load cases with significant bending com-

ponents, shown in Chapter 7. In the preparation of the test, the same procedure employed in the study focusing on the influence of the number of measurements and maximum load level shown in Chapter 4 was applied to determine the minimum number of load steps and maximum load level needed to obtain reliable predictions. In this investigation, it was found that 9 measurements in this case were also sufficient to reduce the variation of the VCT predictions, such that the vast majority of them were within 10% with respect to the baseline predictions employing all available load steps. Conversely, the VCT predictions appeared more sensitive to the maximum load level and vibration mode used than those of the small-scale cylinders, which in turn increased the maximum load level needed to obtain reliable predictions to at least 90%. The experimental results showed a good correlation with the numerical data, with accurate buckling load predictions provided by VCT, as long as the maximum load level taken into account was at least 85%.

Furthermore, when pre-loading the structure to ensure buckling would not occur during the time under which the structure is kept at a constant load to perform the frequency measurement, a sequential pre-load approach instead of a unique one would be preferred. Although this would be more time-consuming as the pre-loads would be applied before multiple vibration measurements, instead of a single pre-load at a high load level, the latter approach comes at a high risk of rendering the subsequent vibration measurements unusable in the context of VCT. Namely, a local event can occur during a single pre-load and remain present for the rest of the test. Given that a change in the structure's equilibrium state typically correlates to a change in its vibration response as well, there is a high risk of losing track of the previously monitored vibration modes beyond this event, thus rendering the subsequent vibration measurements unusable in providing buckling load estimates via VCT.

9.2 Discussion

The limited number of experimental VCT tests available within the literature means that the research conducted and conclusions drawn relied more on numerical, rather

than experimental, results. This, together with the fact that the existing experimental results are covering only small-scale structures, brings some limitations to the conducted study, as enumerated below:

1. While the magnitude of the frequency deviations introduced in the small-scale cylinders investigated in Chapter 4 was representative for their geometry and similar deviations were quoted in the available literature, the same is likely not the case when the scale of the structure is increased. Considering the case of the cylinder representative of a real-scale launcher structure, its frequency decrease between load steps of a 5% load ratio difference was around 0.125Hz. Had random frequency deviations within ±0.5Hz been introduced, there would have been multiple instances in which apparent frequency increases would have been observed as the compression load increased, describing thus an unrealistic behaviour. Therefore, while the investigation is relevant in assessing the qualitative influence of the number of measurements and maximum load level used over the VCT predictions, the threshold values identified are likely structure-specific.

2. In the event of local buckling occurring, the possibility of using load steps exclusively beyond this event to obtain a reliable estimation of the global buckling load was shown in Chapter 5. While in the experimental results of the two cylinders used to validate this observation, the change in frequency response was identical to the one observed in the numerical models due to local buckling, in the absence of additional experimental data, there is no absolute certainty that those changes in the frequency response observed during the test were due to local buckling.

3. The numerical study on the feasibility of VCT to predict the axial load level at which cylindrical shells buckle under combined loading, shown in Chapter 6, used a single approach to define boundary conditions, in which all degrees of freedom besides the ones used to introduce loads were constrained. While the boundary conditions used were also applied in experimental tests, there

were also multiple tests, particularly for shear or bending applied next to compression, in which the boundary conditions used were slightly different. One such case is the experimental campaign in which VCT provided robust buckling load estimations for a cylinder representative to a real-scale launcher structure, shown in Chapter 7. Nevertheless, the two uneven compression load cases under which the cylinder was tested, although presuming significant bending components, the magnitude of bending introduced was not at the level of the pure bending-compression load cases investigated in Chapter 6. Therefore, although the experimental results for the aforementioned test and the numerical results strongly suggest that VCT is able to provide reliable estimations of the axial load level at which cylindrical shells buckle under combined loading, these findings would greatly benefit from additional experimental validations.

9.3 Future research

Throughout the investigations conducted in this thesis, several further research topics that would advance the understanding of VCT's capabilities and limitations (besides the ones stemming from the aforementioned limitations) were identified as listed below:

1. When performing successive VCT predictions, some cases in which a decrease of the VCT predictions as the number of measurements taken into account increased were observed. This behaviour was observed for both experimental and numerical data sets, and while it could generally be identified with ease, it often led to conservative predictions only when load ratios around 80% and above were considered. Thus, understanding the reason behind this behaviour could help in improving the application on VCT, such that higher estimations are obtained consistently when increasing the number of measurements taken into account.

2. Although relatively rare, there were also cases in which the VCT predictions

were unconservative, for a different reason than the aforementioned one. This behaviour was attributed to particular shape imperfection patterns and/or the cylinder configurations. However, the exact reason why, for a given cylinder configuration and shape imperfection pattern, VCT yields poor predictions is not yet understood.

3. The feasibility, in the case local buckling occurs, of using load steps exclusively after this point to predict the global buckling load was supported with both numerical and experimental examples. However, while the frequency response change in the experimental results was very similar in nature to the one observed in the numerical data when local buckling occurred, the occurrence of local buckling in the experimental test was not confirmed. Therefore, further experimental proof would be required to cement this conclusion.

4. In the numerical investigation on the reliability of VCT to predict the axial load level at which cylinders buckle under combined loading, the method was shown to provide reliable estimations. Furthermore, VCT also provided reliable estimations on the buckling loads of a cylinder representative to a real-scale launcher structure, tested under two load cases presuming various degrees of uneven compression designed to induce significant bending loads. While these results are highly encouraging, additional experimental proof, implying different sets of boundary conditions as well, would be greatly beneficial in demonstrating the method's applicability to combined load cases.

To the author's best knowledge, the results shown in Chapter 7 were a first regarding the application of VCT for a real-scale cylinder representative to a launcher structure. While the buckling load predictions were robust and in a good agreement with the numerical results, despite the multiple unforeseen events that occurred during the test, this experimental campaign also revealed additional research topics needing further investigations. Most of these are related exclusively by the significant scale increase when compared to the structures for which VCT was previously applied, which inherently comes with a larger uncertainty and complexity in the structure's

response under loads, and are enumerated as follows:

1. For both of the load cases tested, it was found that the initial vibration measurement was not done at a load level sufficient to provide consistent boundary conditions, therefore also a consistent vibration response with the ones at the subsequent load levels. While it was shown that there is a strong monotonic relation between the maximum load level taken into account and the VCT predictions, the vibration response of the structure tested at low load ratios is also important in describing the change in the frequency response as the load applied increases. Therefore, there is a need of a better understanding of the minimum load level, as a function of the structure tested and test setup, beyond which a consistent vibration response with those in subsequent measurements is found.

2. While there is no available information about the potential frequency measurement deviations for this structure scale, given that the expected frequency decrease as the load increases for the first vibration modes was generally by one order of magnitude smaller than for the small-scale cylinders, in the event such deviations occurs, their influence over the obtained VCT predictions is likely also significantly higher, thus representing an aspect that needs to be further assessed.

3. Real-scale structures may often have additional structural features, the results shown in this research being for a cylinder with eight embossments distributed unequally across its circumference. Although in a study focusing on the applicability of VCT to open hole cylinders it was shown that the method is applicable as long as local buckling in the proximity of the hole is not triggered, an aspect that may hold true also for other types of structural features, a study addressing this topic would be valuable in showing the method's versatility and/or limitations.

A Appendix - Publications

The research conducted in pursuit of this PhD thesis led to several publications, out of which one published in a conference:

- Baciu TD, Degenhardt R, Franzoni F, Gliszczynski A, Arbelo MA, Castro SGP, Kalnins K, *Sensitivity to measurement parameters of the vibration correlation technique to predict shell buckling loads - a numerical study* (Conference: European Conference on Spacecraft Structures, Materials and Environmental Testing: ECSSMET 2021)

and three in scientific journals:

- Baciu TD, Degenhardt R, Franzoni F, Gliszczynski A, Arbelo MA, Castro SGP, Kalnins K, *Sensitivity analysis for buckling characterisation using the vibration correlation technique* (Thin-Walled Structures, Volume 183, 110329, 2023). https://doi.org/10.1016/j.tws.2022.110329.
- Baciu TD, Franzoni F, Degenhardt R, Kalnins K, Bisagni C, *Shape and loading imperfection sensitivity of the vibration-correlation technique for buckling analysis of cylindrical shells* (Engineering Structures, Volume 304, 117605, 2024). https://doi.org/10.1016/j.engstruct.2024.117605.
- Baciu TD, Franzoni F, Degenhardt R, Gliszczynski A, Bisagni C, *Vibration-correlation technique for predicting the compressive buckling load of cylindrical shells under combined loading* (Thin-Walled Structures Volume 216, Part B, 113576, 2025). https://doi.org/10.1016/j.tws.2025.113576

Bibliography

[1] Arbelo MA, Kalnins K, Ozoliņš O, Skukis E, Castro SGP, Degenhardt R, *Experimental and numerical estimation of buckling load on unstiffened cylindrical shells using a vibration correlation technique* (Thin-Walled Structures, Volume 94, pag. 273-279, 2015). https://doi.org/10.1016/j.tws.2015.04.024.

[2] Degenhardt R, Kling A, Bethge A, Orf J, Kärger L, Zimmermann R, *Investigations on imperfection sensitivity and deduction of improved knock-down factors for unstiffened CFRP cylindrical shells* (Composite Structures, Volume 92, Issue 8, pag. 1939–1946, 2010). https://doi.org/10.1016/j.compstruct.2009.12.014.

[3] Kalnins K, Arbelo MA, Ozoliņš O, Skukis E, *Experimental nondestructive test for estimation of buckling load on unstiffened cylindrical shells using vibration correlation technique* (Shock and Vibration, 2015). http://dx.doi.org/10.1155/2015/729684.

[4] Franzoni F, Odermann F, Wilckens D, Skukis E, Kalnins K, Arbelo MA, Degenhardt R, *Assessing the axial buckling load of a pressurized orthotropic cylindrical shell through vibration correlation technique* (Thin-Walled Structures, Volume 137, pag. 353-366, 2019). https://doi.org/10.1016/j.tws.2019.01.009.

[5] Southwell RV, *On the general theory of elastic stability* (Philosophical Transactions of the Royal Society A 1914;213:187–244, 1914). https://doi.org/10.1098/rsta.1914.0005.

[6] Hilburger MW, *Buckling of thin walled circular cylinders, NASA/SP-8007-2020/REV 2* (NASA Langley Research Center, 2020). https://ntrs.nasa.gov/citations/20205011530.

[7] Castro SGP, Zimmermann R, Arbelo MA, Khakimova R, Hilburger MW, Degenhardt R, *Geometric imperfections and lower-bound methods used to calculate knock-down factors for axially compressed composite cylindrical*

shells (Thin-Walled Structures, Volume 74, pag. 118-132, 2014). https://doi.org/10.1016/j.tws.2013.08.011.

[8] Kepple J, Herath M, Pearce G, Prusty G, Thomson R, Degenhardt R, *Improved stochastic methods for modelling imperfections for buckling analysis of composite cylindrical shells* (Engineering Structures, 2015). https://doi.org/10.1016/j.engstruct.2015.06.013.

[9] Thompson JMT, *Advances in shell buckling: Theory and experiments* (International Journal of Bifurcation and Chaos, Volume 25, No. 1, 2015). https://doi.org/10.1142/S0218127415300013.

[10] Arbelo MA, de Almeida SFM, Donadon M, Rett, SR, Degenhardt R, Castro SGP, Kalnins K, Ozoliņš O, *Vibration correlation technique for the estimation of real boundary conditions and buckling load of unstiffened plates and cylindrical shells* (Thin-Walled Structures, Volume 79, pag. 119-128, 2014). https://doi.org/10.1016/j.tws.2014.02.006.

[11] Horák J, Lord GJ, Peletier MA, *Cylinder buckling: The mountain pass as an organizing center* (CSIAM J. APPL. MATH, Volume 66, Issue 5, pag. 1793–1824, 2010). https://doi.org/10.1137/050635778.

[12] Hutchinson JW, Thompson JMT, *Imperfections and energy barriers in shell buckling* (International Journal of Solids and Structures Volumes 148-149, pag. 157-168, 2018). https://doi.org/10.1016/j.ijsolstr.2018.01.030.

[13] Fan H, *Critical buckling load prediction of axially compressed cylindrical shell based on non-destructive probing method* (Thin-Walled Structures, Volume 139, pag. 91–104, 2019). https://doi.org/10.1016/j.tws.2019.02.034.

[14] Li W, Fan H, *Free vibration behaviors and vibration correlation technique of hierarchical Isogrid stiffened composite cylinders* (Thin-Walled Structures, Volume 159, 107321, 2021). https://doi.org/10.1016/j.tws.2020.107321.

[15] Somerfeld A, *Eine einfache Vorrichtung zur Veranschaulichung des Knick-ungsvorganges* (Z Ver Dtsch Ing Volume 49, pag. 1320–1323, 1905).

[16] Melan H, *Kritische Drehzahlen von Wellen mit Langsbelastung* (Zeitschrijt der Osterr lngenieur- und Architekten-Vereines Volume 69, pag. 610-612, 619-621, 1917).

[17] Ban S, *Über die Knicklast und die Eigenschwingungszahl eines längsbelasteten Stabes* (Memoirs of the College of Engineering, Kyoto Imperial University Volume 4, Issue 4, pag. 275-291, 1931). http://hdl.handle.net/2433/280112.

[18] Engler W, *Untersuchung der Knickfestigkeit und des Einspannungsverbältnisses von Balken auf dynamischem Wege* (1922).

[19] Föppl L, *Bestimmung der Knicklast eines Stabes aus Schwingungsversuchen* (Beiträge zur technischen Mechanik und technischen Physik, pag. 82-88, 1924). DOI10.1007/978-3-642-51983-3.

[20] Engler W, *Eine neue Methode zur Untersuchung der Knickfestigkeit und des Einspannungsgrads* (Der Bauingenieur, pag. 343, 1926).

[21] Grauers H, *Transversalschwingungen rechteckiger Platten mit besonderer Rücksicht der Knickung* (Ingeniörs vetenskaps akademiens: handlingar, Nr. 98 Svenska Bokhandelscentralen, 1929).

[22] Schaefer H, Havers A, *Die Eigenschwingungen der in ihrer Ebene allseitig gleichmäßig belasteten gleichseitigen Dreiecksplatte* (Ingenieur-Archiv volume 7, Issue 1, pag. 83-87, 1936). https://doi.org/10.1007/BF02084138.

[23] Stephens BC, *Natural vibration frequencies of structural members as an indication of end fixity and magnitude of stress* (Journal of the Aeronautical Sciences, Volume 4, Issue 2, pag. 54–60, 1936). https://doi.org/10.2514/8.321.

[24] Massonnet CE, *Les Relations entre les modes normaux de vibration et la stabilit´e des syst'emes elastiques* (1940).

[25] Massonnet CE, *Le voilement des plaques planes sollicit´ees dans leur plan* (1948). https://www.e-periodica.ch/cntmng?pid=bse-cr-001:1948:3::128.

[26] Lurie H, *Lateral vibrations as related to structural stability* (ASME Journal of Applied Mechanics Volume 19, pag. 195–204, 1952). https://doi.org/10.1115/1.4010446.

[27] Johnson EE, Goldhammer BF, *The determination of the critical load of a column or stiffened panel by the vibration method* (Proceedings of the Society for Experimental Stress Analysis, Volume 11, pag. 221–232, 1953). .

[28] Ponsford HT, *The effects of stiffness on the buckling of cylinders with moderate wall thickness* (Ph.D. Dissertation, California Institute of Technology, 1953). https://doi:10.7907/JAYX-PF29.

[29] Thielmann W, Garkisch HD, *Einfluss von Schiiringungen auf die Beullast dunnwandiger Kreiszylinderschalen* (DFL Bericht, Braunschweig, 1965).

[30] Bozich WF, *Technical report AFFDL-TR-67-28, The vibration and buckling characteristics of cylindrical shells under axial load and external pressure* (USAF, Air Force Flight Dynamics Lab Wright-Patterson, Air Force Base Ohio, Vehicle Dynamics Division, 1967). https://apps.dtic.mil/sti/pdfs/AD0656302.pdf.

[31] Okubo S, Whittier JS, *A note on buckling and vibrations of an externall pressurized shallow spherical shell* (Journal of Applied Mechanics, Volume 34 Issue 4, pag. 1032–1034, 1967).

[32] Fung YG, Kaplan A, Sechler EE, *Experiments on the vibration of thin cylindrical shells under internal pressure* (The Ramo-Wooldridge Corporation, Guided Missile Research Division, 1955). https://apps.dtic.mil/sti/pdfs/AD0607517.pdf.

[33] Radhakrishnan R, *Prediction of buckling strengths of cylindrical shells from their natural frequencies* (Earthquake Engineering and Strucural Dynamics, Volume 2, pag. 107–115, 1973). https://doi.org/10.1002/eqe.4290020202.

[34] Penzes LE, *Effect of boundary conditions on flexural vibrations of thin orthogonally stiffened cylindrical shells* (The Journal of the Acoustical Society of America, Volume 42, Issue 4, pag. 901–903, 1967). https://doi.org/10.1121/1.1910668.

[35] Bassily SF, Dickenson SM, *Buckling and lateral vibration of rectangular plates subject to inplane loads-A Ritz approach* (Journal of Sound and Vibration, Volume 24, Issue 2, pag. 219-239, 1972). https://doi.org/10.1016/0022-460X(72)90951-0.

[36] Rosen A, Singer J, *Vibrations of axially loaded stiffened cylindrical shells* (Journal of Sound and Vibration Volume 34, Issue 3, pag. 357-378, 1974). https://doi.org/10.1016/S0022-460X(74)80317-2.

[37] Chailleux A, Hans Y, Verchery G, *Experimental study of the buckling of laminated composite columns and plates* (International Journal of Mechanical Sciences, Volume 17, Issue 8, pag. 489–498, 1975). https://doi.org/10.1016/0020-7403(75)90013-2.

[38] Jubb JEM, Phillips IG, Becker H, *Interrelation of structural stability, stiffness, residual stress and natural frequency* (Journal of Sound and Vibration, Volume 39, Issue 1, pag. 121-134, 1975). https://doi.org/10.1016/S0022-460X(75)80212-4.

[39] Rosen A, Singer J, *Vibrations and buckling of eccentrically loaded stiffened cylindrical shells* (Experimental Mechanics, Volume 16, pag. 88–94, 1976). https://doi.org/10.1007/BF02324891.

[40] Singer J, Abramovich H, *Vibration techniques for definition of practical boundary conditions in stiffened shells* (AIAA Journal, Volume 17, Issue 7, pag. 762–769, 1978). https://doi.org/10.2514/3.61215.

[41] Souza MA, Fok WC, Walker AC, *Review of experimental techniques for thin-walled structures liable to buckling: Neutral and unstable buckling* (Experimental Techniques, Volume 7, Issue 9, pag. 21-25, 1983). https://doi.org/10.1111/j.1747-1567.1983.tb01811.x.

[42] Franzoni F, Degenhardt R, Albus J, Arbelo MA, *Vibration correlation technique for predicting the buckling load of imperfection-sensitive isotropic cylindrical shells: An analytical and numerical verification* (Thin-Walled Structures, Volume 140, pag. 236–247, 2019). https://doi.org/10.1016/j.tws.2019.03.041.

[43] Arbelo MA, Castro SGP, Khakimova R, Degenhardt R, *Improving the correlation of finite element models using vibration correlation technique on composite cylindrical shells* (54th Israel Annual Conference on Aerospace Sciences, Tel-Aviv and Haifa, Volume 1, pag. 453-459, 2014). .

[44] Arbelo MA, Herrmann A, Castro SGP, Khakimova R, Zimmermann R, Degenhardt R, *Investigation of buckling behavior of composite shell structures with cutouts* (Applied Composite Materials, Volume 22, pag. 623–636, 2015). https://doi.org/10.1007/s10443-014-9428-x.

[45] Skukis E, Kalnins K, Ozoliņš O, *Application of vibration correlation technique for open hole cylinders* (Proceedings of the 5th International Conference on Nonlinear Dynamics, Kharkov, September 27-30, Volume 5, pag. 377-383, 2016). http://repository.kpi.kharkov.ua/handle/KhPI-Press/24830.

[46] Skukis E, Ozoliņš O, Andersons J, Kalnins K, Arbelo MA, *Applicability of the vibration correlation technique for estimation of the buckling load in axial compression of cylindrical isotropic shells with and without circular cutouts* (Shock and Vibration, Volume 5, pag. 377-383, 2017). https://doi.org/10.1155/2017/2983747.

[47] Labans E, Abramovich H, Bisagni C, *An experimental vibration-buckling investigation on classical and variable angle tow composite shells under axial compression* (Journal of Sound and Vibration, Volume 449, pag. 315-329, 2019). https://doi.org/10.1016/j.jsv.2019.02.034.

[48] Shahgholian-Ghahfarokhi D, Rahimi G, *Buckling load prediction of grid-stiffened composite cylindrical shells using the vibration correlation technique* (Composites Science and Technology, Volume 167, pag. 470–481, 2018). https://doi.org/10.1016/j.compscitech.2018.08.046.

[49] Shahgholian-Ghahfarokhi D, Rahimi G, Liaghat G, Franzoni F, Degenhardt R, *Buckling prediction of composite lattice sandwich cylinders (CLSC) through the vibration correlation technique (VCT): Numerical assessment with experimental and analytical verification* (Composites Part B: Engineering, Volume 199, 2020). https://doi.org/10.1016/j.compositesb.2020.108252.

[50] Skukis E, Jekabsons G, Andersons J, Ozoliņš O, Labans E, Kalnins K, *Robustness of empirical vibration correlation techniques for predicting the instability of unstiffened cylindrical composite shells in axial compression* (Polymers, Volume 12, 2020). https://doi.org/10.3390/polym12123069.

[51] Skukis E, Jekabsons G, Ozoliņš O, Kalnins K, *VCT Vibration correlation technique for assessment of structural load bearing capacity* (Institute of Materials and Structures Riga Technical University, 2020). http://vct.rtu.lv/results.html.

[52] Tian K, Huang L, Sun Y, Yang M, Hao P, Wang B, *Concurrent numerical implementation of vibration correlation technique for fast buckling load prediction of cylindrical shells under combined loading conditions* (Engineering with Computers, Volume 38, pag. 3269–3281, 2021). https://doi.org/10.1007/s00366-021-01458-9.

[53] Tian K, Huang L, Sun Y, Du K, Hao P, Wang B, *Fast buckling load numerical prediction method for imperfect shells under axial compression based on POD and vibration correlation technique* (Composite Structures, Volume 252, 112721, 2020). https://doi.org/10.1016/j.compstruct.2020.112721.

[54] Tian K, Huang L, Sun Y, Zhao L, Gao T, Wang B, *Combined approximation based numerical vibration correlation technique for axially loaded cylindrical shells* (European Journal of Mechanics / A Solids, Volume 93, 104553, 2022). https://doi.org/10.1016/j.euromechsol.2022.104553.

[55] Segall A, Springer GS, *A dynamic method for measuring the critical loads of elastic flat plates* (Experimental Mechanics, Volume 26, pag. 354–359, 1986). https://doi.org/10.1007/BF02320151.

[56] Go CG, Lin YS, Khor EH, *The effects of initial imperfection and changing support conditions on the vibration of structural elements liable to buckling* (Journal of Sound and Vibration, Volume 205, Issue 3, pag. 257-264, 1997). https://doi.org/10.1006/jsvi.1995.1047.

[57] Franzoni F, Odermann F, Lanbans, E, Bisagni C, Arbelo MA, Degenhardt R, *Experimental validation of the vibration correlation technique robustness to predict buckling of unstiffened composite cylindrical shells* (Composite

Structures, Volume 224, 2019).
https://doi.org/10.1016/j.compstruct.2019.111107.

[58] Glantz M and Kissell R, *Multi-asset risk modeling: Techniques for a global economy in an electronic and algorithmic trading era* (Academic Press, 2014). https://doi.org/10.1016/C2012-0-00800-9.

[59] Puth M.T, Neuhäuser M, Ruxton G.D, *Effective use of Spearman's and Kendall's correlation coefficients for association between two measured traits* (Animal Bejaviour, Volume 102, Pages 77-84, 2015). https://doi.org/10.1016/j.anbehav.2015.01.010.

[60] Schober P, Boer C, Schwarte L.A, *Correlation coefficients: Appropriate use and interpretation* (Anesthesia and Analgesia, Volume 126, Issue 5, pag. 1763-1768, 2018). 10.1213/ANE.0000000000002864.

[61] G. van den Berg, Kendall's Tau – Simple Introduction. Https://www.spss-tutorials.com/kendalls-tau/.

[62] Labans E, Bisagni C, *Buckling and free vibration study of variable and constant-stiffness cylindrical shells* (European Conference on Spacecraft Structures, Materials and Environmental Testing (ECSSMET), 2018). https://doi.org/10.1016/j.compstruct.2018.11.061.

[63] Wang B, Zhu S, Hao P, Bi X, Du K, Chen B, Ma X, Chao YJ, *Buckling of quasi-perfect cylindrical shell under axial compression: A combined experimental and numerical investigation* (International Journal of Solids and Structures Volumes 130–131, pag 232-247, 2018). https://doi.org/10.1016/j.ijsolstr.2017.09.029.

[64] Jiao P, Chen Z, Xu F, Tang X, Su W, *Effects of ringed stiffener on the buckling behavior of cylindrical shells with cutout under axial compression: Experimental and numerical investigation* (Thin-Walled Structures, Volume 123, pag. 232–243, 2018). https://doi.org/10.1016/j.tws.2017.11.013.

[65] Jiao P, Chen Z, Tang X, Su W, Wu J, *Design of axially loaded isotropic cylindrical shells using multiple perturbation load approach – Simulation and validation* (Thin-Walled Structures, Volume 133, pag. 1–6, 2018). https://doi.org/10.1016/j.tws.2018.09.028.

[66] Jeon MH, Cho HJ, Sim CH, Kim YJ, Lee MY, Kim IG, Park JS, *Experimental and numerical approach for predicting global buckling load of pressurized unstiffened cylindrical shells using vibration correlation technique* (Composite Structures, Volume 305, 116460, 2023). https://doi.org/10.1016/j.compstruct.2022.116460.

[67] Khakimova R, Wilckens D, Reichardt J, Zimmermann R, Degenhardt R, *Buckling of axially compressed CFRP truncated cones: Experimental and numerical investigation.* (Composite Structures, Volume 146, pag. 232–247, 2016). https://doi.org/10.1016/j.compstruct.2016.02.023.

[68] Holst JMFG, Rotter JM, *Axially compressed cylindrical shells with local settlement* (Thin-Walled Structures, Volume 43, Issue 5, pag. 811-825, 2005). https://doi.org/10.1016/j.tws.2004.10.011.

[69] Błachut J, *Buckling of axially compressed cylinders with imperfect length* (Computers and Structures, Volume 88, Issues 5-6 pag. 365–374, 2010). https://doi.org/10.1016/j.compstruc.2009.11.010.

[70] Cao Q, Zhao Y, *Buckling strength of cylindrical steel tanks under harmonic settlement* (Thin-Walled Structures, Volume 48, Issue 6, pag. 391–400, 2010). https://doi.org/10.1016/j.tws.2010.01.011.

[71] Kriegesmann B, Hilburger M, Rolfes R, *The effects of geometric and loading imperfections on the response and lower-bound buckling load of a compression-loaded cylindrical shell* (53rd AIAA/ASME/ASCE/AHS/ASC Structures, Structural Dynamics and Materials Conference, 2012). https://doi.org/10.2514/6.2012-1864.

[72] Chen Z, Fan H, Cheng, Jiao P, Xu F, Zheng C, *Buckling of cylindrical shells with measured settlement under axial compression* (Thin-Walled Structures, Volume 123, pag. 351–359, 2018). https://doi.org/10.1016/j.tws.2017.11.006.

[73] Wagner HNR, Hühne C, Janssen M, *Buckling of cylindrical shells under axial compression with loading imperfections: An experimental and numerical campaign on low knockdown factors* (Thin-Walled Structures, Volume 151, 106764, 2020). https://doi.org/10.1016/j.tws.2020.106764.

[74] Wagner HNR, Hühne C, Niemann S, Khakimova R, *Robust design criterion for axially loaded cylindrical shells - Simulation and Validation* (Thin-Walled Structures, Volume 115, pag. 154-162, 2017). https://doi.org/10.1016/j.tws.2016.12.017.

[75] Khakimova R, Castro SGP, Wilckens D, Rohwer K, Degenhardt R, *Buckling of axially compressed CFRP cylinders with and without additional lateral load: Experimental and numerical investigation* (Thin-Walled Structures, Volume 119, pag. 178-189, 2017). https://doi.org/10.1016/j.tws.2017.06.002.

[76] Jiao P,Chen Z,Ma H, Ge P, Gu Y, Miao H, *Buckling behaviors of thin-walled cylindrical shells under localized axial compression loads, Part 1: Experimental study* (Thin-Walled Structures, Volume 166, pag. 108118, 2021). https://doi.org/10.1016/j.tws.2021.108118.

[77] Franzoni F, Degenhardt R, Albus J, Arbelo MA, *Numerical assessment of existing vibration correlation techniques* (European Conference on Spacecraft Structures, Materials and Environmental Testing (ECSSMET), 2018). https://elib.dlr.de/124717/.

[78] Yeh MK, Lin MC, Wu WT, *Bending buckling of an elastoplastic cylindrical shell with a cutout* (Engineering Structures, Volume 21, Issue 11, pag. 996-1005, 1999). https://doi.org/10.1016/S0141-0296(98)00058-3.

[79] Li LY, Kettle R, *Nonlinear bending response and buckling of ring-stiffened cylindrical shells under pure bending* (International Journal of Solids and Structures Volume 39, Issue 3, pag. 765-781, 2002). https://doi.org/10.1016/S0020-7683(01)00174-3.

[80] Tafreshi A, Bailey CG, *Instability of imperfect composite cylindrical shells under combined loading* (Composite Structures, Volume 80, Issue 1, pag. 49-64, 2007). https://doi.org/10.1016/j.compstruct.2006.02.031.

[81] Tafreshi A, *Instability of delaminated composite cylindrical shells under combined axial compression and bending* (Composite Structures, Volume 82, Issue 3, pag. 422-433, 2008). https://doi.org/10.1016/j.compstruct.2007.01.021.

[82] Huang H, Han Q, Wei D, *Buckling of FGM cylindrical shells subjected to pure bending load* (Composite Structures, Volume 93, Issue 11, pag. 2945-2952, 2011). https://doi.org/10.1016/j.compstruct.2011.05.009.

[83] Sadowski AJ, Rotter JM, *Solid or shell finite elements to model thick cylindrical tubes and shells under global bending* (International Journal of Mechanical Sciences, Volume 74, pag. 143-153, 2013). https://doi.org/10.1016/j.ijmecsci.2013.05.008.

[84] Sadowski AJ, Rotter JM, Chen L, *Nonlinear stability of thin elastic cylinders of different length under global bending* (International Journal of Solids and Structures, Volume 51, Issues 15–16, pag. 2826-2839, 2014). https://doi.org/10.1016/j.ijsolstr.2014.04.002.

[85] Fajuyitan OK, Sadowski AJ, Wadee MA, Rotter JM, *Nonlinear behaviour of short elastic cylindrical shells under global bending* (Thin-Walled Structures, Volume 124, pag. 574-587, 2018). https://doi.org/10.1016/j.tws.2017.12.018.

[86] Yadav KK, Gerasimidis S, *Instability of thin steel cylindrical shells under bending* (Thin-Walled Structures, Volume 137, pag. 151-166, 2019). https://doi.org/10.1016/j.tws.2018.12.043.

[87] Wagner HNR, Hühne C, Khakimova R, *On the development of shell buckling knockdown factors for imperfection sensitive conical shells under pure bending* (Thin-Walled Structures,Volume 145, 106373, 2019). https://doi.org/10.1016/j.tws.2019.106373.

[88] Li S, Kim DK, Liang QQ, *Fibre-based modelling for predicting the progressive collapse of cylindrical shells under combined axial compression and bending moment* (Engineering Structures, Volume 272, 114988, 2022). https://doi.org/10.1016/j.engstruct.2022.114988.

[89] Kokubo K, Nagashima H, Takayanagi M, Mochizuki A, *Analysis of shear buckling of cylindrical shells* (JSME international journal. Ser. A, Mechanics and material engineering, Volume 36, Issue 3, pag. 259-266, 1993). https://doi.org/10.1299/jsmea1993.36.3_259.

[90] Tsukimori K, *Analysis of the effect of interaction between shear and bending loads on the buckling strength of cylindrical shells* (Nuclear Engineering and Design, Volume 167, Issue 1, pag. 23-53, 1996). https://doi.org/10.1016/S0029-5493(96)01287-3.

[91] Michel G, Limam A, Jullien JF, *Buckling of cylindrical shells under static and dynamic shear loading* (Engineering Structures, Volume 22, Issue 5, pag. 535-543, 2000). https://doi.org/10.1016/S0141-0296(98)00132-1.

[92] Koo GH, Yoo B, Kim JB, *Buckling limit evaluation for reactor vessel of KALIMER liquid metal reactor under lateral seismic loads* (International Journal of Pressure Vessels and Piping Volume 78, Issue 5, pag. 321-330, 2001). https://doi.org/10.1016/S0308-0161(01)00049-7.

[93] Featherston CA, *Imperfection sensitivity of curvedpanels under combined compression andshear* (International Journal of Non-Linear Mechanics Volume 38, Issue 2, pag. 225-238, 2003). https://doi.org/10.1016/S0020-7462(01)00058-0.

[94] Athiannan K, Palaninathan R, *Buckling of cylindrical shells under transverse shear* (Thin-Walled Structures, Volume 42, Issue 9, pag. 1307-1328, 2004). https://doi.org/10.1016/j.tws.2004.03.019.

[95] Gettel M, Schneider W, *Buckling strength verification of cantilevered cylindrical shells subjected to transverse load using Eurocode 3* (Journal of Constructional Steel Research, Volume 63, Issue 11, pag. 1467-1478, 2007). https://doi.org/10.1016/j.jcsr.2007.01.003.

[96] Wang J, Sadowski AJ, *Elastic imperfect tip-loaded cantilever cylinders of varying length* (International Journal of Mechanical Sciences, Volume 140, pag. 200-210, 2018). https://doi.org/10.1016/j.ijmecsci.2018.02.027.

[97] Schmidt M, Winterstetter TA, *Buckling interaction strength of cylindrical steel shells under axial compression and torsion* (Advances in Steel Structures, Proceedings of The Second International Conference on Advances in Steel Structures, Volume 2, pag. 597-604, 1999). https://doi.org/10.1016/B978-008043015-7/50070-1.

[98] Meyer-Piening HR, M Farshad M, Geier B, Zimmermann R, *Buckling loads of CFRP composite cylinders under combined axial and torsion loading – experiments and computations* (Composite Structures, Volume 53, Issue 4, pag. 427-435, 2001). https://doi.org/10.1016/S0263-8223(01)00053-8.

[99] Meyer-Piening HR, M Farshad M, Geier B, Zimmermann R, *A study of elastic-plastic buckling of cylindrical shells under torsion* (Composite Structures, Volume 53, Issue 4, pag. 427-435, 2002). https://doi.org/10.1016/S0263-8223(01)00053-8.

[100] Mao R, Lu G, *A study of elastic-plastic buckling of cylindrical shells under torsion* (Thin-Walled Structures, Volume 40, Issue 12, pag. 1051-1071, 2002). https://doi.org/10.1016/S0263-8231(02)00058-7.

[101] Bisagni C, Cordisco P, *Post-buckling and collapse experiments of stiffened composite cylindrical shells subjected to axial loading and torque* (Composite Structures, Volume 73, Issue 2, pag. 138-149, 2006). https://doi.org/10.1016/j.compstruct.2005.11.055.

[102] Zhang X, Han Q, *Buckling and postbuckling behaviors of imperfect cylindrical shells subjected to torsion* (Thin-Walled Structures, Volume 45, Issue 12, pag. 1035-1043, 2007). https://doi.org/10.1016/j.tws.2007.07.003.

[103] Shen HS, *Boundary layer theory for the buckling and postbuckling of an anisotropic laminated cylindrical shell, Part III: Prediction under torsion* (Composite Structures, Volume 82, Issue 3, pag. 371-381, 2008). https://doi.org/10.1016/j.compstruct.2007.01.013.

[104] Mahdy WM, Zhao L, Liu F, Pian R, Wang H, Zhang J, *Buckling and stress-competitive failure analyses of composite laminated cylindrical shell under axial compression and torsional loads* (Composite Structures, Volume 255, 112977, 2021). https://doi.org/10.1016/j.compstruct.2020.112977.